

**EFFECTS OF VARIED POTASSIUM NUTRITION ON *CELLULOSE SYNTHASE A 4*
(*CESA4*) GENE EXPRESSION IN *ARABIDOPSIS THALIANA* PLANTS**

by

RAVZANUR YAZICIOĞLU BAŞARAN

Submitted to the Graduate School of Engineering and Natural Sciences

in partial fulfillment of the requirements for the degree of

Master of Science

Sabancı University

June 2024

RAVZANUR YAZICIOĞLU BAŞARAN 2024 ©

All Rights Reserved

ABSTRACT

EFFECTS OF VARIED POTASSIUM NUTRITION ON *CELLULOSE SYNTHASE A 4* (*CESA4*) GENE EXPRESSION IN *ARABIDOPSIS THALIANA* PLANTS

RAVZANUR YAZICIOĞLU BAŞARAN

Molecular Biology, Genetics and Bioengineering, MSc, Thesis, June 2024

Thesis Supervisor: Asst. Prof. Stuart James LUCAS

Keywords: potassium deficiency in plants, *Arabidopsis thaliana*, *cellulose synthase A*,
flowering time, PEI-SWNT mediated gene delivery

Plants require a regular nutrient supply to sustain their growth and development. Without adequate mineral nutrition, they cannot perform essential metabolic and physiological functions. One of the most critical nutrients for plants is potassium (K). Potassium is an essential mineral element required for many physiological and biochemical processes including production and transportation of photoassimilates, water and nutrient uptake (in particular nitrogen), and stress mitigation. When plants face K deficiency, they often manifest symptoms like leaf edge yellowing or browning, decreased turgor pressure, and eventual wilting. Increasing number of evidence is available suggesting that K has great contributions to biosynthesis of cellulose and related compounds. The *Cellulose Synthase A 4 (CESA4)* gene holds significant sway in cellulose biosynthesis. In many plant species, cellulose biosynthesis plays a critical role in maintaining axial tension and geometric rigidity, ensuring the upright posture of stems, leaves, and branches. The primary objective of this study was to elucidate the intricate relationship between the *CESA4* gene and the K nutritional status of plants. Various morphological and physiological tests were conducted on the experimental plants, including biomass measurement, shoot elongation analysis, and rosette size measurement. Elemental analysis was realized by using Inductively Coupled Plasma Optical Emission Spectroscopy

(ICP-OES) to evaluate mineral nutritional status of plants. Real-time quantitative PCR (RT-qPCR) was utilized to compare gene activity levels. Differential expression patterns of the *CESA4* gene were discerned in *Arabidopsis thaliana* accessions subjected to varied K treatments from very low to adequate levels. Early flowering ecotypes exhibited higher *CESA4* expression under K deficiency conditions. Examination of potassium accumulation in these plants carrying many single nucleotide polymorphisms (SNPs) in the *CESA4* gene revealed a marked accumulation of potassium in the inflorescence meristems of plants grown under potassium deficiency. High levels of *CESA4* expression were then detected in low K tissues. Building upon these findings, the research delved into functionally characterizing the *CESA4* gene by employing novel gene-editing techniques. The CRISPR/Cas9 system was meticulously engineered to effectuate *CESA4* gene knockout via point mutation. It was administered using the floral dipping transformation methodology. This innovative approach harnessed polyethyleneimine-functionalized single-walled carbon nanotubes (PEI-SWNT) as a promising gene delivery nanovector. The anticipated outcome of this analysis is to enrich the scientific discourse surrounding the possible relations of the *CESA4* gene with potassium nutrition, particularly by shedding light on its unforeseen expression dynamics under potassium deficiency.

ÖZET

ARABIDOPSIS THALIANA BİTKİLERİNDE ÇEŞİTLİ POTASYUM BESLEMESİNİN SELÜLOZ SENTAZ A 4 (CESA4) GEN EKSPRESYONU ÜZERİNE ETKİLERİ

RAVZANUR YAZICIOĞLU BAŞARAN

Moleküler Biyoloji, Genetik ve Biyomühendislik Yüksek Lisans Tezi, Haziran, 2024

Tez Danışmanı: Dr. Öğr. Üyesi Stuart James LUCAS

Anahtar Kelimeler: bitkilerde potasyum eksikliği, *Arabidopsis thaliana*, selüloz sentaz A, çiçeklenme zamanı, PEI-SWNT ile gen aktarımı

Bitkiler, büyüme ve gelişmelerini sürdürebilmek için düzenli mineral besin takviyesine ihtiyaç duyarlar. Yeterli beslenme olmadığında, bitkiler temel metabolik ve fizyolojik fonksiyonları yerine getiremezler. Bitkiler için en önemli besin maddelerinden biri potasyumdur. Potasyum (K), bitki fizyolojisinde önemli birçok rol oynar; örneğin fotoassimilatların biyosentezi ve bitki içinde taşınması, su alımı, besin elentlerin alınması (özellikle azot) ve strese bağlı etkilerin hafifletilmesi. Bitkiler potasyum eksikliği yaşadığında, yaprak kenarlarında sararma veya kahverengileşme, turgor basıncında azalma ve sonunda solma gibi belirtiler gösterirler. Eldeki bilgilere göre K sellulozon ve sellulozla ilişkili ürünlerin biyosentezine önemli katkılar sağlamaktadır. Selüloz biyosentezinin temel süreçlerinden birini yürüten *Selüloz Sentaz A 4 (CESA4)* geni, bitki metabolizmasında önemli bir rol oynar. Bu çalışmanın temel amacı, bitkilerde *CESA4* geni ile potasyum beslenme mekanizması veya potasyum kullanım yolları arasındaki karmaşık ilişkiyi aydınlatmaktır. Deneme, bitkilerde çeşitli morfolojik ve fizyolojik testler yapıldı. Bunlar arasında biyokütle ölçümü, sürgün uzunluğu analizi ve rozet boyutu ölçümü yer almaktadır. Bitkilerin mineral beslenme statüsünü değerlendirmek için İndüktif Eşleşmeli Plazma Optik Emisyon Spektroskopisi (ICP-OES) kullanılarak element analizi

yapıldı. Gerçek zamanlı kantitatif PCR (RT-qPCR) ekipmanı, gen aktivite seviyelerini karşılaştırmak için kullanıldı. Potasyum (K) eksiklik koşullarına maruz kalan *Arabidopsis thaliana* aksesyonlarında *CESA4* geninde farklı ekspresyon seviyeleri tespit edildi. Erken çiçeklenen ekotiplerin, eksiklik koşullarında yüksek *CESA4* ekspresyonu gösterdiği vurgulandı. *CESA4* geninde belirgin tek nükleotid polimorfizm (SNP) taşıyan bu bitkilerde potasyum birikiminin incelenmesi, potasyum eksikliği altında büyütülen bitkilerin çiçeklenme meristemlerinde belirgin bir potasyum birikimi olduğunu ortaya koydu. Gerçekleştirilen analizler sonucunda *CESA4* aktivitesinin de bu dokuda artmış olduğu saptandı. Bu bulguların üzerine, *CESA4* genini fonksiyonel olarak karakterize etmek için yeni gen düzenleme teknikleri kullanılarak araştırmalar yapıldı. CRISPR/Cas9 sistemi, nokta mutasyon yoluyla *CESA4* genini inaktive etmek için özenle tasarlandı ve çiçek daldırma transformasyon yöntemi kullanılarak uygulandı. Yenilikçi bir yaklaşımla, gen taşıma vektörü olarak polietilenimin fonksiyonlu tek duvarlı karbon nanotüplerini (PEI-SWNT) kullanıldı. Bu çalışma, *CESA4* geninin potasyum mekanizmalarındaki rollerine dair bilimsel tartışmayı zenginleştirerek, özellikle potasyum eksikliği altındaki bitkilerde görülen beklenmedik ekspresyon dinamiklerini aydınlatmaktadır.

ACKNOWLEDGEMENTS

First and foremost, I would like to express my heartfelt gratitude to God, who has brought me to this point and given me the strength to undertake this study. I am grateful for always illuminating my path and never leaving me alone. To my dear father, mother, and siblings, I extend my deepest thanks for teaching me to believe in myself and for their invaluable contributions to my life.

I am immensely grateful to my beloved husband, Kutsi, who is the greatest blessing in my life, for his companionship and unwavering support. He has always been by my side whenever I needed him, made everything easier during my toughest times, provided me with the strength to start anew when I felt hopeless and exhausted, and healed me with his patience and love. Without him, I would not be the person I am today.

I extend my sincere thanks to my thesis advisor, Dr. Stuart J. LUCAS, for addressing all my questions and providing invaluable guidance, and to my co-advisor, Dr. Nihal ÖZTOLAN EROL, for believing in me, sharing my dreams, paving the way for me, and mobilizing all possible resources.

I would also like to thank esteemed committee member, Prof. İsmail ÇAKMAK, for generously dedicating his valuable time, offering insightful advice, and providing guidance and feedback that broadened my horizons. My gratitude extends to another committee member, Dr. Bahar SOĞUTMAZ ÖZDEMİR, for making every effort to facilitate my work and for her valuable contributions.

I am grateful to Dr. Zaeema KHAN, for her understanding and the countless professional skills she taught me during my assistantship; and Dr. Atilla YAZICI, Dr. Yusuf TUTUŞ, and the entire greenhouse team for their incredible patience and the invaluable knowledge they shared with me.

I am indebted to our lab team, comprised of the strong women scientists of the future: my esteemed partner Gülnur ŞENER, who provided every possible support under challenging laboratory conditions; Dr. Melike ÇOKOL ÇAKMAK, who introduced me to Sabancı University and supported me unconditionally; Dr. Kadriye KAHRAMAN, our vibrant team leader, for solving all my problems regardless of the time and place; Serap SAKARYA, for

constantly motivating me and coming to my aid during my most stressful times; Gülce GÜRALP, for not only assisting me but also making me laugh whenever I felt overwhelmed.

I consider myself incredibly fortunate to have encountered these remarkable persons.

To my darling husband, Kutsi...

TABLE OF CONTENTS

ABSTRACT.....	i
ÖZET	iii
ACKNOWLEDGEMENTS.....	v
TABLE OF CONTENTS.....	viii
LIST OF FIGURES	xi
LIST OF TABLES.....	xiv
LIST OF ABBREVIATIONS.....	xvi
1. INTRODUCTION	1
1.1. Nutrition of Plants.....	1
1.2. The Genetic and Physiological Characteristics of <i>Arabidopsis thaliana</i> and <i>Triticum aestivum</i> Plants.....	6
1.3. General Characteristics of <i>Cellulose Synthase</i> Genes in Plants.....	8
1.4. Gene Delivery Systems in Plants.....	11
2. SCOPE OF THE THESIS.....	12
3. MATERIALS & METHODS	13
3.1. MATERIALS.....	13
3.1.1. Plant Growth and Phenotyping	13
3.1.2. CRISPR/Cas9-Mediated Gene Knockout System Design.....	14
3.1.3. Floral Dipping Transformation (FDT).....	16
3.1.4. Analysis of Mineral Content of <i>A. thaliana</i> Shoots Grown Under K-Deficiency 17	
3.1.5. Real-Time Quantitative Polymerase Chain Reaction (RT-qPCR) Setup	18
3.2. METHODOLOGY	20
3.2.1. Plant Growth and Phenotyping	20
3.2.1.1. Germination of <i>A. thaliana</i> Seeds.....	20
3.2.1.2. Cultivation of <i>A. thaliana</i> Seedlings.....	20
3.2.1.3. Phenotyping of the Plants	22
3.2.2. CRISPR/Cas9 System Design.....	23
3.2.2.1. gRNA Design for <i>CESA4</i> Gene	23
3.2.2.2. Overlapping PCR.....	24
3.2.2.3. Restriction Digest.....	26
3.2.2.4. Gel Purification.....	27

3.2.2.5.	Plasmid Ligation	28
3.2.2.6.	Preparation of Competent <i>E. coli</i> Cells.....	28
3.2.2.7.	<i>E. coli</i> Transformation	29
3.2.2.8.	Plasmid Isolation.....	29
3.2.2.9.	Confirmation of Integration of the Plasmid DNAs (pDNAs).....	30
3.2.3.	Floral Dipping Transformation (FDT).....	31
3.2.3.1.	Preparation of Polyethyleneimine-Functionalized Single-Walled Carbon Nanotubes (PEI-SWNT)	32
3.2.3.2.	Toxicity Determination for PEI-SWNT in <i>A. thaliana</i> Flowers and Application of CRISPR/Cas9 System for <i>Phytoene Dehydrogenase 3 (PDS3)</i> Gene..	34
3.2.3.3.	Application of CRISPR/Cas9 System for <i>Cellulose Synthase A4 (CESA4)</i> Gene.....	36
3.2.3.4.	Selection of Transformants	36
3.2.4.	Analysis of Mineral Content of <i>A. thaliana</i> Shoots Grown Under K-Deficiency.....	36
3.2.4.1.	Preparation of Plant Samples	36
3.2.4.2.	Operation Procedure of Inductively Coupled Plasma-Optical Emission Spectrometry (ICP-OES)	37
3.2.5.	Real-Time Quantitative Polymerase Chain Reaction (RT-qPCR) Setup	37
3.2.5.1.	RNA Isolation and DNase I Treatment.....	37
3.2.5.2.	Complementary DNA (cDNA) Synthesis.....	39
3.2.5.3.	Real-Time qPCR.....	40
3.2.5.4.	Statistical Analysis.....	40
4.	RESULTS	41
4.1.	Plant Growth and Phenotyping	41
4.2.	CRISPR/Cas9 System Design.....	49
4.3.	Floral Dipping Transformation (FDT).....	57
4.4.	Analysis of Mineral Content of <i>A. thaliana</i> Shoots Grown Under K-Deficiency ...	60
4.5.	Real-Time Quantitative Polymerase Chain Reaction (RT-qPCR) Setup	62
5.	DISCUSSION	70
5.1.	Comparative Analysis of Phenotypic Plasticity and Specific Candidate Gene Expression Levels among <i>A. thaliana</i> Natural Accessions under Nitrogen or Potassium Deficiency	70
5.2.	Association between <i>CESA4</i> Expression Level and Compartmentation of Potassium in Different Plant Tissues.....	76
5.3.	The Potential Correlations of Potassium and the <i>CESA4</i> Gene with Flowering Time.....	80

5.4.	CRISPR/Cas9-Mediated Engineering of <i>CESA4</i> Gene Utilizing PEI-SWNT	81
5.5.	Conclusion	83
5.6.	Future Prospects.....	84
BIBLIOGRAPHY		85
APPENDICES		100

LIST OF FIGURES

Figure 1.1. The naming conventions for transport proteins and the depiction of active transport mechanisms in the membrane (White, 2016)	4
Figure 1.2. Structure of plant cell wall and the plasma membrane (Sticklen, 2008). a: Cell wall comprising soluble proteins, pectin, lignin, hemicellulose, and cellulose microfibrils. b: The enzymes that synthesize cellulose are suspended in the plasma membrane as in the plasma membrane as complexes. c: The S1, S2, and S3 layers of the cell wall are where lignification takes place.	9
Figure 3.1. The scoring system used to classify seen chlorosis, necrosis, and anthocyanin accumulation in <i>A. thaliana</i> leaves (created with BioRender.com).....	23
Figure 3.2. Schematic representation of overlapping PCR reactions (created with BioRender.com).....	24
Figure 3.3. Illustration of floral dipping transformation in <i>A. thaliana</i> using PEI-SWNT and <i>A. tumefaciens</i> . (adapted from Clarck, 2001 and Kram et al., 2009 and created with BioRender.com).....	32
Figure 3.4. Identification of the parts of the plant species for harvesting. <i>Flag leaf (FL)</i> , <i>2. Leaf: Second leaf (SL)</i> , <i>Flag leaf layer: Flag stem (FS)</i> , <i>Leaf 2 layer: Second stem (SS)</i> were used for isolation of <i>T. aestivum</i> . (created with BioRender.com).....	38
Figure 4.1. Mean of length of shoot elongation and rosette size of 4-5 weeks old CS28833 ecotype of <i>A. thaliana</i> plants under potassium deficiency conditions; 1, 25, 200, and 2000 μ M K (grown in the growth chamber conditions given in Table 3.5).....	45
Figure 4.2. K-deficiency symptoms on 4-week-old ecotypes of <i>A. thaliana</i> rosettes. 3 mM K is the control group.	47
Figure 4.3. K-deficiency symptoms on young and old leaves of 4-week-old <i>A. thaliana</i> ecotypes. 3 mM K is the control group.....	47
Figure 4.4. Stem view of 4-week-old CS28833 under 1 μ M, 25 μ M, and 200 μ M K-deficiency. 2000 μ M K is the control group.....	48
Figure 4.5 Stem view of 5-week-old CS28833 under 1 μ M, 25 μ M, and 200 μ M K-deficiency. 2000 μ M K is the control group.....	49
Figure 4.6 Targeted regions on CESA4 protein of gRNAs (red boxes). A: gRNA.5, B: gRNA.7, C: gRNA.8, D: gRNA.8.1. Protein structure was checked with entry number: A0A1R7T3H6 at uniprot.org.....	52

Figure 4.7 Gel electrophoresis images gradient PCR with various annealing temperatures for step 1. NC: negative control, CDS: coding sequence	52
Figure 4.8 Gel electrophoresis images of step 1 PCR for CDSs.....	53
Figure 4.9 Gel images of step 3 PCR. Target 1: CDS1&2, Target 2: CDS3&4, Target 3: CDS5&6, Target 4: CDS:7&8	53
Figure 4.10 Gel images of restriction digested sequences	53
Figure 4.11 Gel image of optimization of time, enzyme amount, and ratio of plasmid ligation. Label numbers are given in Table 4.5.....	54
Figure 4.12 Gel results from plasmid construction.....	54
Figure 4.13 Transformed E. coli bacteria on LB agar plate (100 mg/L Amp). A: Target 1, B: Target 2, C: Target 3, D: Target 4.	55
Figure 4.14 Gel image of confirmation PCR for plasmid integrity. NC: negative control.....	55
Figure 4.15. Maps of the plasmids created with SnapGene Viewer. A: pFGC-pcoCas9 (Addgene, #52256), B: pCESA4-gRNA (SacI and EcoRI regions are shown. Adapted from pUC119-gRNA, Addgene, #52255).	56
Figure 4.16 CS28833 seedlings knocked-out of Phytoene Dehydrogenase 3 (PDS3) Gene with FDT using PEI-SWNT on water agar plates. A: 2 ng/μl, B: 5 ng/μl, C: 10 ng/μl, D: 20 ng/μl, E: 40 ng/μl, and F: 80 ng/μl PEI-SWNT (1:2)	57
Figure 4.17 The albino seedlings belong to 40 ng/μl CNT:pUC119-gRNA plasmid application. 25 seedlings were albino in 150 seedlings.....	58
Figure 4.18 CS28833 ecotype of <i>A. thaliana</i> after floral dipping transformation for <i>CESA4</i> gene with PEI-SWNT. A: Target 2, B: Target 3.....	59
Figure 4.19 <i>CESA4</i> knocked out CS28833 ecotype 10-day-old (T1) seedlings.	59
Figure 4.20 The logarithmic fold change of pheno-groups supplied with 1.6 mM N compared to 8 mM N. <i>CESA4</i> , AT5G44030; <i>SULTR4;1</i> , AT5G13550; <i>MOP9.16</i> , AT5G24320.....	63
Figure 4.21 The logarithmic fold changes of the expression level of the <i>CESA4</i> gene in 4-week-old CS28800, CS28140, CS7611, CS28833, CS28636, and CS76199 ecotypes supplied with 1.6 mM N compared to 8 mM N (n=2).	64
Figure 4.22 The fold changes of the expression level of the <i>CESA4</i> gene in 5-week-old CS76111, CS28140, CS28729, CS76208, CS28812, CS76199, CS28833, CS28787, CS76265, and CS76113. K treatments were normalized with 3 mM (adequate) K. N treatments were normalized with 8 mM N (adequate). Reference gene: Elongation factor-1-α (EF1α).....	65

Figure 4.23 The fold changes in *CESA4* expression level of 4-week-old CS28812 and CS28833 ecotypes. Y: Young leaves, O: Old leaves, S: Stem. Treatments were normalized with 3 mM (adequate) K (n=3).....67

Figure 4.24 The fold changes in *CESA4* expression level in 5-week-old CS28833 ecotype under 1 μ M, 25 μ M, and 200 μ M K deficiency. Treatments were normalized with 2 mM (adequate) K (n=3).....68

Figure 4.25 The logarithmic changes in *CESA4* expression level in *T. aestivum* supplied with 0 ppm K compared to 300 ppm K. *FL*: flag leaf, *FS*: flag stem, *SL*: second leaf, *SS*: second stem provided in Figure 3.4. *3A*: on chromosome 3 in sub-genome A, *3B*: on chromosome 3 in sub-genome B, and *3D*: on chromosome 3 in sub-genome D.....69

LIST OF TABLES

Table 1.1. Basic classification of plant nutrient uptake and function (Mengel and Kirkby, 2001).	2
Table 3.1. Stock solutions for macronutrients.....	21
Table 3.2. Stock solutions for 1000X micronutrient stock.	21
Table 3.3. The required volumes (mL) of stocks needed for 1 L of Hoagland’s solutions. ...	21
Table 3.4. The required concentrations (mM) of elements needed for 1 L of Hoagland’s solutions	22
Table 3.5. Growth chamber settings.....	22
Table 3.6. Components of overlapping PCR steps.....	25
Table 3.7. PCR program of overlapping PCR.....	25
Table 3.8. Reaction mixture of restriction digest protocol.....	26
Table 3.9. Reaction mixture of plasmid ligation protocol.....	28
Table 3.10. Reaction mixture of confirmation PCR.	30
Table 3.11. PCR program used in confirmation PCR.	30
Table 3.12. Reaction mixture of DNase I treatment.	39
Table 3.13. Reaction components and conditions of cDNA synthesis.	39
Table 3.14. Reaction mixture of DNase I treatment.	40
Table 3.15. qPCR conditions for SYBR mix.	40
Table 4.1. Physiological responses of <i>A. thaliana</i> ecotypes and mutants grown with hydroponics and under nutrient deficiency. The system of the 1-to-5 scale is given in Figure 3.1. Each experiment was conducted with at least five biological replicates. Flowering (%) was calculated by number of flowering plants/total number of plants.	42
Table 4.2. The P-values of shoot elongation and rosette size of CS28833 under K-deficiency. (95% confidence interval, n=6, calculated with GraphPad Prism).....	46
Table 4.3 gRNA primers (R1&F2 in Figure 3.2). Efficiency and mismatch values were calculated by the CHOPCHOP Tool.....	50
Table 4.4 gRNA primers (R1&F2 in Figure 3.2). Efficiency and mismatch values were calculated by the CHOPCHOP Tool.....	51
Table 4.5 Usage of primers to amplify coding sequences (CDSs).....	51
Table 4.6 Combinations of plasmid ligation	54
Table 4.7 Dry matter yield of 4-week-old CS28833 (\pm means standard deviation, n=2)	60

Table 4.8 Two-tailed P values of dry matter of 4-week-old CS28833. Student's t-test was performed using GraphPad Prism 10.2 (95% confidence interval, n=2).....	60
Table 4.9 The concentration of mineral elements in 4-week-old CS28833 plants under K deficiency. Analysis was performed using ICP-OES.	61
Table 4.10 Distribution of mean potassium (K) content (%) of 4-week-old CS28833 plants under K deficiency. (Analysis was conducted with two biological and three experimental replicates.).....	62
Table 4.11 Pheno-group classification of <i>A. thaliana</i> ecotypes.....	62
Table 4.12 Positions of SNPs on <i>CESA4</i> gene on the chromosome 5 in CS76113 (Col-0), CS28812, CS28787, CS76199, and CS28833 ecotypes. Col-0 was used as a reference ecotype to determine differences. Matching SNPs with Col-0 were represented in green color. <i>Adapted from HapMap sequencing data</i> (Atwell et al., 2010; Horton et al., 2012; Li et al., 2010).....	66

LIST OF ABBREVIATIONS

μL	Microliter
μM	Micromolar
AKT1	Akt Serine/Threonine Kinase 1
AKT2	Akt Serine/Threonine Kinase 2
AuNP	Gold Nanoparticles
C	Carbon
Ca	Calcium
cDNA	Complementary Deoxyribonucleic Acid
CDS	Coding Sequence
CESA4	Cellulose Synthase A 4
CGR	Crop Growth Rate
CHX	Cation/ H^+ Antiporters
Cl	Chlorine
CNGCs	Cyclic Nucleotide-Gated Channels
CNT	Carbon Nanotube
COOH	Carboxylated
CPA	Cation-Proton Antiporters
CRISPR	Clustered Regularly Interspaced Short Palindromic Repeats
CSC	Cellulose Synthase Complex
DNA	Deoxyribonucleic Acid
DW	Dry Weight
FDT	Floral Dipping Transformation
FS	Flag Stem
FL	Flag Leaf
FT	Flowering Locus T
g_{bs}	Bundle Sheath Cells
g_s	Mesophyll Cells
GT2	Glycosyl Transferases
H	Hydrogen
HAK	High-Affinity K^+ Transporters
HKTs	High-Affinity Potassium Transporters

ICP-OES	Inductively Coupled Plasma Optical Emission Spectroscopy
K	Potassium
KEA	K ⁺ Efflux Antiporters
KT	K ⁺ Transporters
KUP	K ⁺ Uptake Permeases
L	Liter
LDH	Layered Double Hydroxide
M	Molar
Mg	Magnesium
mL	Milliliter
mM	Millimolar
Mn	Manganese
MSN	Mesoporous Silica Particle
N	Nitrogen
Na	Sodium
NaKR1	Sodium-Potassium Root Defective 1
NAPDH	Nicotinamide Adenine Dinucleotide Phosphate Hydrogen
NC	Negative Control,
NFW	Nuclease Free Water
NHX	Na ⁺ /H ⁺ Antiporters
NRT	Nitrate Transceptor
NUE	Nitrogen Use Efficiency
O	Oxygen
P value	Probability Value
PCR	Polymerase Chain Reaction
PCW	Primary Cell Wall
pDNA	Plasmid Deoxyribonucleic Acid
PDS3	Phytoene Dehydrogenase 3
PEG	Polyethylene Glycol
PEI-SWNT	Polyethyleneimine-Functionalized Single-Walled Carbon Nanotubes
RAM	Root Apical Meristem
RNA	Ribonucleic Acid

RNP	Ribonucleic Protein
ROS	Reactive Oxygen Species
RT-qPCR	Real-Time Quantitative Polymerase Chain Reaction
S	Sulfur
SAM	Shoot Apical Meristem
SCW	Secondary Cell Wall
SL	Second Leaf
SNPs	Single Nucleotide Polymorphisms
SS	Second Stem
T-DNA	Transferred Deoxyribonucleic Acid
TMDs	Transmembrane Domains
TPC	Two-Pore Channels
TPK	Tandem-Pore K ⁺
ZnF	Zinc-Finger

1. INTRODUCTION

Plants are sessile organisms, typically remaining permanently at their germination sites. To compensate for their immobility, they have evolved unique mechanisms that allow for rapid responses to constantly changing environmental conditions and flexible adaptation to post-embryonic developmental processes (Hashimoto et al., 2015). Fossils discovered in marine or plain sediments chronicle the evolutionary history of plants. Currently, fossil evidence of terrestrial plants is limited to the Ordovician Period of the Paleozoic Era, spanning from 485.4 to 443.8 million years ago. Nonetheless, studies utilizing the "molecular clock" method, which employs genetic analysis to estimate the divergence time of species from a common ancestor, suggest that plants first colonized terrestrial environments approximately 500 million years ago, during the mid-Cambrian Period (*Plant - Evolution, Paleobotany, Photosynthesis / Britannica*, n.d.). In the history of plant life, the emergence and early diversification of land plants mark a distinct period of innovation. Liverworts, hornworts, mosses, and vascular plants are examples of terrestrial flora that evolved from simple unicellular organisms to complex entities with intricate two-stage life cycles and a remarkable diversity of organ and tissue systems. By the end of the Devonian period, plants had developed specialized sexual organs (gametangia), stems equipped with sophisticated fluid transport mechanisms (vascular tissue), structural tissues (such as wood), epidermal structures for respiratory gas exchange (stomata), various types of leaves and roots, diverse spore-bearing organs (sporangia), seeds, and tree-like forms (Kenrick & Crane, 1997).

1.1. Nutrition of Plants

Plants, which have undergone high evolutionary selection up to the present day, have generally developed as autotrophs. In this case, the nutrients they take from their environment (soil, water, desert sand) are vital for their survival. For over 2000 years, it has been known in agriculture that adding mineral elements, such as plant ash and lime, to the soil can enhance plant development. However, even as recently as 150 years ago, scientists were still debating whether mineral components were utilized as nutrients for plant growth. The 19th century saw the formal recognition of plant nutrition as a scientific field, spurred by the increasing understanding of the role of mineral elements in plant growth (von Liebig, 1841). This advancement led to a rapid increase in the use of mineral fertilizers. In Europe, horticulture and

agriculture began employing disproportionately high concentrations of potash, superphosphate, and later, inorganic nitrogen to promote plant growth (Marschner, 1983).

One of the primary drivers of the surge in research at the end of the last century was the tenuous foundation of Liebig's "mineral element theory." Studies utilizing higher plants in sand and water cultures were conducted to determine the significance of mineral elements for plant growth and their role in plant metabolism. The advancement of this research was closely linked to progress in analytical chemistry, including chemical purification and detection techniques (Marschner, 1983). It is widely accepted that elements should be classified as essential mineral elements (or mineral plant nutrients) only if they meet the following criteria: (a) the element is positively required for normal growth or reproduction; (b) its function cannot be substituted by another element; and (c) it influences plant metabolism, either directly or indirectly (Arnon, 1950). Elements that fulfill these conditions are considered nutrients, but these elements may differ from each other in terms of both biochemical properties and uptake (Table 1.1).

Table 1.1. Basic classification of plant nutrient uptake and function (Mengel and Kirkby, 2001).

Nutrient	Uptake	Biochemical functions
Group 1		
C, H, O, N, S	as CO ₂ , HCO ₃ ⁻ , H ₂ O, O ₂ , NO ₃ ⁻ , NH ₄ ⁺ , N ₂ , SO ₄ ²⁻ , SO ₂ gases from the atmosphere and ions from the soil solution	Principal components of biological matter. Atomic group components that are necessary for enzymatic activities. Oxidation-reduction processes for assimilation.
Group 2		
P, B, Si	such as silic acid, phosphates, and boric acid or borate from the soil solution	Alcohol-group esterification. Esters of phosphate involved in processes involving energy transfer.
Group 3		
K, Na, Ca, Mg, Mn, Cl	as the soil solution's ions	General mechanisms determining osmotic potential. Additional specialized roles for the best validation of enzymes (enzyme activation). Connecting the reaction partners. Anions in balance. Electrochemical potentials and membrane permeability control.
Group 4		
Fe, Cu, Zn, Mo	as chelates or ions derived from the soil solution	In prosthetic groups of enzymes in chelated form. Allow electron transit by valency conversion.

The primary components of organic plant material—carbon (C), hydrogen (H), oxygen (O), nitrogen (N), and sulfur (S)—constitute the first group. These elements are integral to proteins, nucleic acids, amino acids, and enzymes, which are the fundamental building blocks of life. The absorption of these nutrients by plants is directly linked to oxidation-reduction processes. Potassium (K), sodium (Na), calcium (Ca), magnesium (Mg), manganese (Mn), and chlorine (Cl) constitute the third group of plant nutrients. These elements are absorbed from the soil solution as ions and are present in plant cells in their ionic forms. In this state, they serve various general functions, including the creation of electro-potentials (Kirkby, 2023).

In this thesis, nitrogen (N) and potassium (K) nutrition is particularly emphasized. Nitrogen (N) is a key component of organic substances such as proteins, nucleic acids, and amino acids. Its deficiency can lead to delayed phenological development in both vegetative and reproductive stages (Fathi & Zeidali, 2021). Effective use of nitrogen fertilizers can significantly improve biomass, with nitrogen fertilization being the sole condition enabling high biomass (Fathi et al., 2016). N plays a crucial role in sustaining leaf surface integrity, leading to increased leaf longevity, enhanced photosynthesis rates, and ultimately greater dry matter production (Zebarth and Sheard, 2011). Nitrogen deficiency intensifies competition for the element's distribution within the plant, leading to compromised development of reproductive organs due to reduced crop growth rate (CGR), delayed plant phenology, decreased harvest index, and ultimately diminished grain yield (Fathi & Zeidali, 2021). The pathways of nitrogen (N) metabolism in plants—namely, N absorption, N translocation, N assimilation, and N remobilization—are controlled by a variety of genes. The expression of these genes varies depending on the nitrogen conditions. Key genes involved in N metabolism include nitrate transporters (for nitrate and ammonium), reductase (for nitrite and nitrate), synthase (for glutamine and glutamate), aminotransferase (for aspartate and alanine), and glutamate dehydrogenase (P. Kumar et al., 2022). Nitrogen deficiency reduces photosynthesis, leaf area, and the lifespan of green leaves, all of which negatively impact plant productivity. Numerous studies have demonstrated the relationship between photosynthesis and nitrogen availability. Here, we outline the physiological response of photosynthesis to nitrogen deficiency in terms of leaf structure and intraleaf nitrogen distribution (Mu & Chen, 2021). Under severe nitrogen stress, nearly all plants exhibit a reduction in photosynthetic rate due to several factors: (1) a decrease in the content of bioenergetics and light-harvesting proteins, which inhibits the electron transport rate and increases the dissipation of light energy as heat; (2) a reduction in the content and/or activity of photosynthetic enzymes, leading to a lower

carboxylation rate; and (3) a decrease in the stomatal conductance of mesophyll cells (g_s) and bundle sheath cells (g_{bs}), which affects the intercellular CO_2 concentration (Mu & Chen, 2021).

Potassium (K) stands out as the most abundant inorganic cation essential for robust plant growth, making up as much as 10% of the dry weight of a plant (White & Karley, 2010). This vital element activates numerous crucial enzymes responsible for functions such as protein synthesis, sugar transport, nitrogen (N) and carbon (C) metabolism, and photosynthesis. Its presence is indispensable for enhancing both yield and quality (Eichert & Fernández, 2023). Furthermore, potassium is critical in cell proliferation, a fundamental process vital for overall plant development and functionality (Hepler et al., 2001). The mechanism through which potassium (K) promotes cell development is widely acknowledged to involve stimulating and regulating plasma membrane ATPase, leading to acid stimulation that subsequently induces cell wall loosening and activates hydrolases (Oosterhuis et al., 2014). Being highly mobile within plants, potassium plays a crucial role in controlling osmotic pressure within cells and maintaining the proper balance of cations and anions in the cytoplasm (Kaiser, 1982; Zhu et al., 2016). Through these mechanisms, potassium regulates essential physiological functions such as cell elongation, stomatal regulation, and other critical processes. Furthermore, it hampers the rate of net and accelerates leaf senescence (Ding et al., 2005). Moreover, potassium plays a vital role in regulating the opening and closing of stomata, thereby controlling the exchange of oxygen, carbon dioxide, and water vapor. Insufficient potassium or its inadequate provision leads to stunted plant growth and reduced yield. General transport proteins on cellular membranes are represented in Figure 1.1.

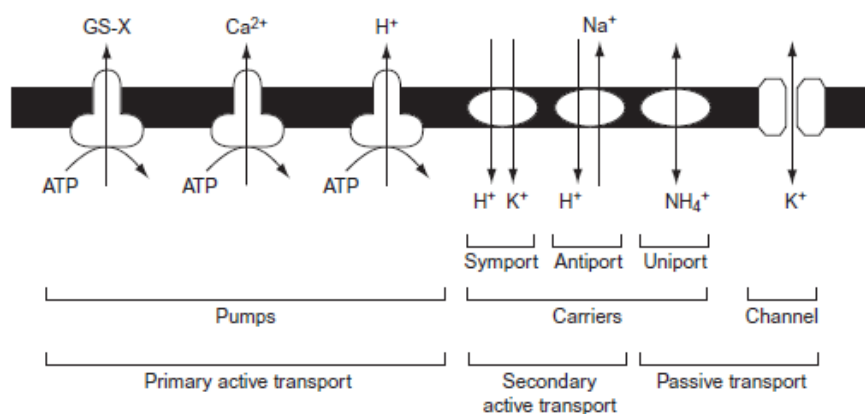


Figure 1.1. The naming conventions for transport proteins and the depiction of active transport mechanisms in the membrane (White, 2016)

Within plants, the uptake and intracellular distribution of potassium ions (K^+) are governed by several families of transporter proteins. These protein families exhibit distinct structural features and modes of transport. Notable among them are the voltage-dependent Shaker-like channels, two-pore channels (TPC), and voltage-independent tandem-pore K^+ (TPK) channels (Hedrich, 2012). Additionally, as per Lebaudy et al. (2007), the Shaker family can be further categorized into five subgroups: weak inward rectifying channels (AKT2-like), silent/regulatory subunit (KAT3-like), inward rectifying channels (AKT1-like), and outward rectifying channels (K-out). Moreover, this mechanism involves cation-proton antiporters (CPA), HKT uniporters and symporters (Hamamoto et al., 2015), and the carrier-like KT/HAK/KUP family (W. Li et al., 2018; Nieves-Cordones et al., 2014). According to Sze and Chanroj (2018), the CPA family comprises three sub-families: NHX, CHX, and KEA antiporters. Additionally, CNGCs and NRT1.5 play a role in maintaining cellular K^+ homeostasis (X. Li et al., 2005). The high-affinity absorption of potassium is facilitated by the KUP/HAK/KT family (W. Li et al., 2018). The regulation of sodium (Na^+) and potassium (K^+) absorption, as well as their homeostasis, relies on the function of HKT proteins. Among these proteins, a subset plays a role in responding to short-term potassium deficiency by increasing sodium absorption, while others are involved in salt tolerance mechanisms. In this context, plant HKT proteins are classified into two groups: class I represents sodium uniporters, while class II encompasses sodium and potassium symporters (Riedelsberger et al., 2021). Signs of potassium (K^+) deficiency in plants include brown scorching and curling of leaf tips, as well as chlorosis between leaf veins, which is closely associated with chlorophyll breakdown (Hafsi et al., 2014). Symptoms of K^+ deficiency typically first appear on older leaves. Plants experiencing K^+ deficiency stress may have evolved this survival strategy, mobilizing K^+ from mature and senescing organs to supply the youngest tissues. According to Cakmak (2005), these symptoms can be attributed to the oxidative destruction of chlorophyll by reactive oxygen species (ROS), a process accelerated by K^+ deficiency. Barley (Drew, 1975) and *Arabidopsis thaliana* (Shin & Schachtman, 2004) grown under low potassium (K^+) concentrations both exhibited a reduction in the number and growth of lateral roots. One of the early responses of plants to potassium (K^+) deficiency stress is the alteration in the distribution of dry matter between roots and shoots. The root/shoot dry weight (DW) ratio under K^+ deficiency varies depending on species and cultural conditions (Andrews et al., 1999). Some studies have reported a decrease in the root/shoot DW ratio in K^+ -deficient plants (Cakmak et al., 1994; Marschner et al., 1996). Additionally, no statistically significant effect on the root/shoot DW

ratio was found in maize (Tewari et al., 2004), *C. rigidum* (Hafsi et al., 2011), and *Arabidopsis thaliana* (Gruber et al., 2013) under K⁺ deficiency.

More recently, molecular, electrophysiological and reverse genetic approaches in plants have identified genes encoding K⁺ transporters and K⁺ channels (Gierth et al., 2005; Lebaudy et al., 2007; Rubio et al., 2000). K⁺ transporters exist in three families of membrane proteins: K⁺ uptake permissives, K⁺ transporter family, and cation proton antiporters (Gierth et al., 2005). Although plant responses to K⁺ deficiency are well documented at physiological and transcriptional levels, the regulatory mechanisms underlying these changes are not fully understood (Ashley et al., 2006). To cope with K⁺ deficiency, plants must sense changes in K⁺ availability and transmit signals to modulate their metabolism. Recent studies have elucidated the sensing and signaling pathway involving components such as ROS, ethylene, Ca²⁺, auxin, jasmonic acid, and phosphatidic acid (Armengaud et al., 2010; Hafsi et al., 2014; Shin & Schachtman, 2004).

1.2. The Genetic and Physiological Characteristics of *Arabidopsis thaliana* and *Triticum aestivum* Plants

The first plant for which the whole genome sequence is known is *Arabidopsis thaliana* (*Arabidopsis* Genome Initiative, 2000). Therefore, *Arabidopsis* could be a helpful tool for identifying the genes responsible for nutrient mobilization. (Himelblau & Amasino, 2001). *Arabidopsis thaliana*, a dicot angiosperm, belongs to the *Cruciferae* (*Brassicaceae*) family within the order *Capparales*. The closest wild relatives of *A. thaliana* are *A. lyrata* and *A. halleri*, both of which are self-incompatible diploids with eight pairs of chromosomes (Mitchell-Olds, 2001). During embryogenesis, angiosperms generate two distinct apical meristems: the shoot apical meristem (SAM) and the root apical meristem (RAM). These meristems serve as a continual source of new cells for organogenesis throughout the plant's life (Fletcher, 2002). Comprised of small populations of pluripotent stem cells, these meristems are morphologically undifferentiated and located at the tips of shoots and roots, respectively. Therefore, the proper functioning of the root and shoot apical meristems is crucial for regular growth and development (Eshed Williams, 2021). In *Arabidopsis*, the SAM is responsible for the sequential initiation of leaves, stems, and flowers. During vegetative development, SAM produces leaf primordia in a standardized spatial arrangement directly from their flanks. At the conclusion of the vegetative phase, environmental and endogenous signals prompt the plant to

transition into flowering and reproductive development (Eshed Williams, 2021). During this phase, the stem elongates, floral meristems form on the sides of both primary and secondary SAMs, and secondary SAMs develop in the leaf axils. The primary reproductive SAM, also referred to as the inflorescence or flower-bearing meristem, gives rise to floral meristems, which are small, spherical clusters of cells that generate four different types of secondary organs arranged in concentric rings known as whorls (Demesa-Arevalo et al., 2024). Sepals form in the outermost whorl, followed by petals in the second whorl, and stamens in the third whorl. Subsequently, the floral meristem is consumed in the formation of central carpels that encase the seeds of the next generation, forming the gynoecium. Thus, while the SAM grows indefinitely, the floral meristem ultimately terminates. This termination of meristem activity in floral meristems is regulated by a temporal feedback loop involving a stem cell regulator and a phase-specific floral patterning factor (Fletcher, 2002). The model plant *Arabidopsis thaliana* is a facultative long-day species, capable of exhibiting either a summer-annual or winter-annual blooming phenotype (Gazzani et al., 2003). It flowers most rapidly during the long photoperiods of spring and early summer. *Arabidopsis* accessions display a range of flowering strategies: some complete their life cycle quickly, while others adopt an annual winter habit, remaining vegetative over winter and flowering when the spring conditions are favorable. Numerous studies have investigated the genetic basis of these flowering behaviors (Alonso-Blanco et al., 1998; Gazzani et al., 2003). *Arabidopsis thaliana* has been utilized as a model organism for plant genome research due to its diploid genetics, rapid growth cycle, relatively low content of repetitive DNA, and small genome size (Goodman et al., 1995).

Triticum aestivum L. belongs to the *Poaceae* (grass) family and is the most economically significant wheat cultivated, owing to its numerous applications and agricultural importance (Knott, 2011). According to Lersten (2015), wheat is a medium-tall annual or winter annual grass characterized by terminal flower spikes with perfect blooms and flat leaf blades. In their vegetative state, plants are identified by tillers that bear axillary, leafy culms. A cultivar consists of five to seven nodes with three to four leaflets. The top leaf, commonly known as the flag leaf, represents the inflorescence (Lersten, 2015). Each cultivar produces an inflorescence, also known as a complex spike, with the fundamental component being the spikelet. Spikelets are separated by short internodes and form on a primary axis or rachis. Each spikelet comprises a compact reproductive stalk made up of two substerile bracts, or glumes. Glumes surround two to five blooms borne on a short axis called a rachilla. Wheat flowers feature large anthers on three stamens, while the pistil has two styles, a single ovary, and two branching, hairy stigmas at the end of each style (Lersten, 2015). *T. aestivum* is hexaploid,

possessing 42 chromosomes in total ($2n=42$; six copies of each of the seven chromosomes) with the genomic constitution AABBDD (Levy & Feldman, 2022). Similarly, many wheat species share members of the fundamental haploid set of seven chromosomes (Lersten, 2015; Levy & Feldman, 2022). Modern wheat cultivars are either tetraploid (durum wheat, AABB) or hexaploid (common wheat and club wheat, *Triticum compactum*, AABBDD).

1.3. General Characteristics of *Cellulose Synthase* Genes in Plants

Plants are renowned for producing a vast array of metabolites, among which cellulose is particularly notable (Delmer, 1999). Cellulose, the most abundant macromolecule on Earth, is the primary component of plant cell walls. It consists of long, linear polymers composed of hundreds of glucose molecules, which form cellulose fibers (Sticklen, 2008). These fibers bundle together into structures known as microfibrils, which typically consist of about 40 fibers. Surrounding the microfibrils is a network formed by hydrated polysaccharides (Cutler & Somerville, 1997). The cell wall is fixed in position by enzymes associated with the cell membrane that assemble precursor components produced within the cell. Plant cell walls are composed of layers containing soluble protein, cellulose microfibrils, hemicellulose, pectin, and lignin (Figure 1.2). This structure is organized into three main layers: the primary cell wall, the middle lamella, and the secondary cell wall. The cell wall, which encases the plasma membrane, provides the cell with tensile strength and protection (Sticklen, 2008).

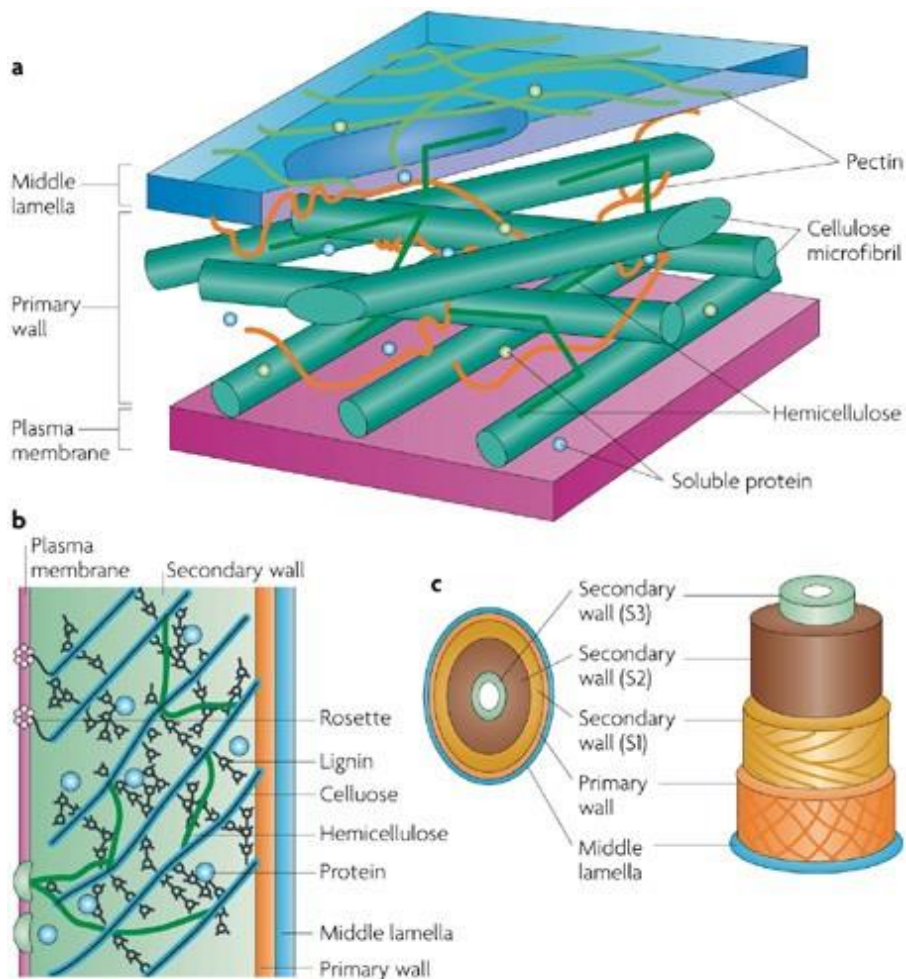


Figure 1.2. Structure of plant cell wall and the plasma membrane (Sticklen, 2008). a: Cell wall comprising soluble proteins, pectin, lignin, hemicellulose, and cellulose microfibrils. b: The enzymes that synthesize cellulose are suspended in the plasma membrane as in the plasma membrane as complexes. c: The S1, S2, and S3 layers of the cell wall are where lignification takes place.

The primary producers of cellulose are cellulose synthase proteins, encoded by *cellulose synthase* genes. These genes were initially identified in bacteria, with divergent homoeologs subsequently discovered in plants (Cutler & Somerville, 1997; Saxena & Brown, 2000). In higher plants, a gene family known as *cellulose synthase A (CESA)* is believed to encode isoforms of the catalytic subunit of cellulose synthase. However, the specific functions of most of these genes in plant development remain largely unknown (Delmer, 1999). Gaining insight into how particular *CESA* genes function in specific tissues or cell types is expected to facilitate the development of valuable analytical and biotechnological tools, enhancing our understanding and management of the factors underlying plant morphogenesis and physiology (Beeckman et al., 2002). Numerous terrestrial plants have been found to carry the *CESA* gene, with ten conserved genes identified in the genome of the model plant *Arabidopsis thaliana* (M.

Kumar et al., 2009). Genetic and biochemical investigations have shown that different combinations of CESA proteins form the terminal complex (Doblin et al., 2002; Mutwil et al., 2008). For example, in *A. thaliana*, a complex consisting of AtCESA1, AtCESA3, and AtCESA6 is involved in the production of the primary cell wall (PCW). Additionally, another complex involved in the production of the secondary cell wall (SCW) is formed by AtCESA4, AtCESA7, and AtCESA8 (Carroll et al., 2012; Gonneau et al., 2014; Taylor et al., 2003). The glycosyl transferases (GT2) family, encompassing plant CESAs, catalyzes the beta connection between glycosyl residues. The catalytic domains of intrinsic plasma membrane proteins, or CESAs, extend into the cytoplasm (Rayon et al., 2014). It is theorized that each of the six subunits of the cellulose synthase complex (CSC) is composed of six active enzyme CESA proteins. Each CESA protein synthesizes a single beta-1,4-linked chain (Morgan et al., 2012; Slabaugh et al., 2014). Following CSC emergence, the numerous chains polymerize into a microfibril outside the plasma membrane through hydrogen bond formation. A CESA protein from higher plants is believed to have eight transmembrane domains (TMDs) that create a gap in the plasma membrane for the newly generated glucan chain to exit. Close to the amino terminus on the cytoplasmic face, two zinc-finger domains (ZnF) are located, bearing a strong resemblance to the RING-finger motif (Slabaugh et al., 2014). The core, or catalytic, domain is situated between the second and third TMDs (S. Li et al., 2014). In all species studied thus far, the catalytic domain of CESA proteins contains three conserved aspartyl residues (D1, D2, and D3) and a QXXRW motif (Kaur et al., 2016).

In bread wheat, there are 22 *CESA* genes with homoeologs present in each of the three genomes. *TaCESA4*, 7, and 8 were identified as specifically involved in secondary cell wall (SCW) synthesis, while *TaCESA1*, 2, and 6 were found to be specific to primary cell wall (PCW) synthesis. Additionally, *TaCESA3*, 5, and 9 were deemed largely redundant one-to-one orthologs to PCW *CESAs* based on ortholog analysis. Intriguingly, *CESA4* exhibited a unique feature with a phase distribution of introns 2, 5, 6, and 7 being 0, indicating distinct characteristics (Kaur et al., 2016). Furthermore, a substitution of the polar amino acid glutamine with the negatively charged amino acid glutamate was observed in SCW *TaCESA4*. The sequence similarity between *Arabidopsis CESA4* and its orthologs from maize, rice, wheat, and barley ranged from 73% to 74%. Group I comprised genes involved in SCW synthesis, namely *TaCESA4A*, *B*, *D*, *TaCESA7B*, *D*, and *TaCESA8B*, *D*, showing minimal expression during PCW development but strong expression in mature tissues, such as stems shortly after anthesis. Notably, three SCW genes (*TaCESA4*, 7, 8) and their homoeologs were found to

exhibit co-expression in mature root tissues, as indicated by RNA-seq expression profiling (Kaur et al., 2016).

1.4. Gene Delivery Systems in Plants

Plant genome engineering typically employs *Agrobacterium*-mediated gene transfer as its primary method. Effective gene delivery systems are crucial for genetic engineering in plants. Traditional gene-transplanting techniques fall into three main categories: physical, chemical, and biological (Zhi et al., 2022). Among physical gene delivery techniques, electroporation and biolistic particle delivery are highly favored. Electroporation utilizes electric field pulses to create pores in cell membranes, while biolistic particle delivery, also known as particle bombardment or gene cannon delivery, propels genetic material into cells. Chemical delivery methods utilize cationic lipids and polymers as transfer agents, with polyethylene glycol (PEG)-mediated transport being a common technique. However, these traditional methods have limitations, including genotype dependence, which restricts the use of genetic engineering and genome editing in many crop plants (Demirer & Landry, 2021). Consequently, there is a pressing need to develop novel gene delivery vectors or methods. Recently, nanomaterials such as mesoporous silica particles (MSNs), AuNPs, carbon nanotubes (CNTs), and layered double hydroxides (LDHs) have emerged as promising vectors for delivering genome engineering tools such as DNA, RNA, proteins, and RNPs to plants. These methods demonstrate high efficiency across various plant species (Shamekhi et al., 2017). Encouraging outcomes have been observed, including successful cargo gene transfer and the development of genome-stable transgenic cotton and maize plants, offering new avenues for genome engineering in plants.

2. SCOPE OF THE THESIS

The objective of this study is to elucidate the reasons behind the increased expression of the *cellulose synthase A 4 (CESA4)* gene in plants under potassium deficiency. To achieve this, we formulated three hypotheses: (i) the *CESA4* gene may play a role in the potassium metabolism within plants; (ii) there may be a connection between the *CESA4* gene and potassium with flowering, as ecotypes exhibiting high *CESA4* expression under potassium deficiency also tend to flower early; and (iii) the activity of the *CESA4* gene may correlate with the compartmentation of potassium within plant tissues. We selected the most suitable *Arabidopsis thaliana* (the thale cress) ecotype to investigate these hypotheses and employed primary mineral element analysis along with real-time quantitative PCR (RT-qPCR) techniques. To deepen the functional analysis of the gene, we performed gene knock-out using CRISPR/Cas9-mediated genetic engineering employing a promising nanovector: polyethyleneimine-functionalized single-walled carbon nanotubes (PEI-SWNT). To determine whether the results were species-specific, we also examined the expression levels of the *CESA4* gene in potassium-deficient *Triticum aestivum* (the common wheat), which is widely used in agriculture.

3. MATERIALS & METHODS

3.1. MATERIALS

The materials used in this study are listed in the following sections.

3.1.1. Plant Growth and Phenotyping

The list below displays the materials required for plant growth at various stages, including germination, cultivation, phenotyping, and harvesting.

- *A. thaliana* seeds of different ecotypes and mutants: SALK-084627, SALK-110333, CS28833, CS76111, CS76199, CS28812, CS28140, CS28800, CS28636, CS76113, CS28729, CS76208, CS28787, CS76265 (ordered from <http://signal.salk.edu/>, <https://arabidopsis.info/>)
- Ammonium nitrate (Merck, CAT: 221244-2.5 KG)
- Calcium nitrate tetrahydrate (PanReac AppliChem, #131231.1211)
- Potassium dihydrogen phosphate (Merck, #1.04873.1000)
- Magnesium(II) sulfate heptahydrate (PanReac AppliChem, #131404.1211)
- Potassium chloride (ISOLAB, CAT: 7447-40-7)
- Boric acid (PanReac AppliChem, #131015.1210)
- Manganese(II) sulfate tetrahydrate ()
- Zinc sulfate heptahydrate (Merck, #1-08883.0500)
- Copper (II) sulfate pentahydrate (Merck, #1.02790.0250)
- Ammonium heptamolybdate tetrahydrate (Merck, #1.001180.0250)
- Ethylenediaminetetraacetic acid iron (III) sodium salt hydrate (Thermo Fisher Scientific, CAT: 088995.22)
- Calcium chloride (Merck, #1.02382.1000)
- Ortho-phosphoric acid, 85% (Merck, 1.00573.2500)
- Hydrochloric acid, 37% (Merck, #100317)
- Sodium hydroxide (Merck, #106498)
- Micropropagation agar, powder (Caisson Labs, CAS: 9002-18-0)

- Agarose, powder (Biomax Prona, CAT: HS-8000)
- UltraPure™ DNase/RNase-Free Distilled Water (Invitrogen, CAT: 10977035)
- Polystyrene Petri dishes, 120 x 17 mm (ISOLAB, REF: 081.02.161)
- Plastic trays (24 Inch x 16 Inch)
- 70-well plastic cube trays
- Plastic bottles (ISOLAB,
- Glass bottles, 1000 mL (ISOLAB, BORO 3.3, REF: 061.02.1000)
- Rockwool cubes (Brodan, Tartes Tarım, CAT: ortam-kayayünü-61638)
- Surgical blades (Medisin, NO: 1)
- Forceps with straight tip (ISOLAB, CAT: 048.07.105)
- ddH₂O
- Ruler

The equipment needed for the plant growth process is listed below.

- Growth Chamber, PG24 (Nordham Technologies, Turkiye)
- Microwave oven, MD595 (Arçelik, Turkiye)
- pH meter (Hanna Instruments, USA)

Tools used in the analysis of the results are given below.

- GraphPad Prism 10.2.3 (Dotmatics, UK)
- Microsoft Excel software

3.1.2. CRISPR/Cas9-Mediated Gene Knockout System Design

The material list for the CRISPR/Cas9 system is provided below, covering gRNA design, plasmid construction, *E. coli* transformation, and plasmid confirmation.

- pUC119-gRNA (Addgene, #52255)
- pFGC-pcoCas9 (Addgene, #52256)
- 5X Phusion® HF buffer (NEB, #B0518)
- 5X Phusion® GC Buffer (NEB #B0519)
- Phusion® High-Fidelity DNA polymerase (NEB, #M0530S)
- 10 mM dNTPs (KAPA, #KK1017)
- Taq PCR Kit (KAPA, #KK1022)

- Custom PCR primers, synthesized to order (SenteBio Lab)
- rCutSmart™ buffer (NEB, #B6004S)
- EcoRI-HF® (NEB, #R3101S)
- SacI-HF® (NEB, #R3156S)
- NucleoSpin Gel and PCR Clean-up Kit (Macherey-Nagel, #740609.50)
- T4 DNA Ligase (NEB, #M0202S)
- *E. coli*, DH5α strain
- LB broth (Sigma, CAT: L3022-250G)
- Sucrose (ISOLAB, #970.053.1000)
- Ampicillin (Duchefa Biochemie, #A0104.0025)
- Kanamycin (PhytoTechnology Laboratories, #K378)
- Plasmid Isolation Kit (EcoSpin, CAT: EcoPI-50x)
- Calcium chloride (Merck, #1.02382.1000)
- Glycerol, ultra-pure (MP Biomedicals, CAT: 800689)
- Agarose, powder (Biomax Prona, CAT: HS-8000)
- 0.5X TBE Buffer
- 0.2 mL PCR tubes (CAPP, #5100201C)
- 10 µL non-filter tips (CAPP, #5130010C)
- 200 µL non-filter tips (CAPP, #4130075C)
- 1000 µL non-filter tips (CAPP, #4130135C)
- Polystyrene Petri dishes, 120 x 17 mm (ISOLAB, REF: 081.02.161)
- UltraPure™ DNase/RNase-Free Distilled Water (Invitrogen, CAT:10977035)
- Ice

The following is the equipment list for this section.

- 10 µL, 100 µL, 1000 µL single channel micropipettes (Thermo Fisher Scientific, USA, #4700860N)
- Mastercycler gradient (Eppendorf, Germany)
- NanoDrop 2000C Spectrophotometer (Thermo Fisher Scientific, USA)
- Gel Electrophoresis System, Advance (Mupid-One, Japan)
- Gel Doc EZ Imager (Bio-Rad, USA)
- Shaking incubator, 3033 (Gujarat Fluorochemicals, India)
- ThermoStat Plus (Eppendorf, Germany)
- Ultracentrifuge, 5418 R (Eppendorf, Germany)

- Safety cabinet, HERAsafe KS (Thermo Fisher Scientific, USA)
- UV/Visible spectrophotometer, WPA Biowave II (Bichrom, USA)
- Microwave oven, MD595 (Arçelik, Turkiye)
- -20°C deep freezer (Arçelik, Turkiye)
- -86°C ultra-low temperature freezer, Forma 890000 (Thermo Fisher Scientific, USA)

The tools used for this part of the study are given below.

- CHOPCHOP Tool (<https://chopchop.cbu.uib.no>)
- NEBicalculator (<https://nebiocalculator.neb.com>)
- Basic Local Alignment Search Tool, NCBI (<https://blast.ncbi.nlm.nih.gov>)
- OligoAnalyzer Tool, IDT (<https://idtdna.com/pages/tools/oligoanalyzer>)
- RCSB Protein Data Bank (RCSB PDB) (<https://rcsb.org/>)
- SnapGene Viewer (Dotmatics, UK)
- GraphPad Prism 10.2.3 (Dotmatics, UK)
- TAIR—The Arabidopsis Information Resource (<http://www.arabidopsis.org/>)
- 1001 Arabidopsis Genomes Project genome browser (<http://signal.salk.edu/atg1001/3.0/gebrowser.php>)

3.1.3. Floral Dipping Transformation (FDT)

The preparation of polyethyleneimine-functionalized single-walled carbon nanotubes (PEI-SWNT) used for transformation is based on the method outlined by Demirer et al. (2019). Transformation of *A. tumefaciens* cells, application of FDT for CRISPR/Cas9, determination of toxicity, and selection of transformants experiments are performed using the materials listed below.

- *A. thaliana* plants at the flowering stage
- PEI-SWNT
- pUC119-gRNA (Addgene, #52255)
- pFGC-pcoCas9 (Addgene, #52256)
- pUC119-gRNA, *CESA4* construct
- Silwet L-77 (PhytoTech Labs, P7777)
- MS Vitamin media (Caisson, #MSP02-50LT)
- Ampicillin (Duchefa Biochemie, #A0104.0025)

- Nutrient-enriched soil (Biomixx, Light-mix)
- UltraPure™ DNase/RNase-Free Distilled Water (Invitrogen, CAT: 10977035)
- 10 µL non-filter tips (CAPP, #5130010C)
- 200 µL non-filter tips (CAPP, #4130075C)
- 1000 µL non-filter tips (CAPP, #4130135C)
- Polystyrene Petri dishes, 60 x 15 mm (ISOLAB, REF: 081.02.161)
- 1.5 mL ultracentrifuge tubes (Capp, #5101500C)
- Surgical blades (Medisin, NO: 1)
- dH₂O
- Plastic pots
- Stretch film

The equipment needed for FDT is listed below.

- Growth Chamber, PG24 (Nordham Technologies, Turkiye)
- Microwave oven, MD595 (Arçelik, Turkiye)
- ZetaSizer Pro (Malvern, UK)
- Shaking incubator, 3033 (Gujarat Fluorochemicals, India)
- 10 µL, 100 µL, 1000 µL single channel micropipettes (Thermo Fisher Scientific, #4700860N)
- NanoDrop 2000C Spectrophotometer (Thermo Fisher Scientific, USA)
- -20°C deep freezer (Arçelik, Turkiye)
- -86°C ultra-low temperature freezer, Forma 890000 (Thermo Fisher Scientific, USA)

The tools needed for the application of FDT are listed below.

- TAIR—The Arabidopsis Information Resource (<http://www.arabidopsis.org/>)
- 1001 Arabidopsis Genomes Project genome browser (<http://signal.salk.edu/atg1001/3.0/gebrowser.php>)

3.1.4. Analysis of Mineral Content of *A. thaliana* Shoots Grown Under K-Deficiency

The following material list represents elemental analysis conducted in two parts: preparation of plant samples and operation of ICP-OES.

- Mature *A. thaliana* plants

- Nitric acid, 65% (Merck, #176737-5G)
- Hydrogen peroxide, 30% (Merck, #1.08597.1000)
- Serological disposable pipettes (Sigma, CAT: CLS7078B25-400EA)
- Vessels, MARSXpress, 75 mL (CEM Corporation, USA)
- Vessel rack, MARSXpress 40 place (CEM Corporation, USA)
- Standard flour (lab product)
- ddH₂O
- Metal spoon

The equipment for the ICP experiment is listed below.

- Bottle-top dispenser, Varispenser (Eppendorf, Germany)
- Balance, CPA2245 (Sartorius, Germany)
- Etuve, UN450 (Mettler, Germany)
- ICP-OES spectrometer, 5110 (Agilent Technologies, USA)
- Autosampler, SPS4 (Agilent Technologies, USA)
- Microwave, MARS 6 (One Touch Technology, UAE)
- Fume hood (Wesem ann, #DG03)

3.1.5. Real-Time Quantitative Polymerase Chain Reaction (RT-qPCR) Setup

Real-time qPCR was conducted with the following steps; RNA isolation, DNase I treatment, cDNA synthesis, and RT-qPCR. The material list for this experiment is provided below.

- Mature *A. thaliana* plants
- Plant Total RNA Kit (ECOTECH, CAT: E2096)
- TRIzol Reagent (Ambion, REF: 14380401)
- 2-propanol (BioFroxx, #1496LT2P5)
- Diethyl Pyrocarbonate (DEPC) (Merck, #D5758-5ML)
- Chloroform (Merck, #1.02445.2500)
- Ethanol, absolute (Merck, #1.00986.2500)
- DNase I Treatment pack (NucleoGene, #NGE024)
- 5X cDNA Synthesis Kit (NucleoGene, #NGMM020)
- SensiFAST™ SYBR® No-ROX Kit (Bioline, CAT: BIO-98020)
- Agarose, powder (Biomax Prona, CAT: HS-8000)

- Liquid nitrogen (Linde, Turkiye)
- UltraPure™ DNase/RNase-Free Distilled Water (Invitrogen, CAT: 10977035)
- LightCycler® 480 Multiwell Plate 96, white (Roche, CAT: 04729692001)
- LightCycler® 480 sealing foil (Roche, CAT: 04729757001)
- 0.2 mL PCR tubes (CAPP, #5100201C)
- 10 µL non-filter tips (CAPP, #5130010C)
- 200 µL non-filter tips (CAPP, #4130075C)
- 1000 µL non-filter tips (CAPP, #4130135C)
- Mortar and pestle, porcelain (ISOLAB, #038.08.100)
- 0.5X TBE Buffer
- Ice
- Aluminum foil

Following is the equipment list for the RT-qPCR experiment.

- 10 µL, 100 µL, 1000 µL single channel micropipettes (Thermo Fisher Scientific, #4700860N)
- Gel Electrophoresis System, Advance (Mupid-One, Japan)
- Gel Doc EZ Imager (Bio-Rad, USA)
- NanoDrop 2000C Spectrophotometer (Thermo Fisher Scientific, USA)
- Mastercycler gradient (Eppendorf, Germany)
- ThermoStat Plus (Eppendorf, Germany)
- Ultracentrifuge, 5418 R (Eppendorf, Germany)
- Ultracentrifuge, Allegra X-I5R (Beckmann Culture, USA)
- LightCycler® 480 II (Roche, Sweden)
- -20°C deep freezer (Arçelik, Turkiye)
- -86°C ultra-low temperature freezer, Forma 890000 (Thermo Fisher Scientific, USA)

The tools for analyzing the results are listed below.

- GraphPad Prism 10.2.3 (Dotmatics, UK)
- Microsoft Excel software

3.2. METHODOLOGY

In this study; plant growth, CRISPR/Cas9 system design, flower dipping transformation, elemental analysis, real-time quantitative PCR, producing an enzymatic assay, and thermogravimetric analysis methods were conducted respectively. The specified procedures are explained below.

3.2.1. Plant Growth and Phenotyping

In this study, various genotypes of *A. thaliana* seeds were utilized to explore the variations caused by polymorphisms among them. This section involves germination, cultivation, phenotyping, and harvesting.

3.2.1.1. Germination of *A. thaliana* Seeds

Due to the small size of *A. thaliana* seeds, they were sown directly in 1% water agar including micropropagation agar to facilitate the planting of seedlings. The seeds on the agar were stratified for 48 hours, then, they were placed into the growth chamber for 72 hours to induce germination. Seeds that did not germinate were treated with 1% water agar containing 10 mM $\text{Ca}(\text{NO}_3)_2$. These seeds were vernalized and acclimated in the same way as previously described.

3.2.1.2. Cultivation of *A. thaliana* Seedlings

After germination, the seedlings were planted on rockwool cubes placed in 70-well plastic cube trays or plastic pots including soil using forceps. For floral dipping transformation (FDT), nutrient-enriched soil was used. However, the experimental setups for nutrient deficiency involved using a hydroponic system with rockwool. The hydroponic solution was prepared based on the study by Hoagland and Arnon (1938). Details of Hoagland's solutions for various deficiency conditions can be found in Tables 3.1 and 3.2. For *A. thaliana* plant, 0.5X strength of the solution was used.

Table 3.1. Stock solutions for macronutrients.

<i>Chemicals</i>	<i>Stock Concentration (M)</i>	<i>Element of Interest</i>	<i>Final Concentration (mM)</i>
<i>NH₄NO₃</i>	0.50	N	2.0
<i>Ca(NO₃)₂·4H₂O</i>	1.00	Ca/N	2.0
<i>KH₂PO₄</i>	0.25	P/K	1.0
<i>MgSO₄·7H₂O</i>	1.00	Mg/S	0.5
<i>KCl</i>	0.25	K	2.0
<i>CaCl₂</i>	0.20	Ca/Cl	2.0
<i>H₃PO₄</i>	0.25	P	1.0

Table 3.2. Stock solutions for 1000X micronutrient stock.

<i>Chemicals</i>	<i>Stock Concentration (mM)</i>	<i>Element of Interest</i>	<i>Final Concentration (μM)</i>
<i>KCl</i>	1	<i>Cl</i>	1
<i>H₃BO₃</i>	25	<i>B</i>	25
<i>MnSO₄·4H₂O</i>	2	<i>Mn</i>	2
<i>ZnSO₄·7H₂O</i>	2	<i>Zn</i>	2
<i>CuSO₄·5H₂O</i>	0,1	<i>Cu</i>	0,1
<i>(NH₄)₆Mo₇O₂₄·4H₂O</i>	0,1	<i>Mo</i>	0,1
<i>Fe-EDTA*</i>	20	<i>Fe</i>	20

*Fe-EDTA stock was prepared and added separately.

Using stock solutions, nutrient contents were adjusted based on the desired deficiency conditions outlined in Table 3.3. and 3.4. The solutions were initially prepared as stocks and then diluted with dH₂O to obtain 50% Hoagland's solution. After adjusting the nutrient concentration, the pH of the solutions was set to 5.5 using 2 M HCl, 10 M NaOH, and a Hanna pH Meter.

Table 3.3. The required volumes (mL) of stocks needed for 1 L of Hoagland's solutions.

	<i>Stock Conc.</i>	<i>0.5X Hoagland</i>	<i>1.6 mM N</i>	<i>2 mM K</i>	<i>200 μM K</i>	<i>25 μM K</i>	<i>1 μM K</i>
<i>NH₄NO₃</i>	0.50 M	4.00	0	8.00	8.00	8.00	8.00
<i>Ca(NO₃)₂·4H₂O</i>	1.00 M	2.00	0.80	0	0	0	0
<i>KH₂PO₄</i>	0.25 M	4.00	4.00	4.00	0.80	0.10	0
<i>MgSO₄·7H₂O</i>	1.00 M	0.50	0.50	0.50	0.50	0.50	0.50
<i>KCl</i>	0.25 M	8.00	8.00	4.00	0	0	0

<i>Microelements</i>	1000X	1.00	1.00	1.00	1.00	1.00	1.00
<i>Fe-EDTA</i>	20 mM	1.00	1.00	1.00	1.00	1.00	1.00
<i>CaCl₂</i>	0.20 M	8.75	8.75	11.25	13.75	13.75	13.75
<i>H₃PO₄</i>	0.25 M	0	0	0	3.20	3.90	4.00

Table 3.4. The required concentrations (mM) of elements needed for 1 L of Hoagland's solutions

	<i>0.5X Hoagland</i>	<i>1.6 mM N</i>	<i>2 mM K</i>	<i>200 μM K</i>	<i>25 μM K</i>	<i>1 μM K</i>
<i>N</i>	8.00	0.50	8.00	8.00	8.00	8.00
<i>P</i>	1.00	1.00	1.00	1.00	1.00	1.00
<i>K</i>	3.00	3.00	2.00	0.20	0.025	0.001
<i>Ca</i>	3.75	2.0	2.25	2.75	2.75	2.75
<i>Mg</i>	0.60	0.60	0.60	0.60	0.60	0.60
<i>S</i>	0.50	0.50	0.50	0.50	0.50	0.50
<i>Cl</i>	5.50	5.50	5.50	5.50	5.50	5.50

After Hoagland's solutions were prepared, rockwool cubes were soaked with the solutions and placed in 70-well plastic cube trays. Then, the trays are located on plastic trays and grounded in the growth chamber. 300 grams of soil was filled up into plastic pots for FDT experiments. Both media are placed on a plastic tray and settled in a growth chamber. The conditions of the growth chamber are given in Table 3.5. In the sequel, plants were irrigated 3 times a week and left to grow for 4 or 5 weeks.

Table 3.5. Growth chamber settings.

Relative humidity (%RH)	Temperature (°C) day/night	Pressure (hPa)	Photoperiod (h) day/night	Light Intensity (μm/m ² s)
70	23/20	100120	12/12	150

3.2.1.3. Phenotyping of the Plants

After the plants had grown for 4 and 5 weeks, Observations of the phenotypes, including physiological changes such as flowering time, chlorosis, necrosis, accumulation of anthocyanin, and biomass, were recorded to identify differences between conditions or genotypes. The scoring system used to classify the phenotypic changes is given in Figure 3.1. Additionally, rosette size and stem length were measured using a ruler.

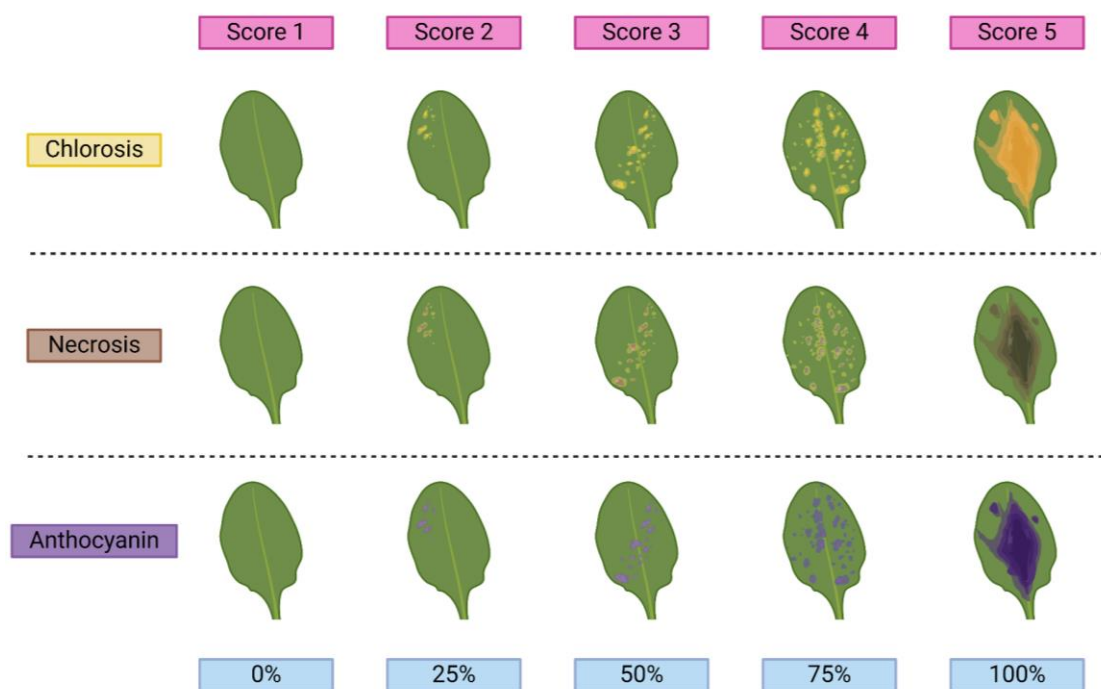


Figure 3.1. The scoring system used to classify seen chlorosis, necrosis, and anthocyanin accumulation in *A. thaliana* leaves (created with BioRender.com).

3.2.2. CRISPR/Cas9 System Design

The CRISPR/Cas9 system was operated by designing gRNAs for the *CESA4* gene, constructing plasmids, transforming the plasmids, and conducting a plasmid confirmation assay.

3.2.2.1. gRNA Design for *CESA4* Gene

Computational design of guide RNA sequences embarked upon using a valuable online tool called CHOPCHOP. “AT5G44030” which is the locus code of the *CESA4* gene was entered as the target for non-synonymous knock-out in this particular gene. The organism was selected as “*A. thaliana* (Araport11)”, and the system was selected as “CRISPR/Cas9” to find target sites. Subsequently, genomic location, GC content (%), risk of self-complementary and mismatch (MM), and efficiency (%) were analyzed using CHOPCHOP tool. The high-impact gRNA candidates were checked in the Protein Data Base (PDB) to comprehend if the knock-out would corrupt the function of the CESA protein (Figure 4.6). Afterwards, four candidates were chosen to knock out the *CESA4* gene by CRISPR/Cas9 and their forward/reverse primers were designed accordingly (Tables 4.3 and 4.4). External primer sequences are included EcoRI and

SacI sticky-end for overhangs, however, internal primers have the gRNA sequence for overlapping.

3.2.2.2. Overlapping PCR

Overlapping PCR was conducted with three steps following the procedure of the study by Hilgarth and Lanigan (2019). In the first step, using Puc119-gRNA plasmid as template DNA, and primers of gRNAs, eight coding sequences (CDS) were amplified (Figure 3.2). External primers including restriction sites and internal primers including gRNA sequences that would be overlapped were combined. After this step, 1% agarose gel was prepared with 0.5X TBE buffer to control CDSs, and PCR products were visualized on the gel after electrophoresis for 30 min at 100 V. In the second step, the same gRNA sequences in the internal primers were nested by amplification without primers. In the last step, the cassette containing the target gRNA sequence was amplified with external primers.

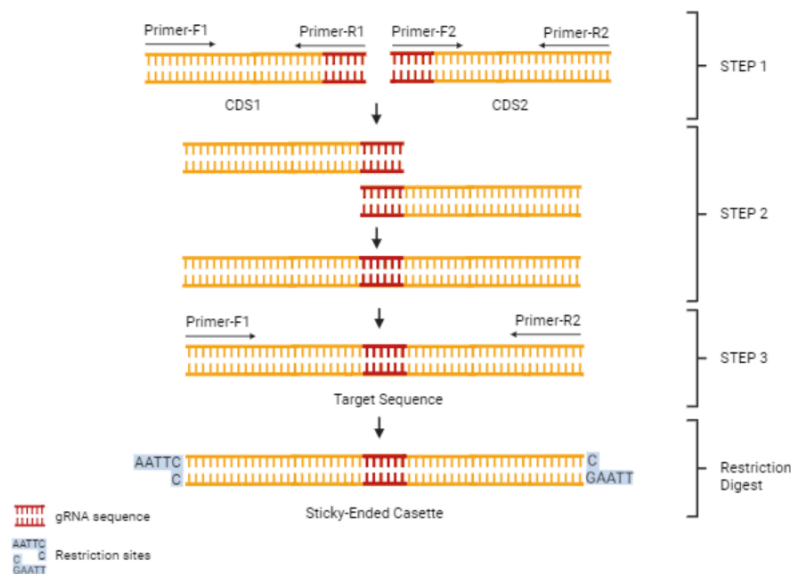


Figure 3.2. Schematic representation of overlapping PCR reactions (created with BioRender.com).

PCR programs and contents are listed in Tables 3.6 and 3.7. Template DNA was input 100 pg for CDS1-to-6, 1 ng for CDS7 and 8.

Table 3.6. Components of overlapping PCR steps.

Step 1		Step 2		Step 3	
Component	Needed Volume (μL)	Component	Needed Volume (μL)	Component	Needed Volume (μL)
5X phusion HF buffer	10	5X phusion HF buffer	10	5X phusion GC enhancer buffer	10
10 mM dNTP mix	1	10 mM dNTP mix	2	10 mM dNTP mix	2
10 μM F-primer	2.5	CDSX*	1	10 μM F-primer	0.2
10 μM R-primer	2.5	CDSY*	1	10 μM R-primer	0.2
Template DNA (pUC119-gRNA)	100 pg-1 ng*	DNA phusion polymerase	0.5	The PCR product from Step 2	4
DNA phusion polymerase	0.5	NFW	35.5	DNA phusion polymerase	0.5
NFW	27			NFW	33.1

*Depends on the template requirements. X and Y represent any CDS couples. NFW: nuclease-free water.

To determine the optimum annealing temperature in step 1 of overlapping PCR, gradient PCR was performed at 62°C, 66.4°C, and 69.4°C.

Table 3.7. PCR program of overlapping PCR.

Step 1	Temperature ($^{\circ}\text{C}$)	Time	Number of Cycles
Initial denaturation	98	30 sec	1
Denaturation	98	15 sec	17
Annealing	66.4*	15 sec	
Extension	72	10 sec	
Denaturation	98	15 sec	23
Annealing	59	15 sec	
Extension	72	10 sec	
Final extension	72	1 min	1
Hold	10		

Step 2	Temperature (°C)	Time	Number of Cycles
Initial denaturation	98	30 sec	1
Denaturation	98	15 sec	9
Extension	72	10 sec	
Denaturation	98	15 sec	5
Annealing	67.5	15 sec	
Extension	72	10 sec	
Final extension	72	1 min	1
Hold	10		
Step 3	Temperature (°C)	Time	Number of Cycles
Initial denaturation	98	30 sec	1
Denaturation	98	15 sec	17
Annealing	64	15 sec	
Extension	72	10 sec	
Denaturation	98	15 sec	23
Annealing	59	15 sec	
Extension	72	10 sec	
Final extension	72	1 min	1
Hold	10		

**Determined with gradient PCR.*

PCR mixes were prepared for each gRNA primer according to Table 3.6 and programs provided in Table 3.7 were carried out with a Mastercycler gradient device. The results were visualized on a 1% agarose gel after electrophoresis for 30 min at 100 V. The developed target sequences were ready to be inserted into the pUC119-gRNA plasmid.

3.2.2.3. Restriction Digest

The gRNA region in the pUC119-gRNA plasmid was excised from the restriction sites located at the 5' ends of Primer-F1 and Primer-R2 sequences. Reaction conditions of restriction digest of pUC119-gRNA are given in Table 3.8.

Table 3.8. Reaction mixture of restriction digest protocol.

<i>Components</i>	<i>Needed Amount per Reaction</i>
<i>10X rCutSmart™ buffer</i>	5 µL

<i>EcoRI-HF (20U/μL)</i>	1 μL
<i>SacI-HF (20U/μL)</i>	1 μL
<i>pDNA</i>	1-5 μg
<i>NFW</i>	Up to 50 μL

The prepared reaction mixture in a 100 μL centrifuge tube was incubated at 37°C for 15 minutes. After digestion, the reaction was heat-inactivated at 65°C for 20 minutes. The same protocol was applied to them to create sticky ends at the ends of the target sequences.

3.2.2.4. Gel Purification

The restricted plasmid (vector) and target (insert) samples were loaded onto 1% agarose gel at max volume (approximately 20 μL) to fit in the wells and electrophoresis for 30 min at 100 V. After gel running was completed, the DNA regions in the gel visualized on a UV light device were separated from the rest of the gel using a sterile blade and weighed. Vector DNA is expected at 3282 bp, and insert DNA is expected at 489 bp. NucleoSpin Gel and PCR Clean-up Kit were used to purify the nucleic acids. For every 100 mg < 2% agarose gel, 200 μL of Buffer NTI was added. The sample was incubated at 50 °C for 5-10 min. The sample was briefly vortexed every 2-3 min until the gel slice was completely dissolved. A NucleoSpin® Gel and PCR Clean-up Column were placed in a Collection Tube (2 mL) and loaded with up to 700 μL of the sample. It was centrifuged at 11,000 x g for 30 seconds. The flow-through was discarded and the column was placed back into the collection tube. 700 μL of Buffer NT3 was added to the NucleoSpin® Gel and PCR Clean-up Column and centrifuged at 11,000 x g for 30 seconds. The flow-through was discarded and the column was placed back into the collection tube and centrifuged at 11,000 x g for 1 min to complete removal of buffer NT3. When removing the spin column from the centrifuge and collection tube, ensure that it did not come into contact with the fluid. The NucleoSpin® Gel and PCR Clean-up Column were placed in a new 1.5 mL microcentrifuge tube and it was labeled in detail. To increase recovery, elution buffer was not added directly. 20 μL of Buffer NE heated at 70°C was added into the column membrane and it was incubated for 5 min at 70°C. The column was centrifuged at 50 x g for 1 min and 11,000 x g for 1 min. This step was repeated once. The purity and concentration values of nucleic acids were then checked using a Nanodrop spectrophotometer.

3.2.2.5. Plasmid Ligation

T4 DNA ligase pack was used for purified insert and vector ligation. Reaction time was tried between 10 min and 2 h to get higher efficiency in ligation. Vector: insert ratio was tried as 3:1 and 1:1. NEBcalculator.com tool was used for necessary mass calculations. Before preparing the reaction mixture provided in Table 3.9, the buffer should be thawed at room temperature and then placed on ice, otherwise precipitation will occur in the buffer. Since the reaction is at room temperature, the enzyme was added last.

Table 3.9. Reaction mixture of plasmid ligation protocol.

<i>Components</i>	<i>Needed Amount per Reaction</i>
<i>10X T4 DNA ligase buffer</i>	2 μ L
<i>Vector DNA (3282 bp)</i>	50 μ g
<i>Insert DNA (489 bp)</i>	7.45 μ g
<i>NFW</i>	Up to 19 μ L
<i>T4 DNA ligase</i>	1 μ L

The reaction mixture was kept at room temperature for 10 min to 2 hours. Then, it was heat-inactivated at 65°C for 15 min. The results were visualized on a 1% agarose gel after electrophoresis for 30 min at 100 V. Plasmid construct bands (~3771 bp) were observed on the gel and ready for transformation.

3.2.2.6. Preparation of Competent *E. coli* Cells

E. coli cells were competent to perform the transformation. *E. coli* bacteria at -80°C without plasmid were inoculated into LB-Agar media, placed in an incubator, and kept at 37°C overnight. Single colonies formed on agar plates were inoculated into 5 mL LB broth. They were incubated in a 200 rpm shanking incubator at 37°C until the OD value was around 1.8. 45 ml of LB broth was added to 5 mL of bacteria and subcultured in a 200 rpm shanking incubator at 37°C until the optical density (OD) was 0.4 at 600 nm. The cultures were divided into several 50 mL tubes and placed on ice for 30 min. After incubation, they were centrifuged at 4000 rpm for 10 min at 4°C. The supernatant was discarded and the remaining media was aspirated. All pellets were thawed with 20 mL ice-cold 0.1 M CaCl₂ and placed on ice for 30

min. Resuspensions were centrifuged at 4000 rpm for 10 min at 4°C and supernatants were discarded. Pellets were resuspended in 5 mL of ice-cold 0.1 M CaCl₂ containing 15% glycerol.

3.2.2.7. *E. coli* Transformation

The prepared competent cells were divided into 200 µL aliquots and kept on ice for heat-shock transformation. 1-5 µL (10 pg-100 ng) plasmid construct was added and incubated on ice for 30 min. Subsequently, cells were heat-shocked by 42°C for 30, 45, or 60 sec and placed on ice for 2 min. Results were compared to obtain a higher yield. 1 mL of LB-broth without antibiotics at 37°C was added into the tubes. The tubes were incubated at 37°C and 200 rpm for 1 hour. 200 µL of transformed *E. coli* cells were spread on an LB-agar plate with 100 µg/mL ampicillin. The remaining cells were centrifuged at 4000 rpm for 5 min and the supernatant was discarded. Pellets were suspended with 100 µL of LB broth and spread on another LB-agar plate with 100 µg/mL ampicillin. This step is critical to increase bacteria growing yield. LB-agar plates were located in a shaking incubator at 37°C and 200 rpm for 2 days. Single colonies were taken and cultured in 5 mL of LB broth with 100 µg/mL ampicillin in a shaking incubator at 37°C and 200 rpm for 2 days to get OD absorbance around 1.5.

3.2.2.8. Plasmid Isolation

Plasmid DNAs were isolated using the EcoSpin Plasmid Isolation Kit according to the manufacturer's instructions. The bacterial culture was harvested by centrifugation at 6000 rpm in a tabletop microcentrifuge for 2 min at room temperature. The supernatant was discarded using a micropipette. The bacterial pellet was resuspended in 250 µL EcoSpin Resuspension Buffer by vortexing until no cell clumps remained. To the resuspended mixture, 20 µL EcoSpin RNase A (+4°C) was added. 250 µl EcoSpin Lysis Buffer was added and the tube was inverted 6-7 times and gently mixed. No vortexing was performed in the following steps to prevent the shearing of genomic DNA. The suspension was incubated at room temperature for 3 minutes. and 350 µL EcoSpin Binding Buffer were added. The tube was inverted 6-7 times and mixed thoroughly. The mixture was centrifuged for 5 minutes at maximum speed at room temperature. An EcoSpin Column was placed in a collection tube and the supernatant was transferred to the EcoSpin Columns. The columns were centrifuged at maximum speed in a tabletop microcentrifuge for 30 seconds at room temperature. Discard the flow-through and add 400 µl

EcoSpin Wash Buffer 1 to the EcoSpin Column. The column was centrifuged at maximum speed in a tabletop microcentrifuge for 30 seconds at room temperature. The flow-through was discarded and 500 µl EcoSpin Wash Buffer 2 was added to the EcoSpin Column. It was centrifuged at maximum speed in a tabletop microcentrifuge for 30 seconds at room temperature. The flow-through was discarded and 200 µl EcoSpin Wash Buffer 2 was added to remove the remaining wash buffer completely and the EcoSpin Column was centrifuged at maximum speed for 2 min. The EcoSpin Column was transferred to a clean and labeled 1.5 mL microcentrifuge tube. 50 µL EcoSpin Elution Buffer was added to the center of the EcoSpin Column membrane and the column was incubated for 1 min at room temperature. The column was centrifuged at maximum speed in a tabletop microcentrifuge for 30 seconds at room temperature. The EcoSpin Column was discarded and purified DNA was stored at -20°C.

3.2.2.9. Confirmation of Integration of the Plasmid DNAs (pDNAs)

A PCR setup was planned to check the integrity of the isolated plasmids and whether the sequences of gRNA candidates belonging to the target regions were inserted. In this PCR, external primers of the target sequence were used. PCR components are provided in Table 3.10 and the PCR program is given in Table 3.11.

Table 3.10. Reaction mixture of confirmation PCR.

<i>Components</i>	<i>Needed Amount per Reaction</i>
<i>10X KAPA Taq PCR buffer with MgCl₂ + Dye</i>	2 µL
<i>10 mM KAPA dNTP mix</i>	0.4 µL
<i>10 µM Primer-F1</i>	0.4 µL
<i>10 µM Primer-R2</i>	0.4 µL
<i>KAPA Taq polymerase</i>	0.1 µL
<i>pDNA constructs</i>	20 µg
<i>NFW</i>	Up to 20 µL

(see appendices for primer sequences)

Table 3.11. PCR program used in confirmation PCR.

Stages	Temperature (°C)	Time	Number of Cycles
Initial denaturation	95	2 min	1
Denaturation	95	15 sec	35
Annealing	54	30 sec	

Extension	72	1 min	
Final extension	72	3 min	1
Hold	10		

In addition, two different negative control samples which are restricted and gel-purified pUC119-gRNA plasmid and no-template sample were included in the PCR setup. Positive control was included non-treated pUC119-gRNA plasmid. The results were visualized on a 1% agarose gel after electrophoresis for 30 min at 100 V.

3.2.3. Floral Dipping Transformation (FDT)

Flower dipping transformation (FDT) was chosen as a relatively easy and time-saving method to produce transformants without the need for tissue culture. Since the main target for transformation here was the ovule, cutting open flowers before initiation greatly increased transformation efficiency, as it would prevent self-pollination and the proliferation of untransformed embryos. Care was taken to ensure that the 4-week-old *Arabidopsis thaliana* plants were in the inflorescence phase I. Although the transformation agents carbon nanotube and *A. tumefaciens* functionalized with pDNA as given in sections 3.2.3.1 and 3.2.3.2 were used for pairwise comparison, the FDT application technique was the same. In both methods, Silwet L-77 was added to the infiltration medium to a final concentration of 0.02% (vol/vol) just before starting the flower dip transformation. The flower parts and inflorescence parts of the plants were inverted and immersed in the transformation suspension for 10 sec. This process was repeated 5 times. The representation of floral dipping transformation is provided in Figure 3.3.

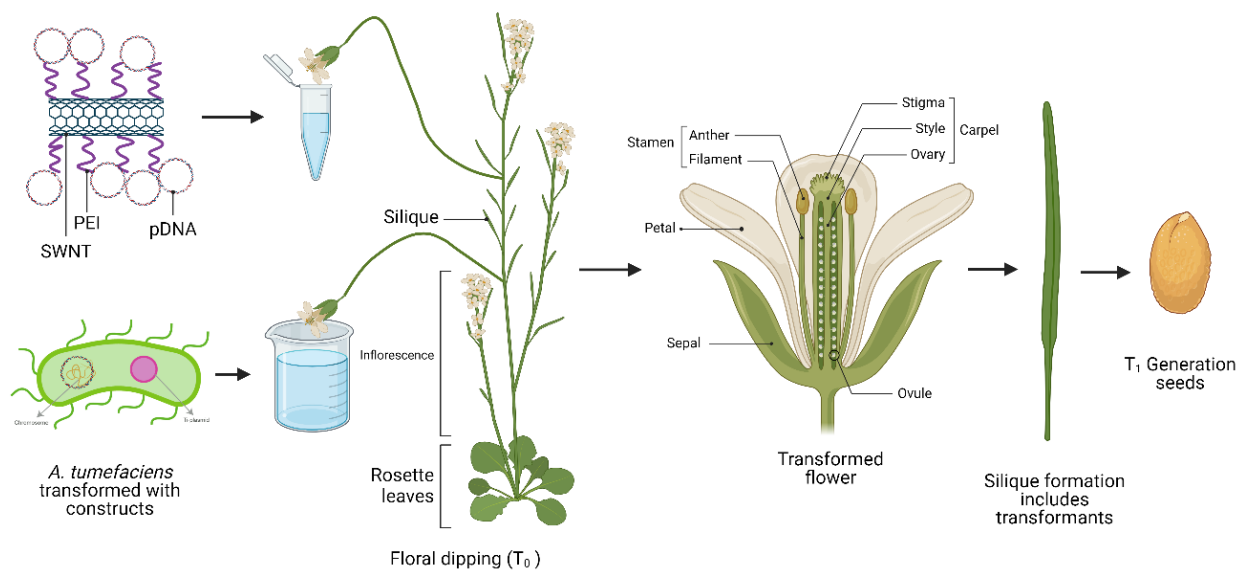


Figure 3.3. Illustration of floral dipping transformation in *A. thaliana* using PEI-SWNT and *A. tumefaciens*. (adapted from Clark, 2001 and Kram et al., 2009 and created with BioRender.com)

After transformation, the plants were transferred to the acclimatization cabinet and were grown in 5 × 5 cm pots filled with soil under 16 h light/8 h dark conditions for 2-3 weeks at 23 °C until seed set. Mature seeds were harvested after 3-4 weeks.

3.2.3.1. Preparation of Polyethyleneimine-Functionalized Single-Walled Carbon Nanotubes (PEI-SWNT)

Carbon nanotube-mediated DNA delivery without transgene integration protocol in intact 4-week-old *Arabidopsis thaliana* plants was adapted from Demirer et al. (2019). In summary, the preparation of the nanotubes was started with the suspension of carboxylated single-walled carbon nanotubes (COOH-SWNT). 30 mg of dry COOH-SWNT was weighed in a chemical fume hood into a 50 mL conical tube and 30 mL of nuclease-free water was added. The mixture was bath-sonicised for 10 min at room temperature. COOH-SWNTs were visibly suspended in water to form a dark black solution. Using an ultrasonic homogenizer, 30-40 W probe tip sonication was performed continuously for 30 min at 10% amplitude (with a 6 mm probe tip) in an ice bath. The tube was removed from the ice bath and allowed to rest at room temperature for 10 min. The suspension was centrifuged at 5000 g for 1 h at room temperature. Then, the supernatant containing individually suspended COOH-SWNTs was collected and COOH-SWNT concentration was determined.

The volume of COOH-SWNT required to react with 2 mg for PEI functionalization was calculated. An appropriate volume of 500 mM MES (pH 4.5-5) buffer solution was added to 2 mg of suspended COOH-SWNT so that the final MES concentration was 100 mM. To 2.5 mL of 100 mM MES solution was added 10 mg EDC and 10 mg NHS. The entire EDC-NHS solution was slowly added dropwise to the COOH-SWNT suspension under stirring. Bath-sonicisation was carried out for 15 min at room temperature. The reaction was allowed to continue for 45 min on an orbital shaker at ~180 rpm at room temperature. Two 100,000-MWCO filters were prewashed once with 15 mL 0.1× PBS to wet the membranes by centrifugation at maximum speed for 2 min at room temperature. To remove free EDC, NHS, and by-products, EDC-NHS-activated COOH-SWNT solution was washed three times with 0.1× PBS (pH 7.4) three times using the washed 100,000-MWCO filters. After each washing step, the activated COOH-SWNT solution was briefly vortexed. After recovery from the filters, the activated COOH-SWNT solutions were combined into a single tube. 0.1× PBS (pH 7.4) was added to 20 mL of activated COOH-SWNT solution before adding MES buffer. Washed and activated COOH-SWNTs were resuspended by bath sonication for 15 min. 40 mg PEI (25,000 MW, branched) was added to 5 mL 0.1× PBS and completely dissolved. The pH of this PEI solution was fixed to 7.4-7.6 with 5 M HCl. Activated COOH-SWNTs were added dropwise to the PEI solution. The reaction was carried out overnight (~16 h) at room temperature on an orbital shaker at ~180 rpm. Two 100,000-MWCO filters were prewashed once with 15 mL nuclease-free water to wet the membranes by centrifugation at maximum speed for 2 min at room temperature. The PEI-SWNT reaction solution was divided in half and half of each solution (prewashed) was transferred to one of the 100,000-MWCO filters. PEI-SWNT solutions were washed six times with nuclease-free water. After the final washing step, two 100,000 MWCO filters (tops only) containing the PEI-SWNT solution were subjected to bath sonication for 1 min while pipetting up and down, and then the collected PEI-SWNTs were combined into a single tube. The washed PEI-SWNTs were resuspended by bath and probe tip sonication. PEI-SWNTs were subjected to bath sonication for 15 min, and then PEI-SWNTs were sonicated at 10% amplitude for 15 min. The supernatant was collected from tubes that were centrifuged at 16,000 g for 1 hour at room temperature. PEI-SWNT concentration was measured via absorbance at 632 nm. The zeta potential and dimensions of positively charged PEI-SWNTs were measured using Zetasizer Pro to evaluate their colloidal stability and verify PEI attachment.

To load PEI-SWNT with plasmid DNA at a PEI-SWNT: DNA mass ratio of 2:1, which was optimal according to ZetaSizer Pro results, PEI-SWNT, which was determined to be non-toxic (section 3.2.3.3), was first diluted in 100 μL of MES dispersion buffer per infiltration. Diluted PEI-SWNTs were added dropwise to the plasmid solution. They were pipetted up and down 10 times to mix. It was incubated at room temperature for 30 minutes to form the DNA-PEI-SWNT complex. After incubation, 0.05% Silwet L-77 was added and FDT was applied as described in section 3.2.3.

3.2.3.2. Toxicity Determination for PEI-SWNT in *A. thaliana* Flowers and Application of CRISPR/Cas9 System for *Phytoene Dehydrogenase 3 (PDS3)* Gene

For the nano-toxicity study of PEI-SWNT, half-weight pUC199-gRNA and pFGC-pcoCas9 plasmids and PEI-SWNT at rates of 2, 5, 10, 20, 40, 80 $\text{ng}/\mu\text{l}$ were applied with floral dipping. The pDNA couples were separately bound on the surface of the PEI-SWNT to ensure equal uptake of them. The NEBcalculator.com online tool was used to ensure that the plasmids were molarly equal. Based on the zeta potential data (see Appendices), the total weight ratio of PEI-SWNT to plasmid should be 2:1. However, since two plasmids are being used, their molar amounts were equalized to ensure precision. Despite this, both plasmids were not bound to PEI-SWNT in the same reaction. Instead, to ensure that both plasmids were carried by carbon nanotubes (CNTs), the following calculations were performed. The total weight of the plasmids was set to be half of the CNT weight, while their molar amounts were kept equal. The required amount of PEI-SWNT (C) was incubated with the plasmids in a total volume of 500 μL MES-delivery buffer for thirty minutes. After incubation, the two pDNA:PEI-SWNT suspensions were combined. Prior to application, 0.02% (vol/vol) Silwet L-77 was added to the tubes.

Molarity of pFGC-proCas9 plasmid: 79.39 $\text{fmol}/\mu\text{l}$, concentration: 325.9 $\text{ng}/\mu\text{l}$ = A

Molarity of pUC119-gRNA plasmid: 271.2 $\text{fmol}/\mu\text{l}$, concentration: 314.9 $\text{ng}/\mu\text{l}$ = B

Concentration of PEI-SWNT: 115 $\text{ng}/\mu\text{l}$ = C

Toxicity test for 2 $\text{ng}/\mu\text{l}$ PEI-SWNT:

CNT 1000 ng, pDNA 500 ng:

$$79.39 \times A = 271.2 \times B \rightarrow A = 3.42 \times B \rightarrow A = 3.42x, B = 1x$$

$$\rightarrow A + B = 4.42x = 500 \text{ ng} \rightarrow A = 387 \text{ ng}, B = 113 \text{ ng}$$

$$\text{Needed volume for} \rightarrow A = 1.2 \mu\text{l}, B = 0.4 \mu\text{l}, C = 8.7 \mu\text{l}$$

Toxicity test for 5 ng/μl PEI-SWNT:

CNT 2500 ng, pDNA 1250 ng:

$$79.39 \times A = 271.2 \times B \rightarrow A = 3.42 \times B \rightarrow A = 3.42x, B = 1x$$

$$\rightarrow A + B = 4.42x = 1250 \text{ ng} \rightarrow A = 967.2 \text{ ng}, B = 282.8 \text{ ng}$$

$$\text{Needed volume for} \rightarrow A = 3 \mu\text{l}, B = 0.9 \mu\text{l}, C = 21.7 \mu\text{l}$$

Toxicity test for 10 ng/μl PEI-SWNT:

CNT 5000 ng, pDNA 2500 ng:

$$79.39 \times A = 271.2 \times B \rightarrow A = 3.42 \times B \rightarrow A = 3.42x, B = 1x$$

$$\rightarrow A + B = 4.42x = 2500 \text{ ng} \rightarrow A = 1934.4 \text{ ng}, B = 565.6 \text{ ng}$$

$$\text{Needed volume for} \rightarrow A = 6 \mu\text{l}, B = 1.8 \mu\text{l}, C = 43.5 \mu\text{l}$$

Toxicity test for 20 ng/μl PEI-SWNT:

CNT 10000 ng, pDNA 5000 ng:

$$79.39 \times A = 271.2 \times B \rightarrow A = 3.42 \times B \rightarrow A = 3.42x, B = 1x$$

$$\rightarrow A + B = 4.42x = 5000 \text{ ng} \rightarrow A = 3868.8 \text{ ng}, B = 1131.2 \text{ ng}$$

$$\text{Needed volume for} \rightarrow A = 11.9 \mu\text{l}, B = 3.6 \mu\text{l}, C = 87 \mu\text{l}$$

Toxicity test for 40 ng/μl PEI-SWNT:

CNT 20000 ng, pDNA 10000 ng:

$$79.39 \times A = 271.2 \times B \rightarrow A = 3.42 \times B \rightarrow A = 3.42x, B = 1x$$

$$\rightarrow A + B = 4.42x = 10000 \text{ ng} \rightarrow A = 7737.6 \text{ ng}, B = 2262.4 \text{ ng}$$

$$\text{Needed volume for} \rightarrow A = 23.8 \mu\text{l}, B = 7.2 \mu\text{l}, C = 173.9 \mu\text{l}$$

Toxicity test for 80 ng/μl PEI-SWNT:

CNT 40000 ng, pDNA 20000 ng:

$$79.39 \times A = 271.2 \times B \rightarrow A = 3.42 \times B \rightarrow A = 3.42x, B = 1x$$

$$\rightarrow A + B = 4.42x = 20000 \text{ ng} \rightarrow A = 15475.1 \text{ ng}, B = 4524.9 \text{ ng}$$

$$\text{Needed volume for} \rightarrow A = 47.5 \mu\text{l}, B = 14.4 \mu\text{l}, C = 347.8 \mu\text{l}$$

Prepared transformation suspensions were applied on the flowers of 4-week-old *A. thaliana* with double biological replicates. In this way, the transformation efficiency threshold of nanotubes was also determined by screening albino seedlings after the application.

3.2.3.3. Application of CRISPR/Cas9 System for *Cellulose Synthase A4 (CESA4)* Gene

Plasmid constructs containing four different gRNAs described in section 3.2.2 were molarly equalized (as explained in section 3.2.3.2) with the pFGC-pcoCas9 plasmid and bound to PEI-SWNTs at a ratio of 1:2. The pDNA couples were separately bound on the surface of the PEI-SWNT to ensure equal uptake of them. Prepared transformation suspensions were applied on the flowers of 4-weeks-old *A. thaliana* with triple biological replicates. After transformation, T₀ plants were left in a growth chamber for 3-4 weeks.

3.2.3.4. Selection of Transformants

To screen T₁ seeds, MS vitamin media was prepared using 4.3 g/L of MS vitamin powder and 7.5 g/L of micropropagation agar. Before adding agar, the media were adjusted to pH 5.8 using 2 M HCl, 10 M NaOH, and a pH meter. After that, agar was added and the media were filled up to 1 L with ddH₂O. Then, the media were autoclaved and left to cool at 45-50°C. To provide a selection, MS agar plates were poured with either 100 mg/L or 500 mg/L of Ampicillin to optimize the antibiotic need. T₁ seeds were spread on the plates and vernalized for 2 days. In the sequel, the seeds were placed in a growth chamber for 2 weeks. A hundred seeds were sown from each plant, and the number of phenotypic changes observed was counted and compared to the total to determine transformants.

3.2.4. Analysis of Mineral Content of *A. thaliana* Shoots Grown Under K-Deficiency

Elemental analysis was conducted to ensure the suitability of plant nutrition conditions in *A. thaliana* plants grown under potassium (K) deficiency. This section describes the preparation and ICP-OES analysis of 4-week-old plant samples grown in environments with 1 μM, 25 μM, 200 μM, and 2000 μM (control) potassium concentrations.

3.2.4.1. Preparation of Plant Samples

Potassium-deficient plant samples were harvested at exactly 4 weeks old, including all green tissues except siliques and flowers. During the harvest, the stem (inflorescence) and leaf

(rosette) parts were collected separately. Cauline leaves on the stem were detached and included in the leaf portion (Figure 3.3). The harvested tissues were first washed with dH₂O, then twice with ddH₂O, and placed into paper bags for 24 hours to dry completely.

3.2.4.2. Operation Procedure of Inductively Coupled Plasma-Optical Emission Spectrometry (ICP-OES)

The dried plant tissues were ground into a fine powder using a grinder. The tissues were placed into labeled plastic bags. Approximately 0.3 grams of the powdered tissues were measured and loaded into MARSXpress vessels. Then, 5 mL of 65% nitric acid and 2 mL of 35% hydrogen peroxide were added, and the samples were digested in a MARS 6 microwave at 200°C for 20 minutes. After cooling, 13 mL of ddH₂O was added to the digested samples, which were then filtered into containers using filter paper. The filtrates were analyzed using an Agilent 5110 ICP-OES device. The raw data were processed and analyzed to calculate concentration and content of mineral elements using Microsoft Excel. Statistical data analysis was performed by a student's t-test using GraphPad Prism 10.2.3.

3.2.5. Real-Time Quantitative Polymerase Chain Reaction (RT-qPCR) Setup

The following sections explain the steps required for a real-time quantitative PCR (RT-qPCR) with plant tissue.

3.2.5.1. RNA Isolation and DNase I Treatment

For RNA isolation, various tissues of the plant were used. During the harvest of *A. thaliana*, inflorescence parts, regardless of being primary or secondary, were separated from siliques, flowers, and cauline leaves before being harvested. For leaf harvests, young and old leaves were harvested separately for some experiments. For total harvests, flower buds (if present) were discarded, and the entire rosette was harvested. Cauline leaves were included in the young leaf portion during the young leaf harvest (if harvested separately), but they were not included in the entire rosette harvest. In the case of *T. aestivum* (common wheat), the flag leaf and the second leaf were harvested separately, excluding the collar parts of the leaves. For stem harvest,

the flag leaf layer and leaf 2 layer were harvested separately after the sheath removal. The regions pointed to harvested regions used to isolate nucleic acid are shown in Figure 3.4.

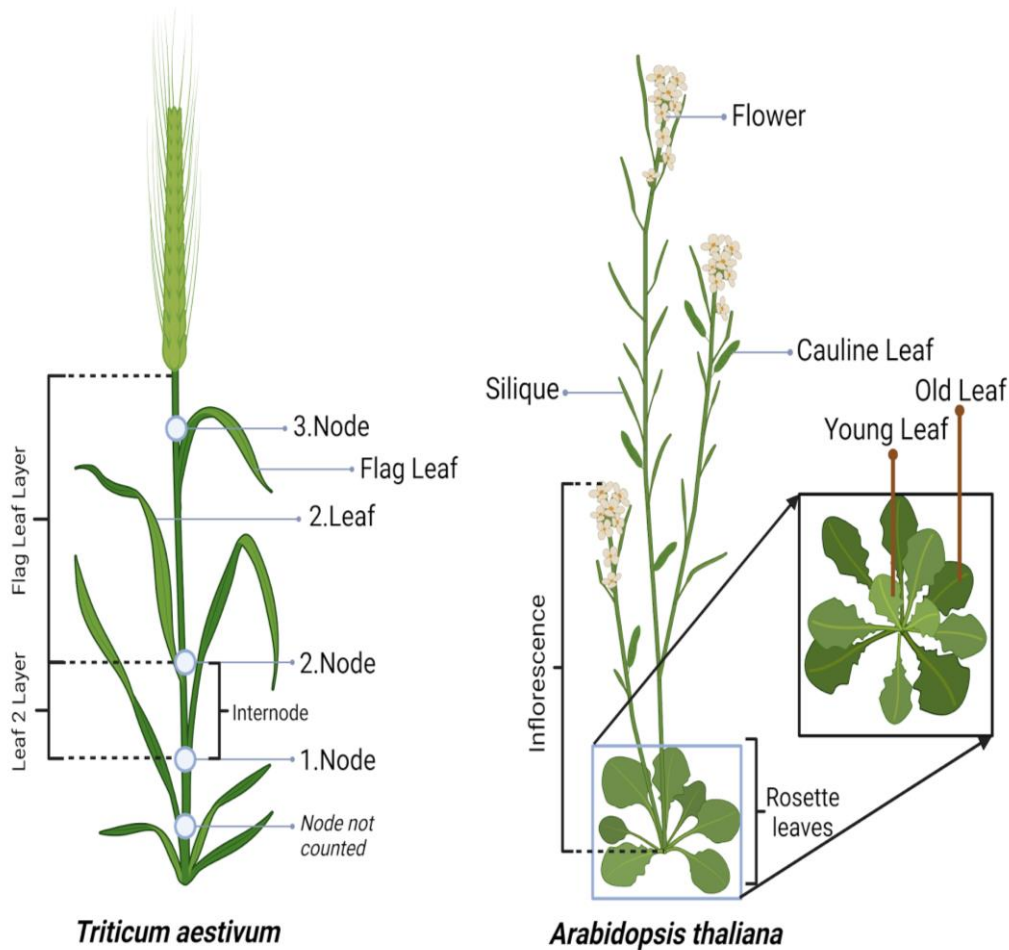


Figure 3.4. Identification of the parts of the plant species for harvesting. *Flag leaf (FL)*, *2.Leaf: Second leaf (SL)*, *Flag leaf layer: Flag stem (FS)*, *Leaf 2 layer: Second stem (SS)* were used for isolation of *T. aestivum*. (created with BioRender.com).

To determine if there were differences in extraction yield from these tissues, a TRIzol-based extraction method and the EcoSpin Plant Total RNA kit were used. For *A. thaliana* ecotypes, the kit method followed the provider's instructions. In the kit isolations, after adding wash buffer I, 2.5 μ L NucleoGene DNase I buffer, and 1 μ L NucleoGene DNase I were added and incubated for half an hour at 37°C for DNase I treatment. The isolation then continued with wash buffer 2.

TRIzol extraction was used for comparative applications of *A. thaliana* and for *Triticum aestivum* plants. In this method, 100 mg of plant tissue was weighed and ground with liquid nitrogen. The tissue was transferred to a 2 mL centrifuge tube, 1 mL TRIzol was added, and

the mixture was pipetted and mixed. The mixture was left at room temperature for 5 minutes. Then, 200 μ L chloroform was added to a fume hood and vigorously mixed. After leaving the mixture on the bench for 2-3 minutes, it was centrifuged at maximum speed for 10 minutes at +4°C. The upper phase was transferred to a new 1.5 mL centrifuge tube. 0.5 mL isopropanol was added to this phase, and after standing at room temperature for 10 minutes, it was centrifuged at 4°C for 10 minutes. The supernatant was carefully discarded. The pellet was washed once with 1 mL ice-cold 75% ethanol. At this stage, the pellet was gently dislodged to ensure the ethanol reached all areas but was not dissolved in ethanol. Then, it was centrifuged at maximum speed for 5 minutes. The ethanol was carefully discarded, and the remaining ethanol was removed using a fine-tipped pipette, followed by air drying for 5-10 minutes. Finally, the pellet was dissolved in 50 μ L NFW. For DNase I treatment of TRIzol isolates, Ambion DNase I and Ambion 10X DNase I buffer were used. The mixture was prepared as shown in Table 3.12 and incubated at 37°C for 20 minutes. It was then heat-inactivated at 75°C for 10 minutes. All products were run on a 2% agarose gel using 0.5X DEPC-treated TBE buffer and visualized by a gel imager.

Table 3.12. Reaction mixture of DNase I treatment.

<i>Components</i>	<i>Needed Amount per Reaction</i>
<i>Thermo Ambion 10X DNase I buffer</i>	5 μ L
<i>Ambion 10X DNase I (2U/μL)</i>	2.5 μ L
<i>RNase Inhibitor (20U/μL)</i>	2 μ L
<i>RNA isolate</i>	10 ug<
<i>NFW</i>	Up to 50 μ L

3.2.5.2. Complementary DNA (cDNA) Synthesis

Synthesis of complementary DNA (cDNA) was performed by using NucleoGene 5X RNA to cDNA mix and instructions of the manufacturer. Reaction components and conditions of cDNA conversion are provided in Table 3.13.

Table 3.13. Reaction components and conditions of cDNA synthesis.

<i>Components</i>	<i>Needed Amount per Reaction</i>	<i>Reaction Temperature (°C)</i>	<i>Time (min)</i>
<i>5X RNA to cDNA mix</i>	4 μ L	25	5
<i>Template RNA</i>	100 ng	50	30
<i>NFW</i>	Up to 20 μ L	85	5

3.2.5.3. Real-Time qPCR

To screen the expression level of *cellulose synthase A catalytic subunit 4 (CESA4)* or other genes of interest in different tissues, the real-time quantitative PCR (RT-qPCR) technique was used. For the experimental setup, SensiFAST™ SYBR® No-ROX Kit was used as shown in Table 3.14, and qPCR conditions are provided in Table 3.15. Housekeeping genes *EF1ALPHA* (AT5G60390) and *alpha-tubulin (TUB, U76558)* were used for *A. thaliana* and *T. aestivum* samples (see appendices for primer sequences).

Table 3.14. Reaction mixture of DNase I treatment.

<i>Components</i>	<i>Needed Amount per Reaction</i>
2X SensiFAST™ SYBR® No-ROX mix	10 µL
10 µM F-primer	0.8 µL
10 µM R-primer	0.8 µL
cDNA template (5ng/µL)	3 µL
NFW	5.4 µL

Table 3.15. qPCR conditions for SYBR mix.

Step 1	Temperature (°C)	Time	Number of Cycles
Initial denaturation	95	5	1
Denaturation	95	10	45
Annealing	60	10	
Extension	72	10	
Final extension	72	2	1
Hold	4		

3.2.5.4. Statistical Analysis

Processing the data from RT-qPCR is performed by Microsoft Excel software. First, fold change values were calculated using the $2^{\Delta\Delta Ct}$ formula. Then, a student t-test ($P < 0.05$, 95% confidence interval) was performed to determine if there was a significant difference between the means of treatment and control groups using Graph Prism 10.2.3.

4. RESULTS

Results of the phenotyping, CRISPR/Cas9 system design, flower dipping transformation, elemental analysis, real-time quantitative PCR, enzymatic assay, and thermogravimetric analysis experiments were provided respectively.

4.1. Plant Growth and Phenotyping

Phenotyping results belonging to different ecotypes and mutants of *A. thaliana* grown under nutrient deficiency conditions are given in Table 4.1. 3 mM K, 2 mM K, and 8 mM N were considered as control groups (Hoagland and Arnon, 1950). Based on the phenotyping results in Table 4.1, non-flowering and flowering ecotypes exhibited a gradient of decreased biomass in response to reduced nutrition. The plants showed increased chlorosis, necrosis, and anthocyanin accumulation as the deficiency worsened. It can be stated that the general symptoms observed in plants under nutrient deficiency conditions include a decrease in biomass and an increase in fresh weight as the plant ages and grows. However, early flowering plants, particularly CS76199 and CS28833, displayed increased biomass despite reduced nutrition at 5 weeks old. Furthermore, their physiological responses closely resembled those of the control groups. Additionally, in CS76199 and CS28833 ecotypes, flowering exhibited an increase as their potassium nutrition decreased, with the fastest flowering observed under the most deficient conditions. In the Col-0 (CS76113) ecotype, despite no physiological change under normal conditions, necrosis and anthocyanin accumulation were observed under moderate or marginal conditions with decreased high nutrient supply. In the CS28729 plant, flowering was observed under all conditions, with an increase in flowering correlating with increased nitrogen deficiency. This plant exhibited the highest anthocyanin accumulation compared to other conditions. The CS76265 ecotype did not flower under any conditions within 4 weeks. Symptoms included intense anthocyanin accumulation and some chlorosis and necrosis. In the CS76111 ecotype, no flowering was observed under any conditions for 5 weeks. However, the plant exhibited intense symptoms outside of normal conditions. Similarly, no flowering was observed in the CS76208 ecotype under any conditions, and the plant generally tended to accumulate anthocyanin. In the CS28812 ecotype, no flowering was observed for 5 weeks, and the symptoms shown by the plant were consistent with the level of nutrient deficiency. The CS76199 plant exhibited flowering in almost all conditions and

harvests, with an increase in flowering correlating with increased nutrient deficiency. Physiological responses to deficiencies intensified as the deficiency increased. The CS28833 ecotype flowered under all conditions, showing increased flowering and physiological deficiency symptoms as nutrient deficiency intensified. The CS28140 ecotype did not flower under any conditions and exhibited symptoms only under very low deficiency conditions. The CS28787 ecotype showed anthocyanin or necrosis even under control conditions and flowered under some low nutrient conditions. Regarding the SALK mutants, they are known as T-DNA insertion mutants of the *CESA4* gene (*SIGNAL*: *Salk Institute Genomic Analysis Laboratory Home Page*, n.d.). Both exhibited high flowering rates under all conditions and increased physiological symptoms as the deficiency intensified.

Table 4.1. Physiological responses of *A. thaliana* ecotypes and mutants grown with hydroponics and under nutrient deficiency. The system of the 1-to-5 scale is given in Figure 3.1. Each experiment was conducted with at least five biological replicates. Flowering (%) was calculated by number of flowering plants/total number of plants.

<i>Ecotype</i>	<i>Nutrition</i>	<i>Age</i>	<i>Average of Fresh Weight (g)</i>	<i>Flowering (%of plant individual)</i>	<i>Chlorosis (1-5)</i>	<i>Necrosis (1-5)</i>	<i>Anthocyanin Accumulation (1-5)</i>
CS76113	3 mM K	4 weeks	0.54	75	-	-	-
	750 μ M K	4 weeks	0.61	25	1	2	-
	187.5 μ M K	4 weeks	0.55	-	1	2	2
	8 mM N	4 weeks	0.18	50	-	-	-
	2 mM N	4 weeks	0.10	25	-	-	1
	0.5 mM N	4 weeks	0.03	-	-	2	2
CS28729	3 mM K	4 weeks	0.97	50	-	-	1
	750 μ M K	4 weeks	0.85	100	-	-	2
	187.5 μ M K	4 weeks	0.89	75	2	-	3
	8 mM N	4 weeks	0.24	25	-	-	-
	2 mM N	4 weeks	0.13	75	-	-	1
	0.5 mM N	4 weeks	0.03	50	-	2	2
CS76265	3 mM K	4 weeks	0.89	-	-	1	1
	750 μ M K	4 weeks	0.78	-	1	-	-
	187.5 μ M K	4 weeks	0.75	-	2	1	3
	8 mM N	4 weeks	0.36	-	-	-	-
	2 mM N	4 weeks	0.21	-	-	-	1
	0.5 mM N	4 weeks	0.05	-	1	1	2
CS76111	3 mM K	4 weeks	1.14	-	-	-	-

<i>Ecotype</i>	<i>Nutrition</i>	<i>Age</i>	<i>Average of Fresh Weight (g)</i>	<i>Flowering (%of plant individual)</i>	<i>Chlorosis (1-5)</i>	<i>Necrosis (1-5)</i>	<i>Anthocyanin Accumulation (1-5)</i>
	750 μ M K	4 weeks	0.82	-	1	-	-
	187.5 μ M K	4 weeks	1.17	-	2	-	3
	8 mM N	4 weeks	0.42	-	-	-	-
	2 mM N	4 weeks	0.20	-	-	-	1
	0.5 mM N	4 weeks	0.05	-	-	1	2
	2 mM K	5 weeks	1.02	-	-	-	-
	200 μ M K	5 weeks	0.87	-	1	1	-
	25 μ M K	5 weeks	0.56	-	3	3	1
	1 μ M K	5 weeks	0.34	-	4	3	1
<i>CS76208</i>	3 mM K	4 weeks	0.93	-	1	-	1
	750 μ M K	4 weeks	0.86	-	-	-	3
	187.5 μ M K	4 weeks	0.67	-	3	-	3
	8 mM N	4 weeks	0.41	-	-	-	1
	2 mM N	4 weeks	0.24	-	-	1	2
	0.5 mM N	4 weeks	0.07	-	1	2	2
<i>CS28812</i>	3 mM K	4 weeks	0.82	-	-	-	-
	750 μ M K	4 weeks	0.75	-	-	-	-
	187.5 μ M K	4 weeks	0.73	-	1	1	3
	8 mM N	4 weeks	0.27	-	1	1	1
	2 mM N	4 weeks	0.18	-	-	-	1
	0.5 mM N	4 weeks	0.06	-	-	1	3
	2 mM K	5 weeks	0.78	-	-	-	-
	200 μ M K	5 weeks	0.57	-	1	1	1
	25 μ M K	5 weeks	0.35	-	3	1	1
1 μ M K	5 weeks	0.26	-	4	2	3	
<i>CS76199</i>	3 mM K	4 weeks	1.04	67	1	-	1
	750 μ M K	4 weeks	0.93	-	1	1	1
	187.5 μ M K	4 weeks	0.62	100	3	1	4
	8 mM N	4 weeks	0.28	50	-	-	-
	2 mM N	4 weeks	0.24	50	-	-	1
	0.5 mM N	4 weeks	0.09	67	-	1	2
	2 mM K	5 weeks	2.76	50	-	-	-
	200 μ M K	5 weeks	1.79	75	-	-	-
	25 μ M K	5 weeks	0.93	75	1	-	1
1 μ M K	5 weeks	0.87	100	2	-	1	
<i>CS28833</i>	3 mM K	4 weeks	0.81	80	1	-	1

<i>Ecotype</i>	<i>Nutrition</i>	<i>Age</i>	<i>Average of Fresh Weight (g)</i>	<i>Flowering (%of plant individual)</i>	<i>Chlorosis (1-5)</i>	<i>Necrosis (1-5)</i>	<i>Anthocyanin Accumulation (1-5)</i>
	750 μ M K	4 weeks	1.02	100	1	-	1
	187.5 μ M K	4 weeks	0.71	67	1	1	3
	8 mM N	4 weeks	0.22	67	1	-	-
	2 mM N	4 weeks	0.24	75	1	1	1
	0.5 mM N	4 weeks	0.05	100	-	1	2
	2 mM K	5 weeks	2.92	50	-	-	-
	200 μ M K	5 weeks	1.87	50	-	-	-
	25 μ M K	5 weeks	1.21	75	1	-	1
	1 μ M K	5 weeks	0.94	100	2	-	2
CS28140	3 mM K	4 weeks	0.35	-	-	-	-
	187.5 μ M K	4 weeks	0.54	-	1	1	3
	8 mM N	4 weeks	0.27	-	-	-	-
	2 mM N	4 weeks	0.03	-	-	-	1
	0.5 mM N	4 weeks	0.06	-	-	1	3
CS28787	3 mM K	4 weeks	0.68	-	-	3	1
	750 μ M K	4 weeks	0.32	100	2	1	2
	187.5 μ M K	4 weeks	0.69	-	-	-	3
	8 mM N	4 weeks	0.11	-	-	-	-
	2 mM N	4 weeks	0.17	-	-	-	1
	0.5 mM N	4 weeks	0.07	50	-	1	2
SALK-084627	3 mM K	4 weeks	0.40	75	-	-	-
	750 μ M K	4 weeks	0.20	75	-	-	-
	187.5 μ M K	4 weeks	0.06	100	1	1	1
	8 mM N	4 weeks	0.64	100	2	1	1
	2 mM N	4 weeks	0.20	75	-	-	2
	1.6 mM N	4 weeks	0.24	75	1	-	3
	0.5 mM N	4 weeks	0.04	50	2	2	3
SALK-110333	3 mM K	4 weeks	0.52	100	-	-	-
	750 μ M K	4 weeks	0.12	75	-	-	-
	187.5 μ M K	4 weeks	0.11	100	-	1	1
	8 mM N	4 weeks	0.53	100	2	2	1
	2 mM N	4 weeks	0.30	75	-	-	1
	1.6 mM N	4 weeks	0.24	50	2	1	1
	0.5 mM N	4 weeks	0.05	50	2	3	3

K: potassium, N: nitrogen

Shoot elongation and rosette size of 4 or 5-week-old CS28833 ecotype grown with 1, 25, 200, and 2000 μM K were measured. In Figure 4.1, it is evident that 4-week-old plants exhibited greater size and height as potassium deficiency increased. On the other hand, 5-week-old plants showed reduced height when there was a decrease in potassium nutrition. These observations indicate that the plants displayed higher biomass production within the first 4 weeks; however, they exhibited typical symptoms one week later.

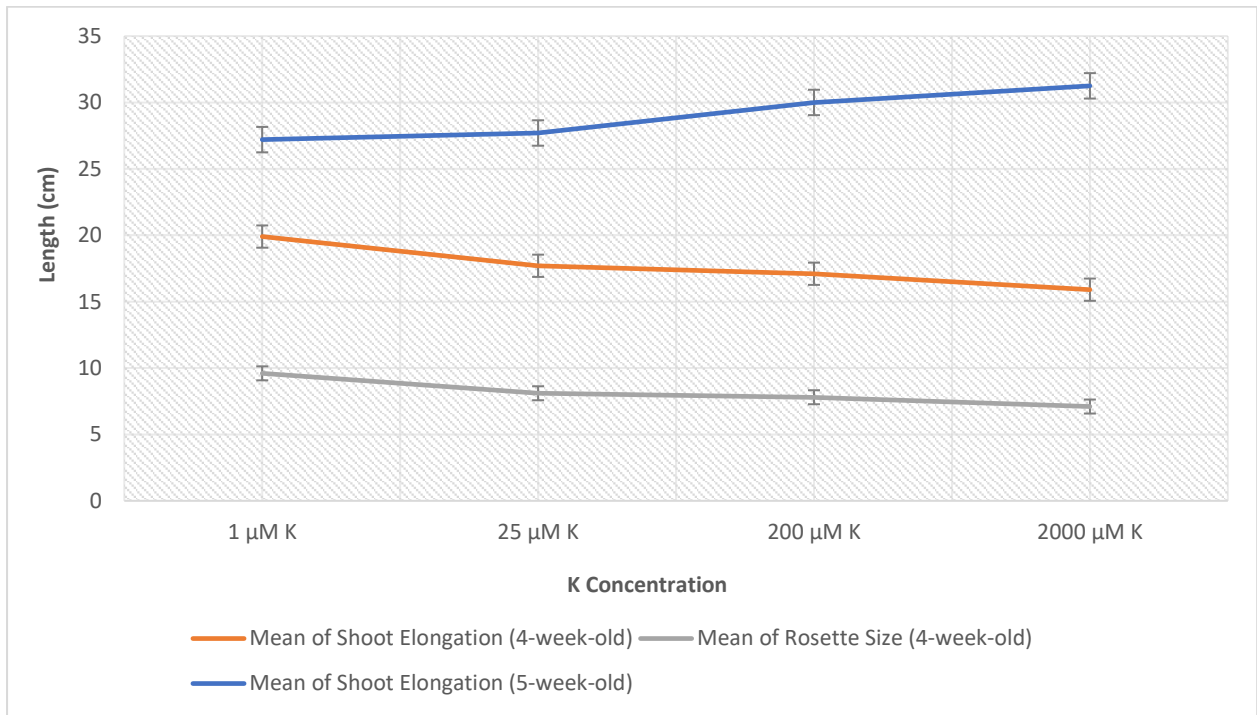


Figure 4.1. Mean of length of shoot elongation and rosette size of 4-5 weeks old CS28833 ecotype of *A. thaliana* plants under potassium deficiency conditions; 1, 25, 200, and 2000 μM K (grown in the growth chamber conditions given in Table 3.5).

The results of the two-tailed student t-test ($P < 0.05$, 95% confidence interval) performed on the data compared to the control (2 mM K) condition are provided in Table 4.2. Shoot elongation and rosette size of 4-week-old plants in 2000 μM K supply was significantly lower than others. However, shoot elongation of 5-week-old plants was not significantly different from each other.

Table 4.2. The P-values of shoot elongation and rosette size of CS28833 under K-deficiency. (95% confidence interval, n=6, calculated with GraphPad Prism)

<i>SE (4-week-old)</i>	<i>1 μM K</i>		<i>25 μM K</i>		<i>200 μM K</i>	
<i>Compared to;</i>	P Value	Significance	P Value	Significance	P Value	Significance
<i>2000 μM K</i>	0.0022	**	<0.0000	****	<0.0000	****
<i>200 μM K</i>	0.0252	*	0.5603	ns	-	
<i>25 μM K</i>	0.0659	ns	-		0.060	**
<i>RS (4-week-old)</i>						
<i>Compared to;</i>	P Value	Significance	P Value	Significance	P Value	Significance
<i>2000 μM K</i>	<0.0000	****	0.0002	****	0.0164	*
<i>200 μM K</i>	0.0011	**	0.5346	ns	-	
<i>25 μM K</i>	<0.0000	****	-		0.5346	ns
<i>SE (5-week-old)</i>						
<i>Compared to;</i>	P Value	Significance	P Value	Significance	P Value	Significance
<i>2000 μM K</i>	0.1020	ns	0.0513	ns	0.2754	ns
<i>200 μM K</i>	0.1680	ns	0.0603	ns		
<i>25 μM K</i>	0.7769	ns			0.0603	ns

SE: shoot elongation, *RS*: rosette size, *ns*: not significant, * = $P < 0.05$, ** = $P < 0.01$, *** = $P < 0.001$, **** = $P < 0.0001$

The visual symptoms of 46.9 μM, 187.5 μM, and 750 μM K-deficiency in 4-week-old *A. thaliana* genotypes (CS28833, CS76199, CS28812, CS76111) are shown in Figures 4.2 and 4.3 (grown in the growth chamber conditions given in Table 3.5). As seen in the figures, chlorosis, necrosis, and anthocyanin accumulation increased with increasing K deficiency. Young leaves are greener and healthier than old leaves. As determined through experimental and biological replicates conducted at different times, the CS28833 and CS76199 ecotypes flowered early (at 2-3 weeks), whereas the CS28812 and CS76111 ecotypes flowered late (at 5-6 weeks).

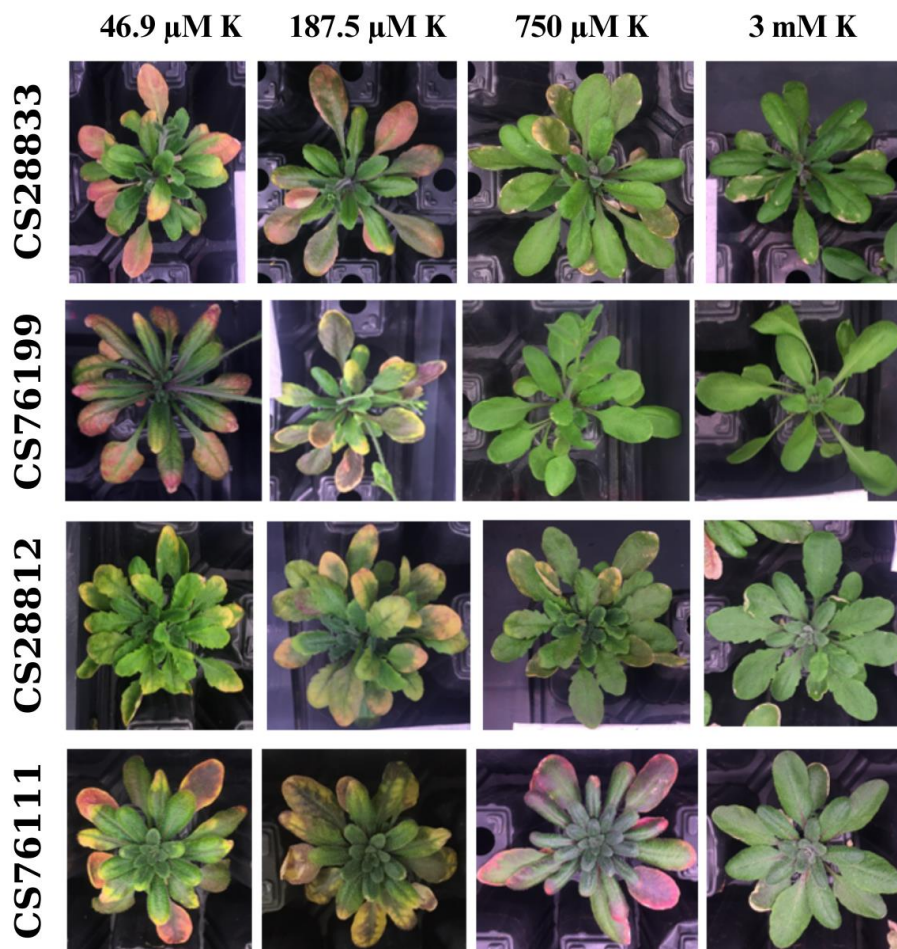


Figure 4.2. K-deficiency symptoms on 4-week-old ecotypes of *A. thaliana* rosettes. 3 mM K is the control group.

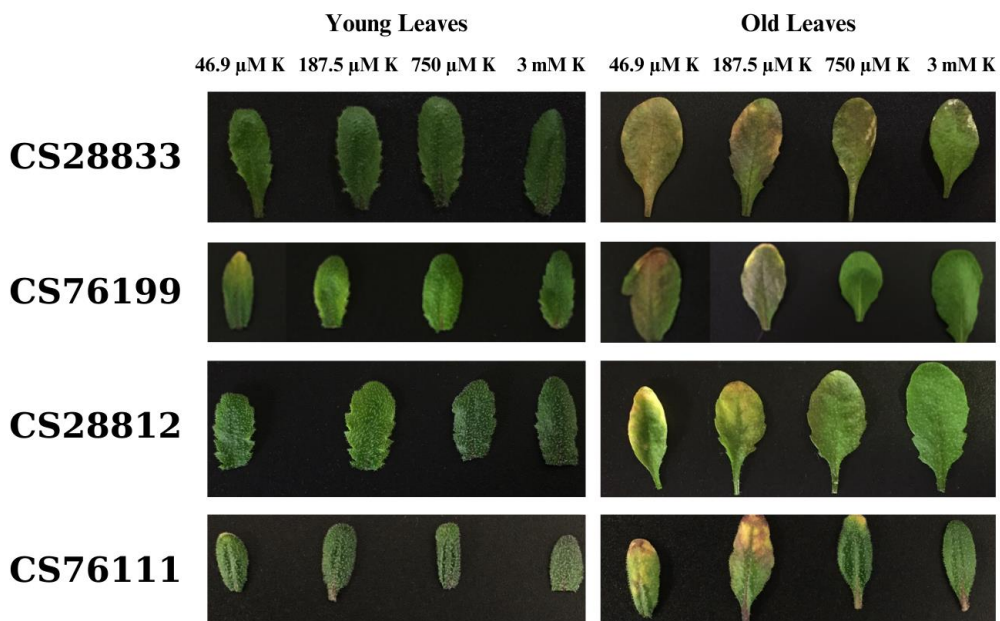


Figure 4.3. K-deficiency symptoms on young and old leaves of 4-week-old *A. thaliana* ecotypes. 3 mM K is the control group.

Based on these results, it was decided to continue with ecotype CS28833 due to its fast growth and flowering, stable symptoms, and high level of *CESA4* gene expression. The images of the CS28833 ecotype grown under K deficiency again at 4 and 5 weeks of age are given in Figures 4.4 and 4.5. Although germination rates were different, the chlorosis rate increased as K-deficiency increased. Interestingly, plants growing under low K in 4-week-old CS28833 plants were larger and taller than the control. Similarly, in 4-week-old plants, the longest stem was observed in the lowest K condition, while the shortest stem was observed in the control condition. The earliest flowering condition was associated with the lowest potassium (K) level, and as the potassium deficiency decreased, the flowering rate also decreased. The stems of these plants were found to be quite erect and healthy-looking. In contrast to the 4-week-old plants, from the 5th week onwards the situation went in the opposite direction. While the control plants continued to overgrow, the size and length of the K-deficient plants continued to grow at a slower rate or entered the senescence stage. In 5-week-old plants under nutrient deficiency, the longest stem was in the control, while the shortest was in the lowest K condition. On the other hand, K-deficiency was observed in cauline leaves of 1 μM and 25 μM K-deficient plants at 5 weeks of age. Almost all rosette leaves dried up and lost their cellular activity in plants with 1 μM , 25 μM , and 200 μM K.

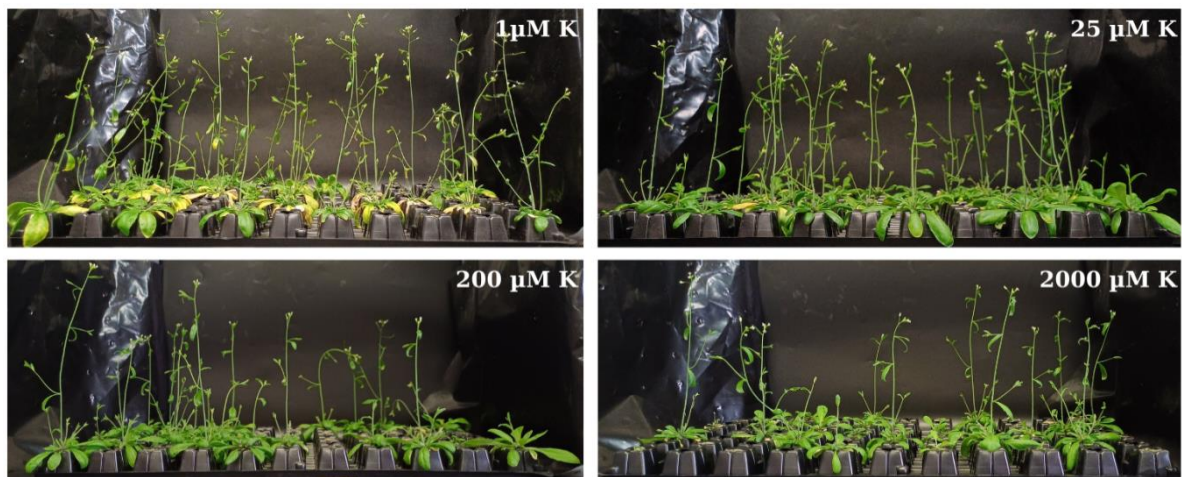


Figure 4.4. Stem view of 4-week-old CS28833 under 1 μM , 25 μM , and 200 μM K-deficiency. 2000 μM K is the control group.

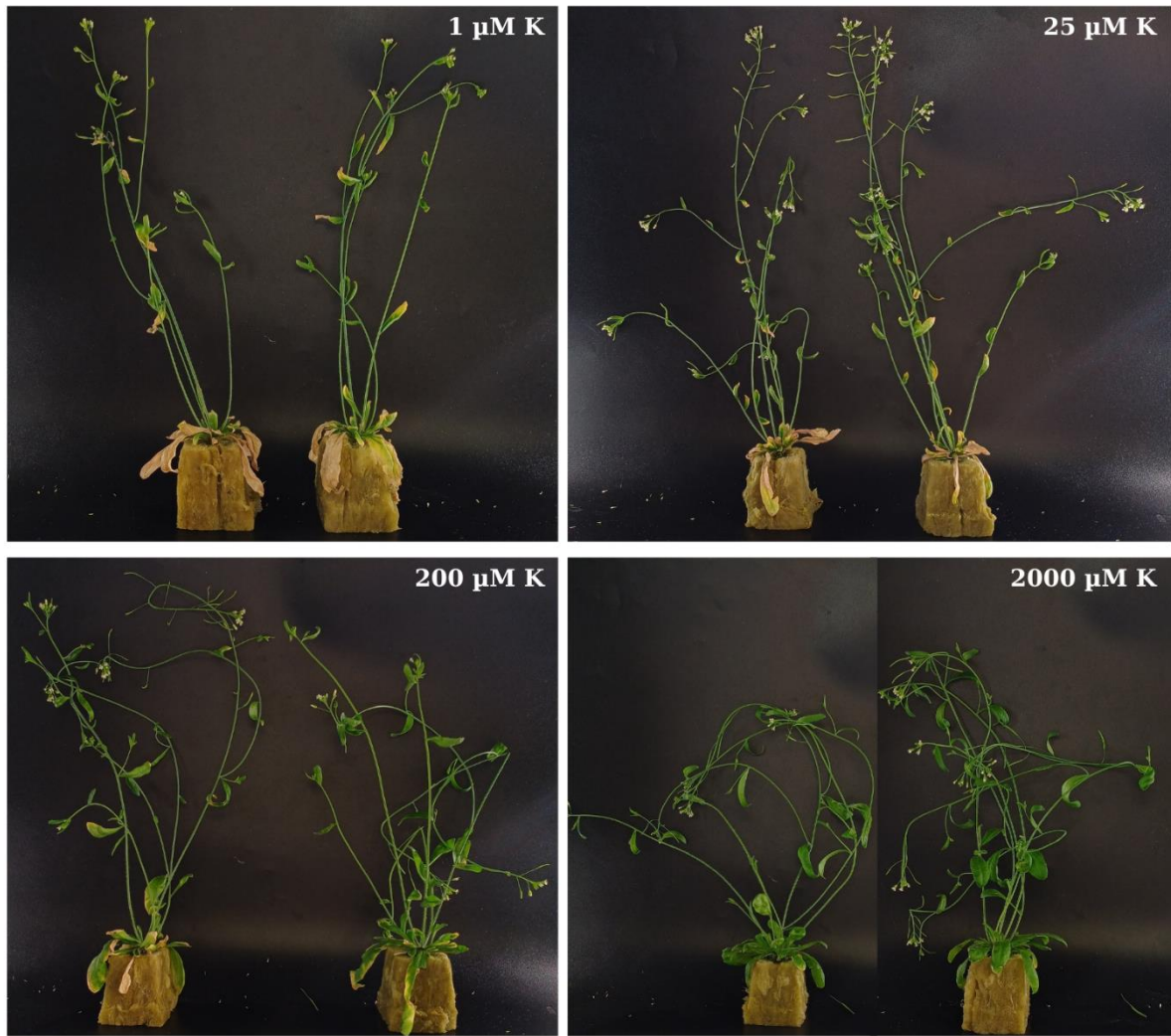


Figure 4.5 Stem view of 5-week-old CS28833 under 1 μM , 25 μM , and 200 μM K-deficiency. 2000 μM K is the control group.

Based on these results, we decided to design a knock-out system to determine whether there is a link between differences in the CS28833 genotype and the *CESA4* gene.

4.2. CRISPR/Cas9 System Design

The creation of the CRISPR/Cas9 system began with the design of gRNA sequences to knock out the *CESA4* gene, as detailed in Tables 4.3 and 4.4. 4 different gRNAs were designed using the CHOPCHOP tool and NCBI Blast. gRNA.8 contains an intron region, so an alternative, gRNA8.1, was designed. 8 primer sequences were designed to create 8 coding sequences (CDSs) given in Table 4.5.

Table 4.3 gRNA primers (R1&F2 in Figure 3.2). Efficiency and mismatch values were calculated by the CHOPCHOP Tool.

<i>Name of gRNA</i>	<i>Sequence of gRNA</i>	<i>Mismatch</i>	<i>Efficiency (%)</i>	<i>Primers</i>	<i>Length (bp)</i>	<i>T_m at Step 1 (°C)</i>	<i>T_m at Step 2&3 (°C)</i>
<i>gRNA#5 (Target 1)</i>	CGGCTATCT TAGAACTC CGG TGG	-	66.03	R 1 5'- CCGGAGTTC TAAGATAGC CGAATCACT AC-3'	29	63.1	62.9
				F 2 5'- CGGCTATCTT AGAACTCCG GGTTTTAGA G-3'			
<i>gRNA#7 (Target 2)</i>	TGATGCTTA CACCCTC CAC CGG (- strand)	-	65.34	R 1 5'- TGATGCTTAC ACCACTCCA CAATCACT-3'	27	63.7	63.5
				F 2 5'- GTGGAGTGG TGTAAGCAT CAGTTTTAG AGC-3'			
<i>gRNA#8 (Target 3)</i>	TTATAACA G AATAACA TGAG AGG	-	64.74	R 1 5'- CTCATGTTTA TCTGTTATAA AATCACTAC TTCGTCT-3'	36	62.7	62.5
				F 2 5'- TTATAACAG ATAAACATG AGGTTTTAG AGCTAGAAA TAG-3'			

<i>gRNA#8.1</i> (Target 4)	CATGTGATT	-	57.02	5'-	28	64.5	64.3
	GTTGGCCG			R 1			
	TCG TGG			A-3'			
				5'-	28	64.9	64.6
				F 2			
				A-3'			

***Intron regions, PAM sequences**

Table 4.4 gRNA primers (R1&F2 in Figure 3.2). Efficiency and mismatch values were calculated by the CHOPCHOP Tool.

Name of Primers	Sequences of Primers	Length (bp)	T _m at Step 1 (°C)	T _m at Step 2&3 (°C)
F1-primer	F1 5'-CGAGAGCTCAGAAATCTCAAATTCGG-3'	28	63	62.8
R2-primer	R2 5'-GAATTCCTCGAGTACGTAGGATCCATTAAA-3'	31	62.6	62.3

Table 4.5 Usage of primers to amplify coding sequences (CDSs)

Coding Sequence (CDS)	Forward Primer	Reverse Primer
CDS 1	F1-primer	gRNA#5.R1
CDS 2	gRNA#5.F2	R2-primer
CDS 3	F1-primer	gRNA#7.R1
CDS 4	gRNA#7.F2	R2-primer
CDS 5	F1-primer	gRNA#8.R1
CDS 6	gRNA#8.F2	R2-primer
CDS 7	F1-primer	gRNA#8.1.R1
CDS 8	gRNA#8.1.F2	R2-primer

The targeted regions within the CESA4 protein are illustrated in Figure 4.6. The gRNA.5 is placed on the 2688th base pair of the gene sequence and the 896th amino acid of the protein sequence. It is on one of the transmembrane helices. The gRNA.7, which is on the same helix as gRNA.5, targets the 2705th base pair and the 902nd amino acid. Both are considered as

efficient for a non-synonymous knock-out. The gRNA.8 targets the 1737th base pair and the 579th amino acid in the structure. The gRNA.8.1 targets the 1874th base pair and 625th amino acid. Both are targeted to the nucleotide-diphospho-sugar transferase enzymatic domain and found to be as effective candidates.

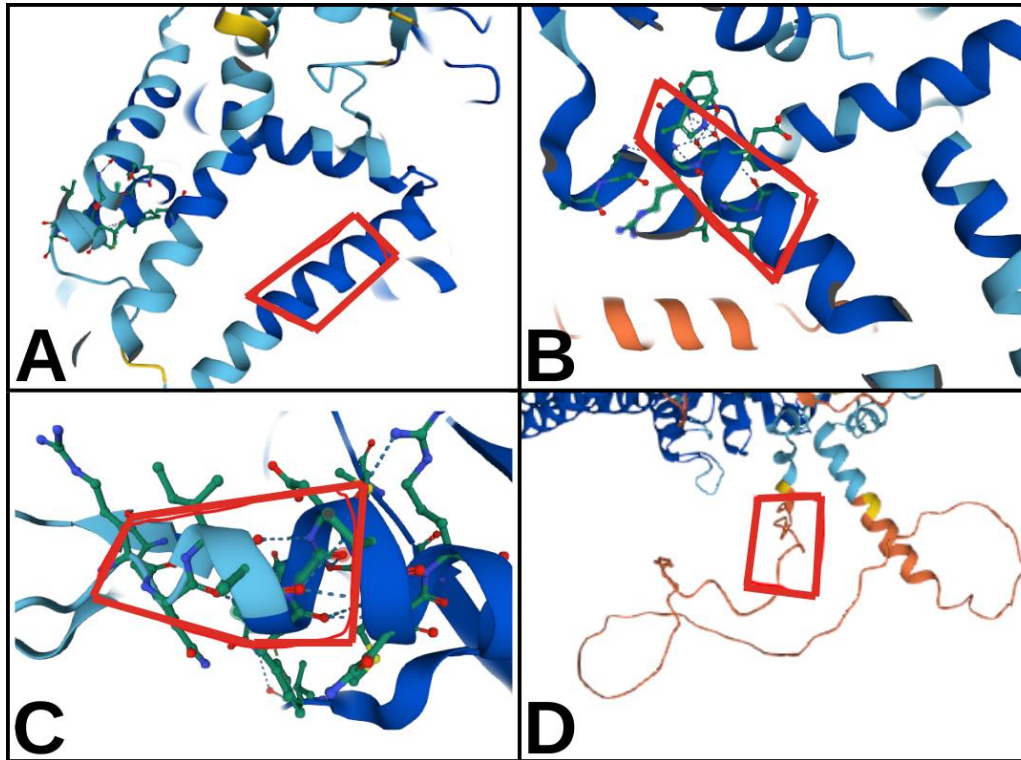


Figure 4.6 Targeted regions on CESA4 protein of gRNAs (red boxes). A: gRNA.5, B: gRNA.7, C: gRNA.8, D: gRNA.8.1. Protein structure was checked with entry number: A0A1R7T3H6 at uniprot.org.

To determine the optimum annealing temperature in step 1 of overlapping PCR, gradient PCR was performed at 62°C, 66.4°C, and 69.4°C. According to the gel electrophoresis, 66.4°C which gives the most intensive band was the best temperature (Figure 4.7).

		CDS3	CDS7	CDS3	CDS7	CDS3	CDS7
Annealing Temp:	NC	62°C	62°C	66.4°C	66.4°C	69.4°C	69.4°C
~330 bp		[Gel electrophoresis image showing bands for each condition]					

Figure 4.7 Gel electrophoresis images gradient PCR with various annealing temperatures for step 1. NC: negative control, CDS: coding sequence

Step 1 PCR was visualized at 66.4°C annealing temperature using gel electrophoresis (Figure 4.8). The CDSs were ready to proceed with step 2. Step 2 PCR was performed to overlap gRNA sequences without primers as explained in section 3.2.2.2 and presented in Figure 3.2.

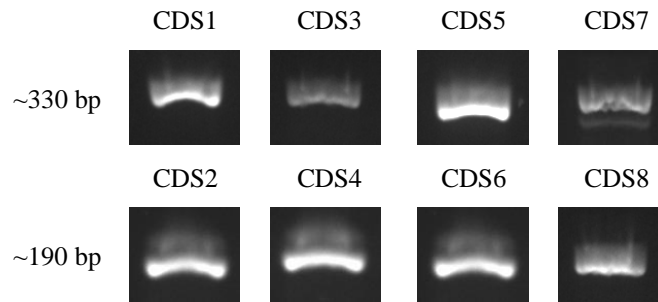


Figure 4.8 Gel electrophoresis images of step 1 PCR for CDSs.

Step 3 PCR, which occurs immediately after step 2, was visualized on gel electrophoresis as shown in Figure 4.9. According to the images, the targets were ready for restriction digest.

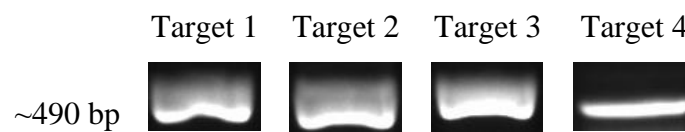


Figure 4.9 Gel images of step 3 PCR. Target 1: CDS1&2, Target 2: CDS3&4, Target 3: CDS5&6, Target 4: CDS:7&8

To transfer the inserts, pUC119-gRNA plasmid was restriction digested from SacI and EcoRI sites. To create sticky ends to help overhang the ends of the targets, they were likewise digested with SacI and EcoRI enzymes (Figure 4.10). These sites were previously inserted into primers F1 and R2.

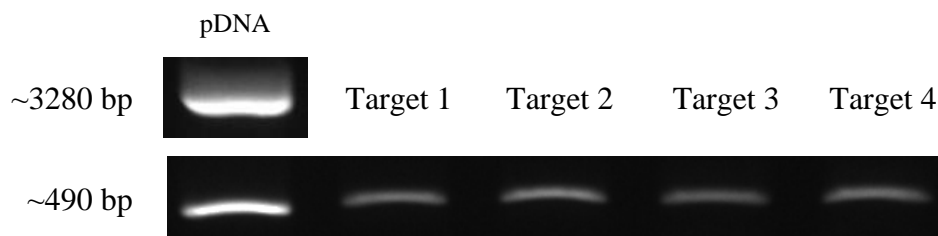


Figure 4.10 Gel images of restriction digested sequences

These bands were isolated from agarose gel to avoid contamination of the gRNA sequence of the plasmid. Then, combinations in Table 4.6 were visualized on an agarose gel to optimize the ratio of insert, amount of ligase enzyme, and vector and time (Figure 4.11). Although the vector band (~3284 bp) could not be completely eliminated by optimization, its intensity was reduced and the intensity of the band belonging to the plasmid (~3771 bp) was increased. The condition with the most intense plasmid band (7) was preferred.

Table 4.6 Combinations of plasmid ligation

	Insert:Vector	Ligase	Incubation		Insert:Vector	Ligase	Incubation
1	2:1	1 μ l	10 min	5	1:1	1 μ l	10 min
2	2:1	2 μ l	10 min	6	1:1	2 μ l	10 min
3	2:1	1 μ l	30 min	7	1:1	1 μ l	30 min
4	2:1	2 μ l	30 min	8	1:1	2 μ l	30 min

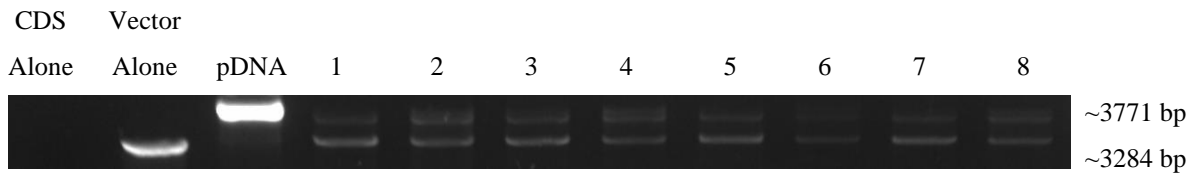


Figure 4.11 Gel image of optimization of time, enzyme amount, and ratio of plasmid ligation. Label numbers are given in Table 4.5.

It was observed that the construct (~3771 bp) band increased as the dwell time of the plasmids increased. Therefore, the dwell time was extended up to 2 hours. Since the 1:1 ratio of the insert and 1 μ l ligase amount were found to be appropriate, the experiment was performed again with this ratio Figure 4.12. Plasmid bands were generally seen as two bands close to each other.

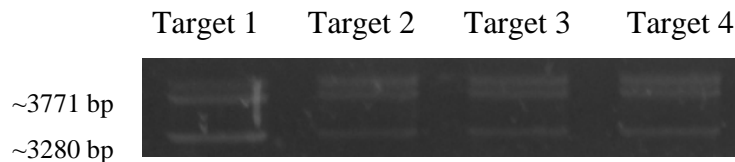


Figure 4.12 Gel results from plasmid construction.

Plasmid constructs (100 ng) were transfected into competent *E. coli* cells. Ampicillin-resistant colonies obtained after 2 days at 37°C incubation is shown in Figure 4.13. At the end of the incubation period, about 50 single colonies were obtained from all targets.

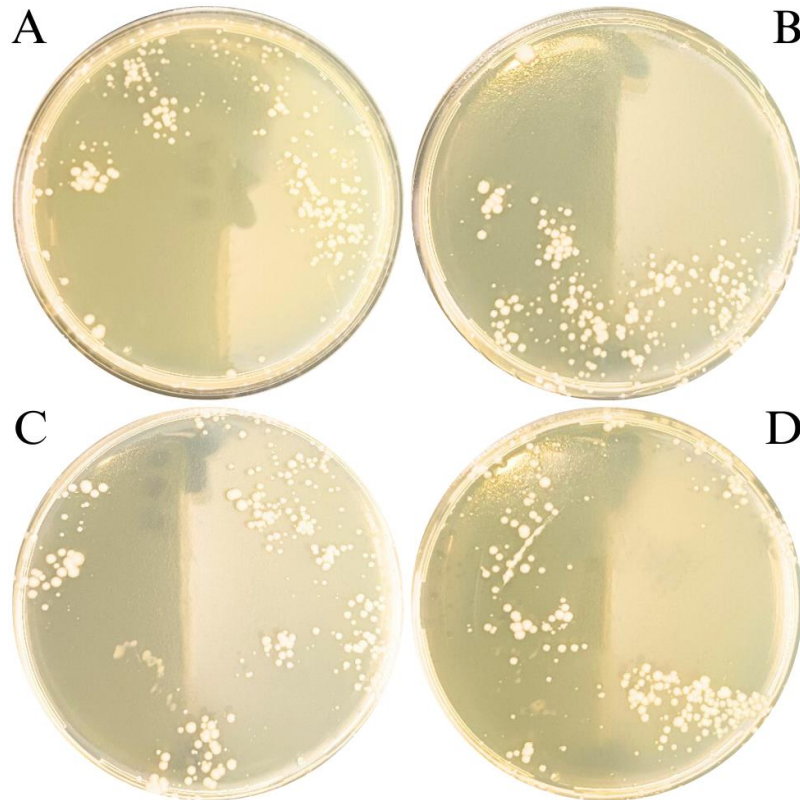


Figure 4.13 Transformed *E. coli* bacteria on LB agar plate (100 mg/L Amp). A: Target 1, B: Target 2, C: Target 3, D: Target 4.

Single colonies were isolated by placing them in a liquid LB-amp medium. A PCR confirmation was then performed to check the integrity of these plasmids. In this PCR, Primer F1 and Primer R2 were used to construct the target regions. The images of the PCR products run on gel are given in Figure 4.14 and the products were sequenced. The targets were found to be intact.

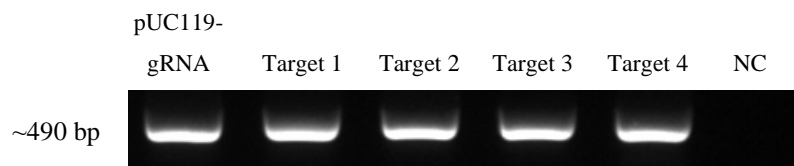


Figure 4.14 Gel image of confirmation PCR for plasmid integrity. NC: negative control

The pCESA4-gRNA plasmid formed after removing the gRNA region targeted to the *PDS3* gene in the pUC119-gRNA (Addgene, #52255) plasmid and inserting 4 different gRNA regions targeted to *CESA4* is given in Figure 4.15.B. The pFGC-pcoCas9 plasmid used to provide Cas9 activity is shown in Figure 4.15.A.

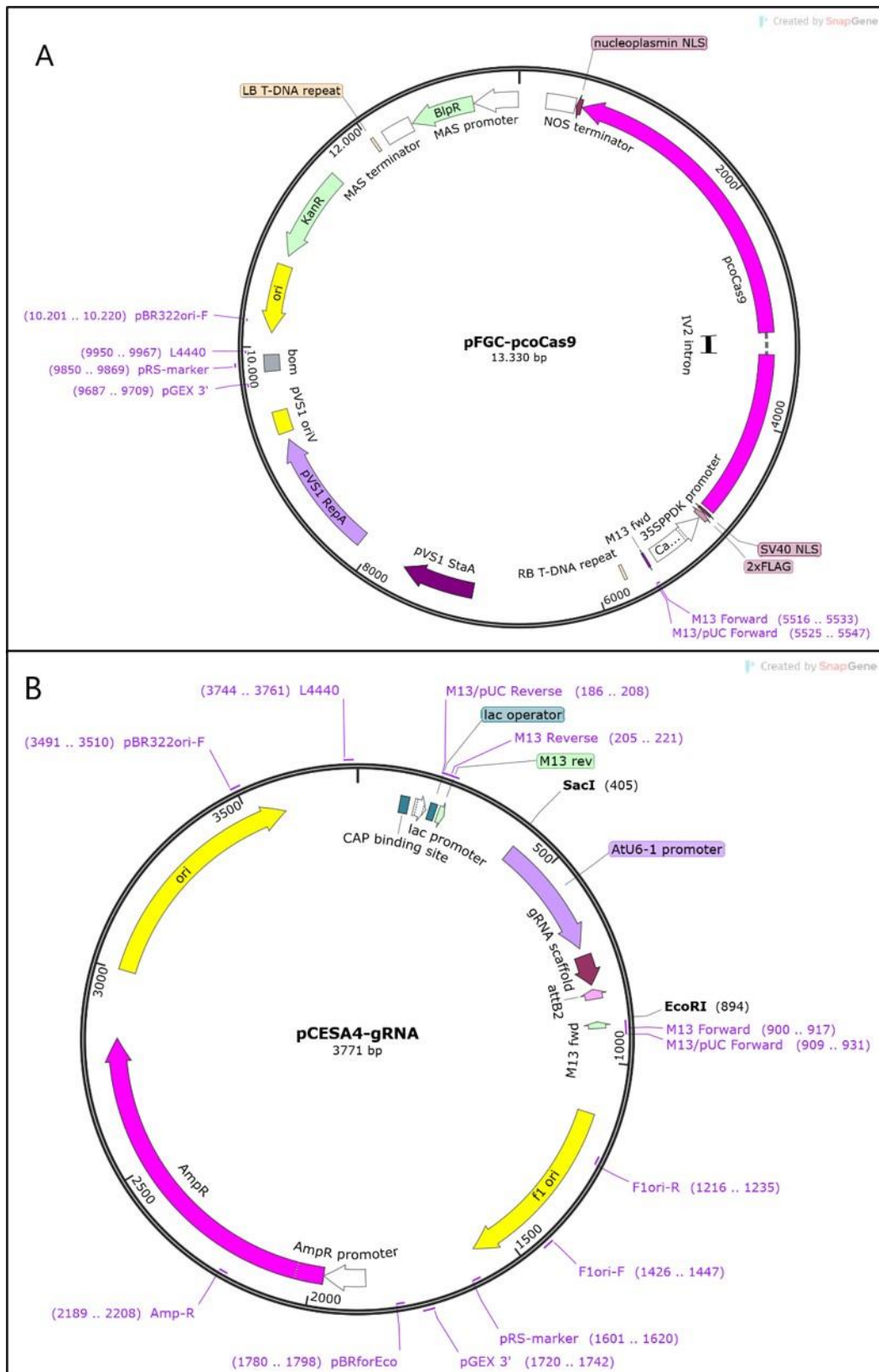


Figure 4.15. Maps of the plasmids created with SnapGene Viewer. A: pFGC-pcoCas9 (Addgene, #52256), B: pCESA4-gRNA (SacI and EcoRI regions are shown. Adapted from pUC119-gRNA, Addgene, #52255).

4.3. Floral Dipping Transformation (FDT)

To transfer these constructs to the CS28833 ecotype, floral dipping was performed using PEI-functionalized single-walled carbon nanotubes (PEI-SWNT) and *A. tumefaciens*. Before the plasmids targeted the *CESA4* gene, the toxicity of PEI-SWNT on the flowers of the plant was determined with the pUC119-gRNA plasmid, which can be obtained phenotypically. Although drying of the flower tips and some leaves of the plant was observed, none of the concentrations (2 ng/ μ l, 5 ng/ μ l, 10 ng/ μ l, 20 ng/ μ l, 40 ng/ μ l, and 80 ng/ μ l) prevented seed formation (Figure 4.16).

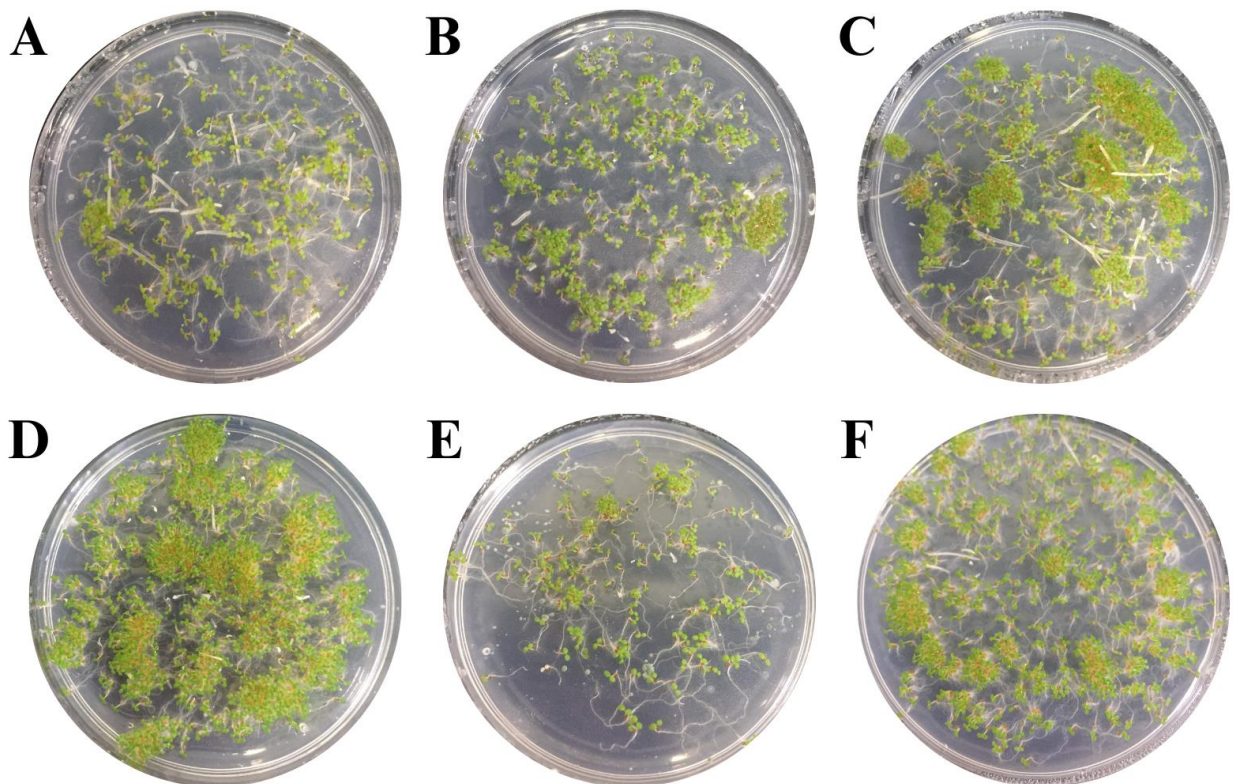


Figure 4.16 CS28833 seedlings knocked-out of Phytoene Dehydrogenase 3 (*PDS3*) Gene with FDT using PEI-SWNT on water agar plates. A: 2 ng/ μ l, B: 5 ng/ μ l, C: 10 ng/ μ l, D: 20 ng/ μ l, E: 40 ng/ μ l, and F: 80 ng/ μ l PEI-SWNT (1:2)

In this case, the most effective transformation was achieved using the pUC119-gRNA plasmid at a ratio of 1:2 (plasmid:CNT). The transformation of *PDS3* was most efficient (~15-20%) when 40 ng/ μ l CNT was applied. At other concentrations, the efficiency was around 5%. The *PDS3* knock-outed albino seedlings applied 40 ng/ μ l CNT and 20 ng/ μ l pDNA can be seen in

Figure 4.17. Based on this situation, the percentage of transformants in the application of 40 ng/ μ l was considered appropriate. The concentration was determined as the appropriate concentration for *CESA4*-targeted CRISPR/Cas9 applications.

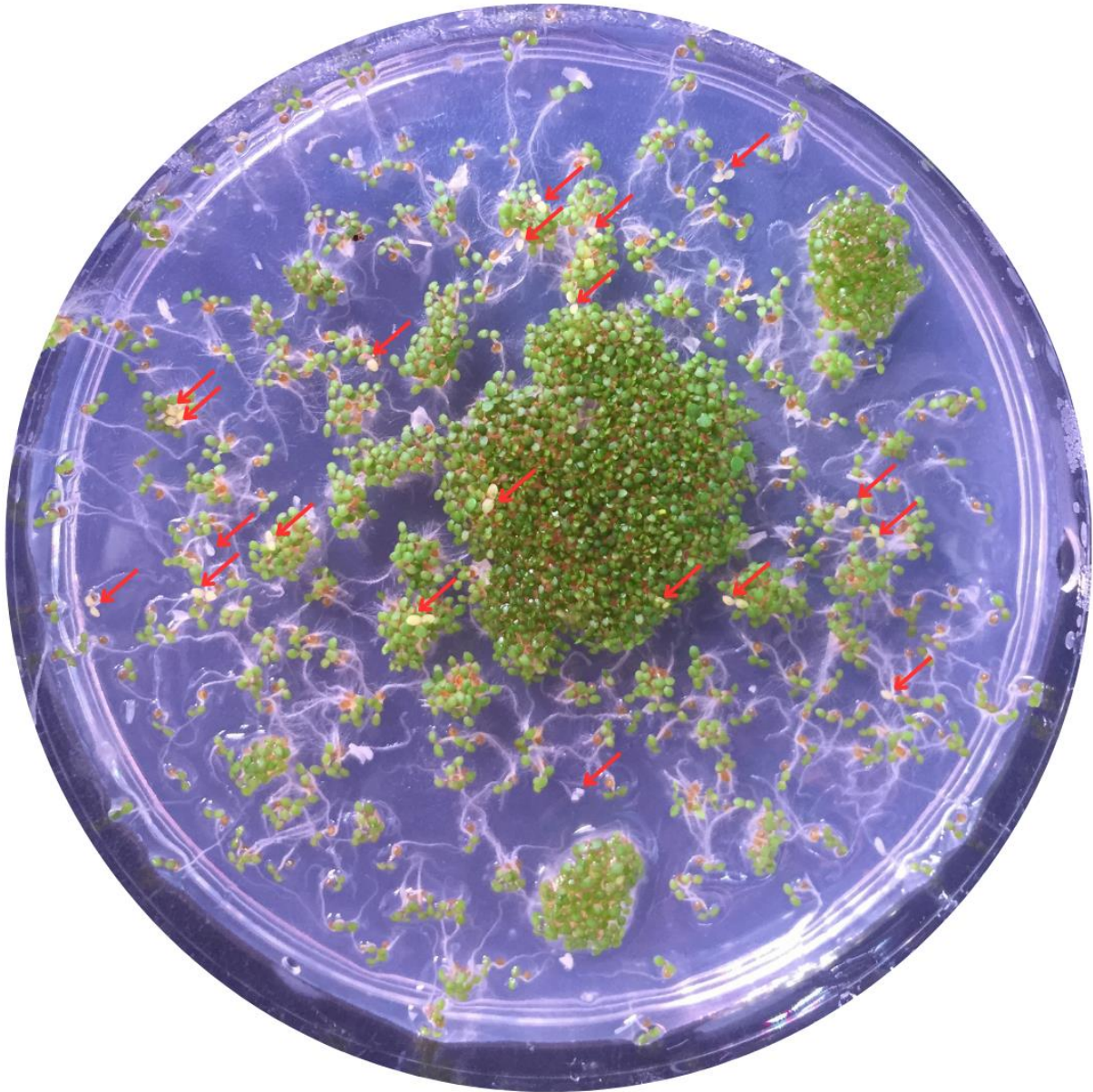


Figure 4.17 The albino seedlings belong to 40 ng/ μ l CNT:pUC119-gRNA plasmid application. 25 seedlings were albino in 150 seedlings.

A previous *CESA4* knock-out floral dipping application with PEI-SWNT was performed. After application (Figure 4.18), the plants were healthy and gave seeds. The T₁ seeds were planted on LB-Amp (100 mg/L and 500 mg/L) plates for selection of transformants (Figure 4.19).

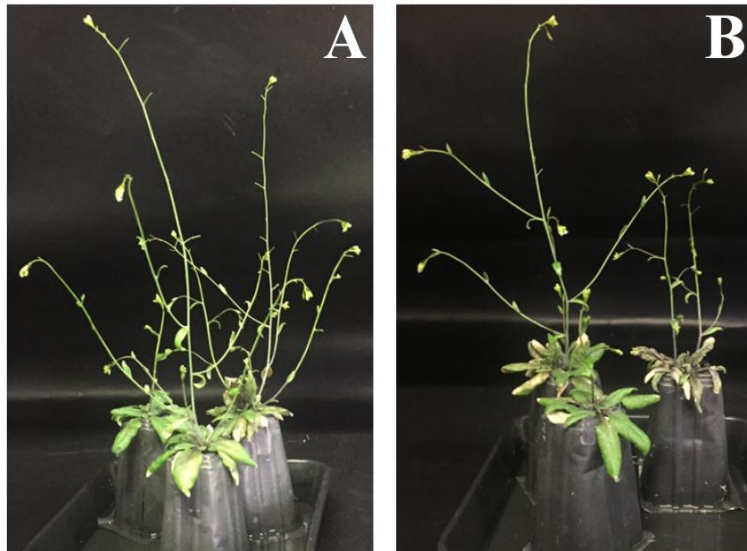


Figure 4.18 CS28833 ecotype of *A. thaliana* after floral dipping transformation for *CESA4* gene with PEI-SWNT. A: Target 2, B: Target 3

In the first 10 days, no significant difference was observed between Col-0, cultured as a positive control, and CS28833 samples knock-out with targets 2 and 3 (Figure 4.19). All the seeds had grown cotyledons.

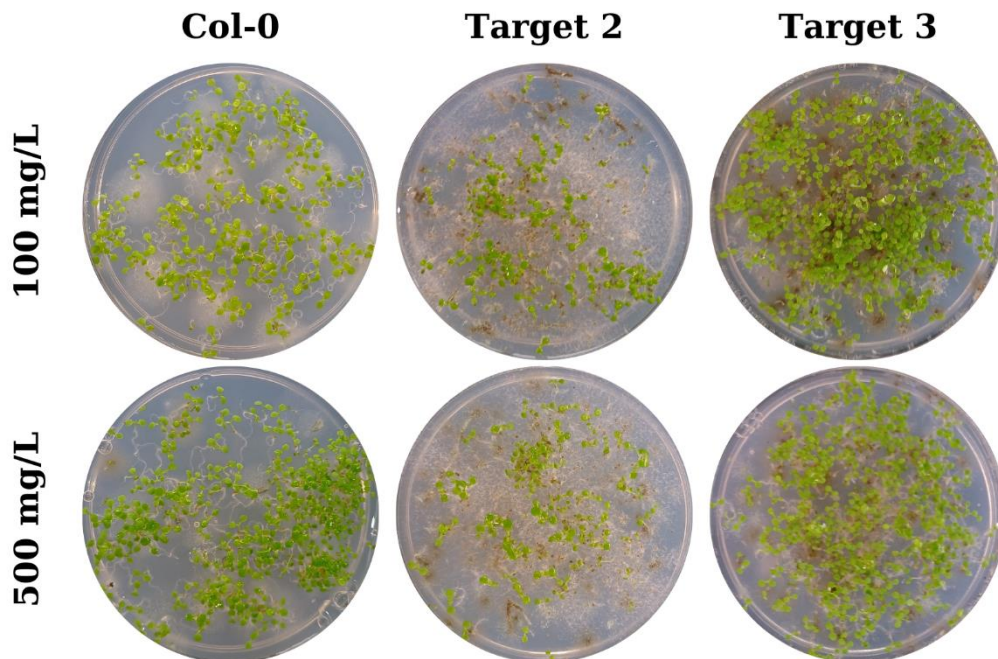


Figure 4.19 *CESA4* knocked out CS28833 ecotype 10-day-old (T1) seedlings.

4.4. Analysis of Mineral Content of *A. thaliana* Shoots Grown Under K-Deficiency

The 4-week-old CS28833 ecotypes were completely dried, and to determine the growth of plants their weights were measured. The plants grown under control conditions (2000 μM K) exhibited the lowest weights (Table 4.7). This decrease in dry weight may be attributed to a deficiency in building blocks such as cellulose or high K-induced Ca or Mg deficiency stress. It is known that high levels of K have inhibitory effects on both root uptake and/or cellular utilization of Ca and Mg within plant tissues (Ashley et al., 2006). In good agreement with this, increasing K supply clearly reduced tissue concentrations of Ca and Mg while this inhibitory effect of increasing K was not found in the case of other mineral nutrients (Table 4.9). A Student's t-test was conducted to assess the significance of the similarity between the values (Table 4.8). The results indicated that all dry weights under K deficiency conditions were significantly different from the control. Comparative analyses revealed statistically significant differences in dry weights across all treatments, except for those under 200 and 25 μM K deficiency conditions. The weights at 25 and 200 μM K deficiency were similar and represented the maximum values among all treatments. Under the lowest K condition, although biomass decreased compared to the 25 and 200 μM K conditions, it remained higher than the control. The test was performed using two biological replicates.

Table 4.7 Dry matter yield of 4-week-old CS28833 (\pm means standard deviation, n=2)

K dose μM	Dry matter (g plant⁻¹)
1	109 \pm 4
25	119 \pm 6
200	114 \pm 2
2000	90 \pm 9

Table 4.8 Two-tailed P values of dry matter of 4-week-old CS28833. Student's t-test was performed using GraphPad Prism 10.2 (95% confidence interval, n=2)

<i>P values</i>	<i>1 μM K</i>		<i>25 μM K</i>		<i>200 μM K</i>	
<i>Compared to 2000 μM K</i>	P Value	Significance	P Value	Significance	P Value	Significance
	0,0264	*	0,0042	**	0,0007	***

200 μM K	0,0072	**	0,2255	ns	-
25 μM K	0,0192	*	-	0,2255	ns

ns: not significant, * = $P < 0.05$, ** = $P < 0.01$, *** = $P < 0.001$, **** = $P < 0.0001$

There appears to be an inverse relationship between cellulose production and potassium (K) content. For better understanding of this possible connection, the K nutritional status of the experimental plants was examined, and elemental analysis was performed using ICP-OES (Table 4.9). The mineral analysis results indicated an increasing K deficiency in plants supplied with low potassium. However, in all plants, the stems contained 1.5 to 4 times more potassium than the leaves. Specifically, this difference was approximately 1.5 times in the 2000 μM K (adequate) sample, about 3 times in the 200 μM K (moderate) sample, and 4 times in both the 25 μM K (low) and 1 μM K (marginal) samples. No significant differences were observed between treatments for other elements. The results indicate preferential accumulation of K in the stem parts of plants, probably due to its involvement in the ligno-cellulosic compounds (White & Karley, 2010).

Table 4.9 The concentration of mineral elements in 4-week-old CS28833 plants under K deficiency. Analysis was performed using ICP-OES.

K dose	Tissue	K	P	S	Mg	Ca	Na
		%	%	%	%	%	%
1 μM	Stem	1,95 \pm 0,17	0,85 \pm 0,02	0,66 \pm 0,04	0,25 \pm 0,00	1,44 \pm 0,04	0,24 \pm 0,00
	Leaf	0,50 \pm 0,01	0,86 \pm 0,05	0,76 \pm 0,06	0,29 \pm 0,03	3,31 \pm 0,05	0,17 \pm 0,01
25 μM	Stem	2,40 \pm 0,03	0,92 \pm 0,01	0,73 \pm 0,01	0,20 \pm 0,00	1,30 \pm 0,06	0,17 \pm 0,00
	Leaf	0,60 \pm 0,03	0,79 \pm 0,01	0,73 \pm 0,00	0,30 \pm 0,00	3,40 \pm 0,00	0,23 \pm 0,01
200 μM	Stem	3,47 \pm 0,07	0,99 \pm 0,05	0,88 \pm 0,04	0,20 \pm 0,02	1,31 \pm 0,09	0,20 \pm 0,02
	Leaf	1,24 \pm 0,06	0,82 \pm 0,00	0,71 \pm 0,01	0,28 \pm 0,02	3,34 \pm 0,02	0,25 \pm 0,02
2000 μM	Stem	5,63 \pm 0,69	0,88 \pm 0,06	0,80 \pm 0,05	0,16 \pm 0,00	1,00 \pm 0,05	0,05 \pm 0,00
	Leaf	3,61 \pm 0,48	0,77 \pm 0,06	0,72 \pm 0,05	0,25 \pm 0,00	2,90 \pm 0,02	0,07 \pm 0,00
		Fe	Mn	Zn	B	Cu	Mo
		mg/kg	mg/kg	mg/kg	mg/kg	mg/kg	mg/kg
1 μM	Stem	61 \pm 5	28 \pm 1	29 \pm 1	21 \pm 1	4 \pm 0	6 \pm 1
	Leaf	106 \pm 0	107 \pm 0	43 \pm 1	90 \pm 7	5 \pm 1	15 \pm 2
25 μM	Stem	47 \pm 0	28 \pm 1	37 \pm 0	17 \pm 0	3 \pm 0	7 \pm 0
	Leaf	79 \pm 1	92 \pm 0	40 \pm 1	97 \pm 1	3 \pm 0	12 \pm 0
200 μM	Stem	58 \pm 5	28 \pm 1	41 \pm 3	19 \pm 2	4 \pm 0	7 \pm 1
	Leaf	85 \pm 1	86 \pm 1	43 \pm 2	84 \pm 2	4 \pm 0	12 \pm 1
2000 μM	Stem	47 \pm 0	30 \pm 3	41 \pm 7	18 \pm 0	4 \pm 0	7 \pm 0
	Leaf	86 \pm 5	93 \pm 5	43 \pm 2	76 \pm 0	4 \pm 0	11 \pm 0

Using the mineral element concentration and dry weight of plant tissues, the distribution of potassium (K) content in specific tissues was calculated (Table 4.10). The results indicated that K-deficient plants accumulated the majority of their potassium in the stems. In contrast, when potassium was supplied adequately, the plants accumulated the majority of their potassium in the leaves.

Table 4.10 Distribution of mean potassium (K) content (%) of 4-week-old CS28833 plants under K deficiency. (Analysis was conducted with two biological and three experimental replicates.)

		K	
K dose	Tissue	Content Distribution	
		%	
1 μ M	Stem	65,8	\pm 0,03
	Leaf	34,2	\pm 0,03
25 μ M	Stem	60,4	\pm 0,02
	Leaf	39,6	\pm 0,02
200 μ M	Stem	46,1	\pm 0,04
	Leaf	53,9	\pm 0,04
2000 μ M	Stem	36,2	\pm 0,03
	Leaf	63,8	\pm 0,03

4.5. Real-Time Quantitative Polymerase Chain Reaction (RT-qPCR) Setup

Based on the findings obtained, changes in the expression levels of the *CESA4* gene and several other genes in certain *A. thaliana* ecotypes under nitrogen or K deficiency were investigated. CS28833 and other ecotypes with unexpected results were evaluated. The real-time quantitative PCR (RT-qPCR) method was used to determine expression levels. In all experiments, RNA integrity and purity were assessed using Nanodrop spectrometry and gel electrophoresis. Subsequently, RNA samples were treated with DNase I, and C_t values obtained from cDNA were monitored. All experiments were conducted with two biological replicates and three experimental replicates. Initially, ecotypes exhibiting similar physiological responses and phenotypes were grouped. Ecotypes with early flowering were designated as pheno-group 1, while those with late flowering were designated as pheno-group 2 (Table 4.11). Gene expression experiments were subsequently initiated on these groups.

Table 4.11 Pheno-group classification of *A. thaliana* ecotypes.

Pheno-group 1		Pheno-group 2	
Name	ABRC stock number	Name	ABRC stock number
Bur-0	CS76105	Br-0	CS76101

Aa-0	CS28007	CIBC-17	CS76111
Ca-0	CS28128	PHW-36	CS28636
Kelsterbach-2	CS28382	WAR	CS28812
GT3885	CS28729	Paw-3	CS76208
Ag-0	CS76087	TOU-I-6	CS76265
Ven-1	CS28800	CIBC2	CS28140
Wt-3	CS28833	Uk-1	CS28787
NFA-8	CS76199		

These pheno-groups were analyzed using *cellulose synthase A4* (*CESA4*, AT5G44030), *sulfate transporter 4.1* (*SULTR4;1*, AT5G13550), *transducin/WD40 repeat-like superfamily protein* (*MOP9.16*, AT5G24320) genes. In this setup, gene expression changes in plants supplied with 1.6 mM (deficient) N and 8 mM (adequate) N were analyzed. According to RT-qPCR results, the N-deficient group 1 exhibited approximately a 180-fold increase in the *CESA4* gene, a 140-fold increase in the *SULTR4;1* gene, and a 20-fold increase in the *MOP9.16* gene. In N-deficient group 2, there was an approximately 100,000-fold increase in the *CESA4* gene, a 150-fold increase in the *SULTR4;1* gene, and a 50,000-fold increase in the *MOP9.16* gene. Log($2^{-\text{ddCt}}$) values were used in Figure 4.20 to enhance the readability of the data.

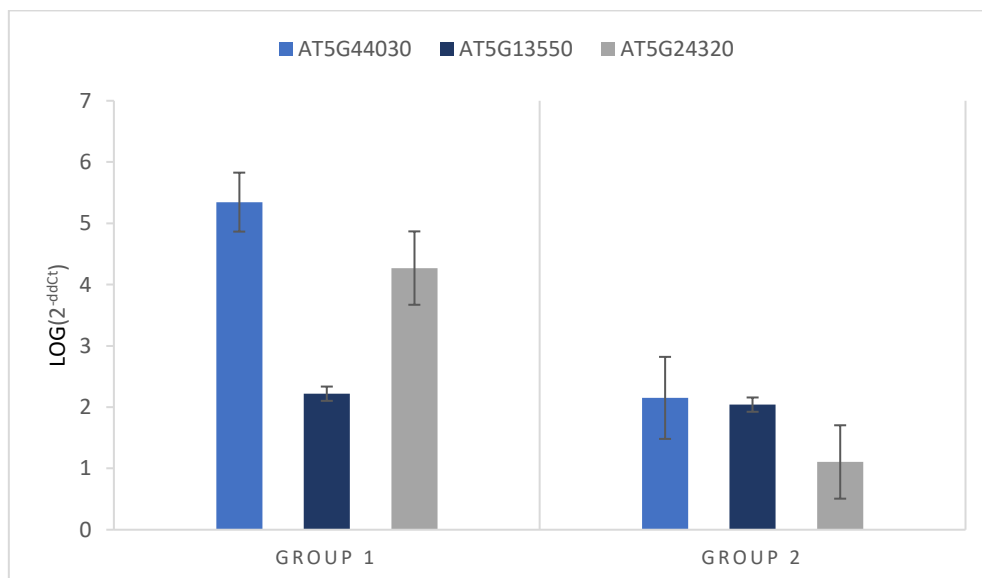


Figure 4.20 The logarithmic fold change of pheno-groups supplied with 1.6 mM N compared to 8 mM N. *CESA4*, AT5G44030; *SULTR4;1*, AT5G13550; *MOP9.16*, AT5G24320.

After these interesting results, the group members were analyzed one by one. Among the 3 genes, it was decided to continue with the *CESA4* gene, where the highest expression level was observed in both groups. The logarithmic change of *CESA4* expression results in 4-week-old CS28800, CS28140, CS7611, CS28833, CS28636, and CS76199 plants grown in 1.6 mM N and 8 mM N medium is given in Figure 4.21. *CESA4* expression in N deficiency was increased approximately 1,000-fold in CS28800, 300,000-fold in CS28140, 100-fold in CS7611, 10,000-fold in CS28833, 1,500-fold in CS28636, and 1,000-fold in CS76199.

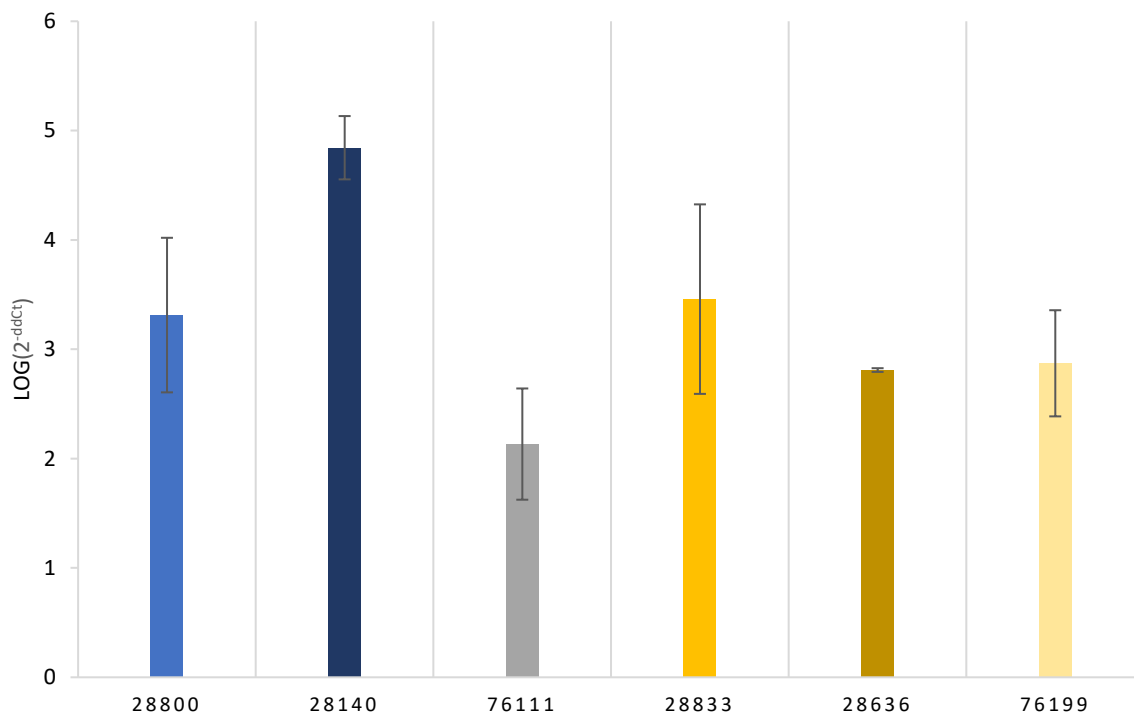


Figure 4.21 The logarithmic fold changes of the expression level of the *CESA4* gene in 4-week-old CS28800, CS28140, CS7611, CS28833, CS28636, and CS76199 ecotypes supplied with 1.6 mM N compared to 8 mM N (n=2).

Given that nitrogen is a building block for proteins, it was hypothesized whether similar changes in expression data would occur in the absence of another macroelement, potassium. Since potassium is not directly involved in protein or cellulose structure, it was anticipated that its absence might provide a different perspective on the underlying mechanism. RT-qPCR of plants grown in 1.6 mM N deficiency normalized to 8 mM N was repeated. In 1.6 mM N deficiency, *CESA4* expression increased 2-fold in CS76111, 5-fold in CS28140, 9-fold in CS28729, 3-fold in CS76199 and 4-fold in CS28833. However, no significant expression difference was observed in CS76208, CS28812, CS28787, CS76265, and CS76113. In addition, the *CESA4* expression changes of plants grown in 0.75 mM K and 0.1875 mM K

deficiency normalized to 3 mM K were examined (Figure 4.22). No significant expression difference was observed in CS76111, CS28140, CS28812, and CS76265 in K deficiency. In the CS28729 ecotype, *CESA4* expression increased 5-fold at 0.75 mM K, with no significant difference observed at 0.1875 mM K. Similarly, in the CS76208 ecotype, *CESA4* expression increased 2.5-fold at 0.75 mM K, with no significant difference observed at 0.1875 mM K. For the CS28787 ecotype, *CESA4* expression increased 1.5-fold at 0.75 mM K, with no significant difference observed at 0.1875 mM K. In contrast, the CS76199 ecotype exhibited a 5-fold increase in *CESA4* expression at 0.75 mM K and a 7-fold increase at 0.1875 mM K. The CS28833 ecotype showed a 2-fold increase in *CESA4* expression at 0.75 mM K and a 4-fold increase at 0.1875 mM K. Lastly, the CS76113 ecotype demonstrated a 3-fold increase in *CESA4* expression at 0.75 mM K and a 2-fold increase at 0.1875 mM K.

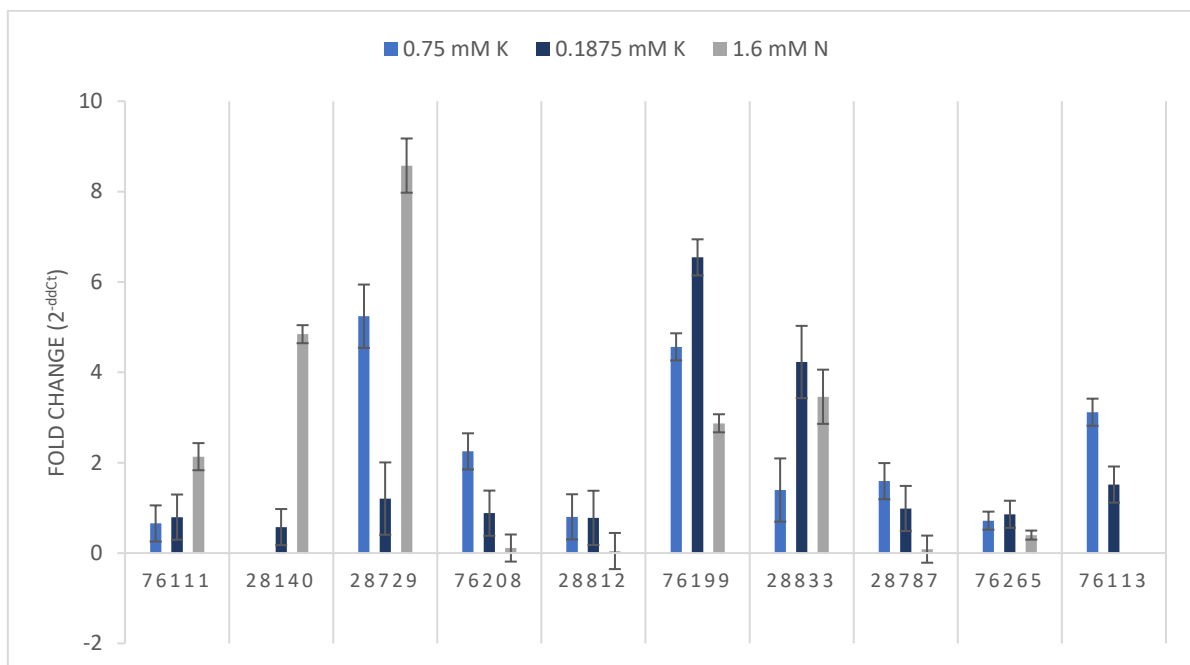


Figure 4.22 The fold changes of the expression level of the *CESA4* gene in 5-week-old CS76111, CS28140, CS28729, CS76208, CS28812, CS76199, CS28833, CS28787, CS76265, and CS76113. K treatments were normalized with 3 mM (adequate) K. N treatments were normalized with 8 mM N (adequate). Reference gene: Elongation factor-1- α (EF1 α)

To examine the expression level differences between individuals, single nucleotide polymorphisms (SNPs) in the *CESA4* gene located on chromosome 5 were analyzed in the CS28812, CS26787, CS76199, and CS28833 ecotypes using HapMap (2012) data. Differences in SNPs were analyzed regarding the Col-0 (CS76113) ecotype. The CS28812 ecotype, which did not exhibit a significant expression difference in K deficiency, had exactly the same SNPs as Col-0. In the CS28787 ecotype, which showed a 2-fold difference in *CESA4* expression at

0.75 mM K, 15 different SNPs were identified. In the CS76199 ecotype, which exhibited significant differences in *CESA4* expression at both 0.75 mM K and 0.1875 mM K, 18 different SNPs were identified. Similarly, in the CS28833 ecotype, which also showed significant differences at both potassium levels, 16 different SNPs were detected (Table 4.12).

Table 4.12 Positions of SNPs on *CESA4* gene on the chromosome 5 in CS76113 (Col-0), CS28812, CS28787, CS76199, and CS28833 ecotypes. Col-0 was used as a reference ecotype to determine differences. Matching SNPs with Col-0 were represented in green color. *Adapted from HapMap sequencing data* (Atwell et al., 2010; Horton et al., 2012; Li et al., 2010).

Positions	CS76113	CS28812	CS76199	CS28787	CS28140	CS28833
17714543	T	T	T	C	C	C
17714736	C	C	C	T	T	T
17714887	T	T	T	C	C	C
17715333	G	G	A	G	G	G
17715354	C	C	T	T	T	T
17715545	G	G	A	G	G	G
17715808	C	C	T	C	C	C
17715928	T	T	A	A	A	A
17716123	C	C	G	G	G	G
17716147	G	G	G	T	T	T
17716357	T	T	C	C	C	C
17716420	T	T	C	C	C	C
17716668	C	C	T	T	T	T
17716713	C	C	C	C	C	C
17717050	C	C	A	A	A	A
17717232	C	C	C	C	C	C
17717343	G	G	G	G	G	G
17717478	G	G	G	G	G	G
17717520	A	A	A	A	A	A
17717729	C	C	G	G	G	G
17718276	A	A	A	G	G	G
17718489	A	A	C	A	A	A
17718507	C	C	T	C	C	C
17718549	C	C	C	T	T	T
17718722	T	T	C	C	C	C
17718985	T	T	T	T	T	T
17719004	T	T	T	T	T	T
17719123	T	T	C	T	C	T
17719162	T	T	C	T	T	T

17719213	C	C	T	C	C	C
17719252	C	C	T	C	C	C

Based on these results, an experiment was designed comparing the CS28812 ecotype, which is identical to Col-0 and does not have any changes in the *CESA4* gene, and with the CS28833 ecotype, which contains 16 different SNPs compared to Col-0 and exhibits increasing *CESA4* expression levels as K deficiency increases. To replicate the experiment, a marginal 46.9 μM K condition was added to the feeding conditions of 0.75 mM K and 0.1875 mM K. The plants were analyzed in three different parts: old leaves, young leaves, and stems. Due to the late flowering of CS28812, stem isolation could not be performed. As seen in Figure 4.23, significant changes in *CESA4* expression were again observed in CS28833. While no obvious expression change was observed in young leaves of CS28812, a 2.5-fold increase in *CESA4* expression was observed only in mature leaves of plants grown in 750 μM K. Furthermore, in CS28833, the highest *CESA4* expression was observed at 187.5 μM K, followed by 750 μM K, and the lowest at 46.9 μM K. Among the tissues, young leaves exhibited the highest expression, while mature leaves and stems showed similar results (Figure 4.23).

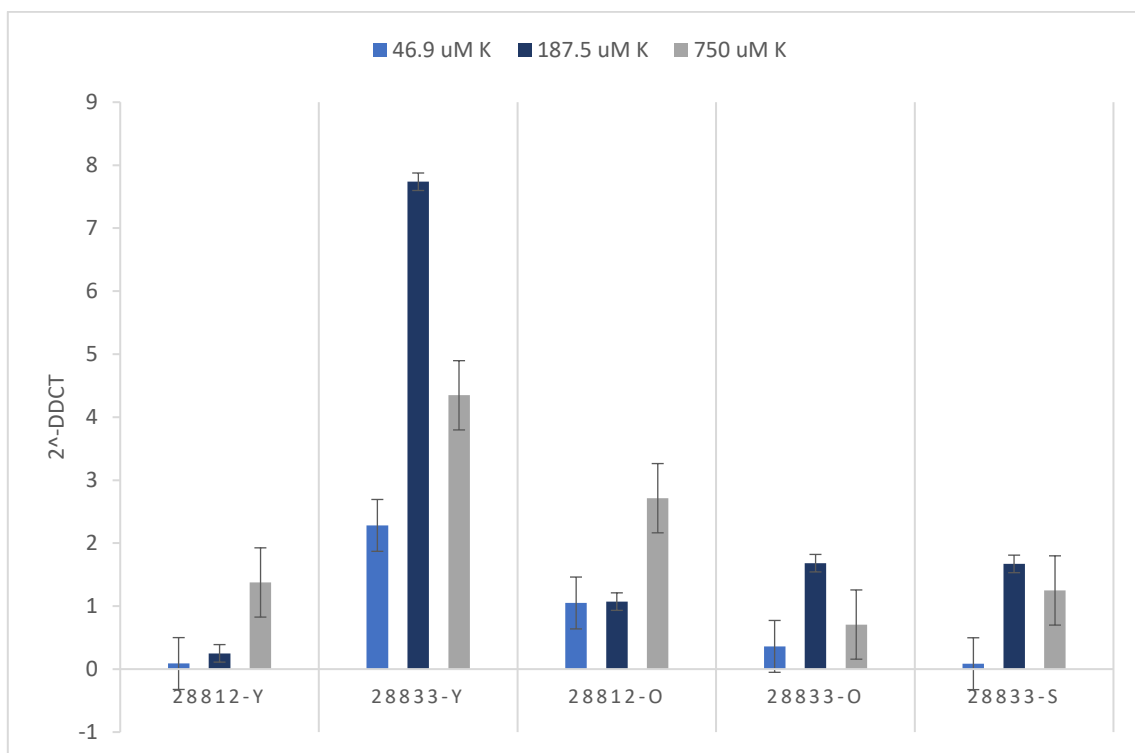


Figure 4.23 The fold changes in *CESA4* expression level of 4-week-old CS28812 and CS28833 ecotypes. Y: Young leaves, O: Old leaves, S: Stem. Treatments were normalized with 3 mM (adequate) K (n=3).

CS28833 plants grown under more marginal potassium (K) conditions were examined to determine if a similar decrease in expression would occur. Therefore, the *CESA4* expression was analyzed in CS28833 plants grown in 1 μM , 25 μM , and 200 μM K conditions. Young leaf and stem tissues were evaluated separately in 5-week-old plants. As the 5-week-old CS28833 ecotypes had entered the senescence stage in mature leaves, isolation could not be performed. As expected, no significant change in *CESA4* expression was observed in young leaves under 1 μM and 25 μM K conditions. However, in stem tissues, there was approximately a 1.5-fold increase at 1 μM K and about a 2-fold increase at 25 μM K. In the 200 μM K samples, young leaves exhibited a 1.5-fold increase in *CESA4* expression, while the stem showed a 3-fold increase as provided in Figure 4.24.

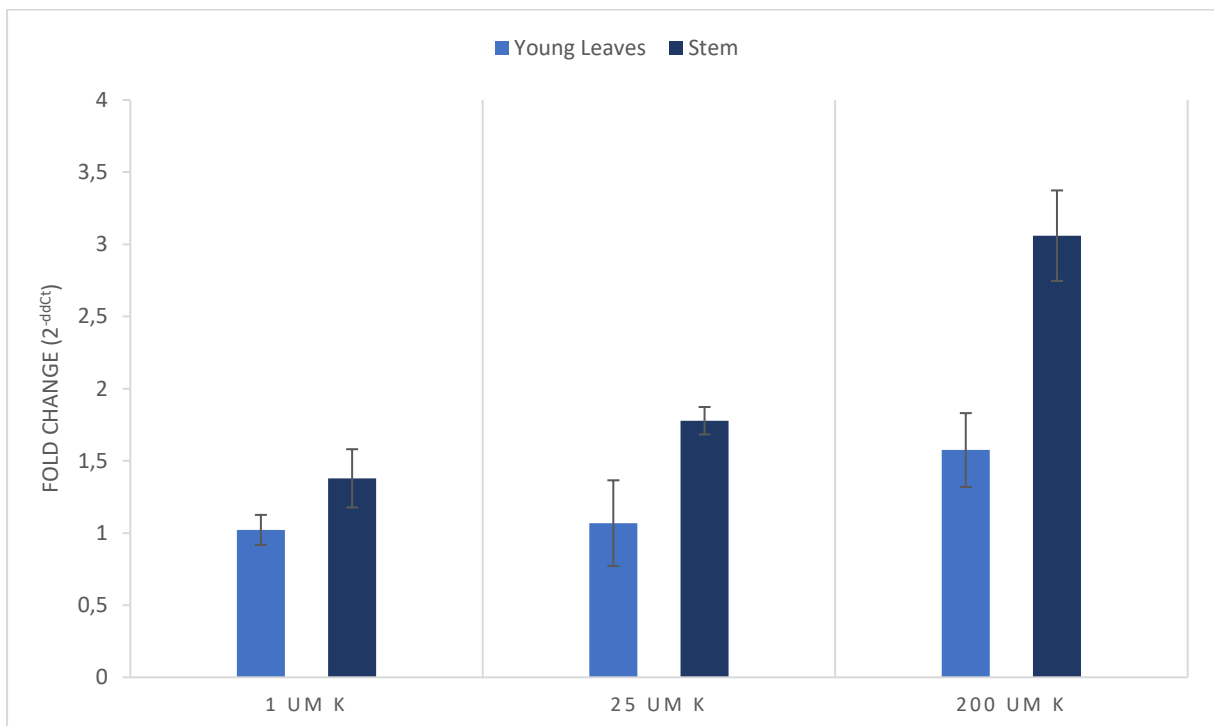


Figure 4.24 The fold changes in *CESA4* expression level in 5-week-old CS28833 ecotype under 1 μM , 25 μM , and 200 μM K deficiency. Treatments were normalized with 2 mM (adequate) K (n=3).

The investigation aimed to determine whether the *CESA4* gene exhibits different expression levels in response to potassium deficiency in other plants. Therefore, bread wheat (*Triticum aestivum*) plants were grown under 0 ppm (deficient) and 300 ppm (adequate) potassium levels, and changes in *TaCESA4* expression were examined. Harvested wheat samples were separated into flag leaves, flag stems, second leaves, and second stems, as shown in Figure 3.4, and the three homoeologs of the *AtCESA4* gene were individually investigated. According to the results in Figure 4.25, in the flag leaf, *TaCESA4* gene expression increased approximately 6-fold in

the 3A homoeolog and 9.5-fold in the 3D homoeolog, while no change was observed in the 3B homoeolog. The flag stem did not exhibit any significant differences in expression across all three homoeologs. In the second leaf, expression increased 30-fold in the 3A homoeolog, 4.5-fold in the 3B homoeolog, and 50-fold in the 3D homoeolog. In the second stem, expression increased 45-fold in the 3A homoeolog, 100-fold in the 3B homoeolog, and 13-fold in the 3D homoeolog. It was observed that the *TaCESA4* gene was expressed more in the relatively older second leaves and stems compared to the control, rather than in the younger flag leaves and stems.

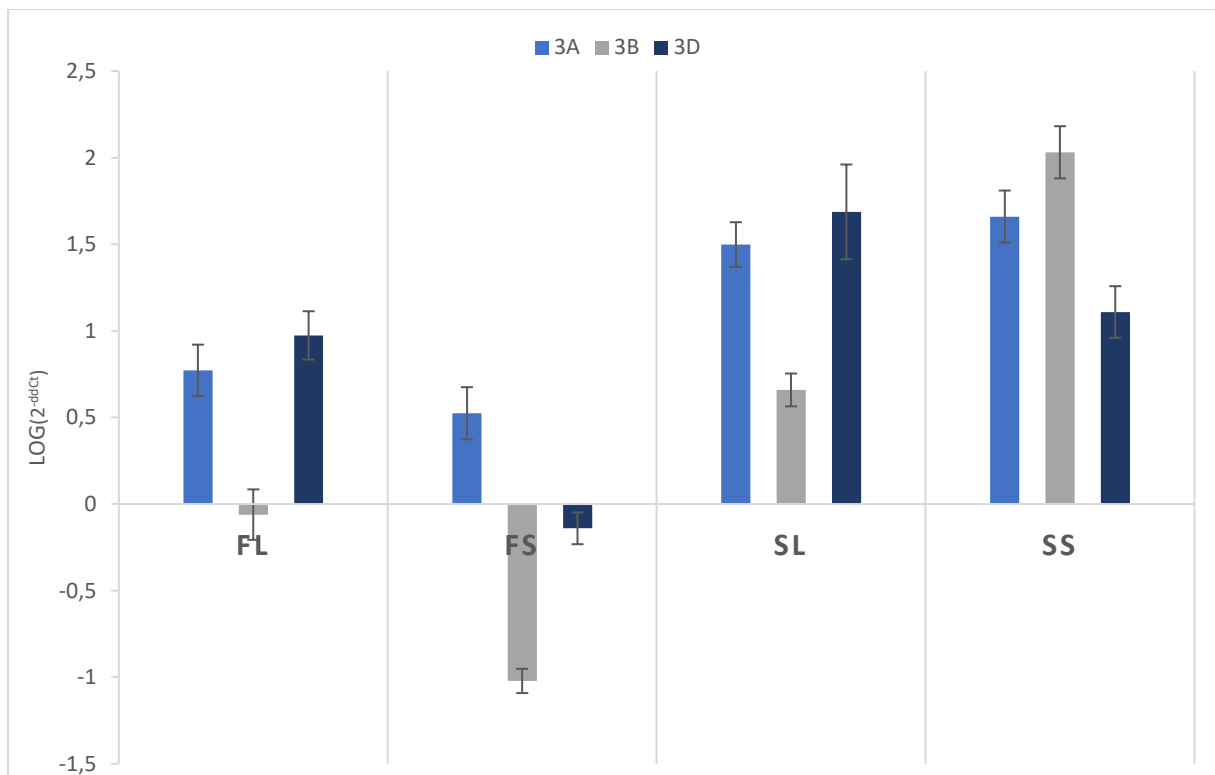


Figure 4.25 The logarithmic changes in *CESA4* expression level in *T. aestivum* supplied with 0 ppm K compared to 300 ppm K. *FL*: flag leaf, *FS*: flag stem, *SL*: second leaf, *SS*: second stem provided in Figure 3.4. *3A*: on chromosome 3 in sub-genome A, *3B*: on chromosome 3 in sub-genome B, and *3D*: on chromosome 3 in sub-genome D

5. DISCUSSION

In this section, a comprehensive discussion and analysis of the study's findings were delved into. Initially, nitrogen and potassium metabolisms among different natural accessions of *Arabidopsis thaliana* are compared using specific candidate genes. This involves comparing the phenotypic plasticity of these ecotypes to pinpoint the most accurate candidate gene and accession. Subsequently, I endeavored to identify correlations between the observed differences in *CESA4* expression levels, analyzed through statistical methods, and the potassium concentrations in various plant tissues. Furthermore, the potential relationships among potassium, the *CESA4* gene, and flowering time are explored, drawing insights from existing data. Lastly, a detailed examination of the CRISPR/Cas9-mediated knockout of the *CESA4* gene using PEI-SWNT is conducted to wrap up the study and address any lingering questions. The discussion encompasses both positive and negative aspects of the outcomes, consistent and inconsistent elements of the results, and potential causes of discrepancies. Through an analysis grounded in cause-and-effect relationships, various phenomena are explored to establish connections among concepts.

5.1. Comparative Analysis of Phenotypic Plasticity and Specific Candidate Gene Expression Levels among *A. thaliana* Natural Accessions under Nitrogen or Potassium Deficiency

In this study, plant growth in hydroponics was conducted using 50% Hoagland's solution, as provided in the Material and Method section. This enabled the use of an irrigation system containing the required levels of micro and macro elements. One of the most important environmental variables to adjust to ensure the availability of nutrients to plants is the pH value (Wiser et al., 2016). As demonstrated in many studies, a slightly acidic or neutral pH of the growth medium provides the optimal growth and root uptake of mineral nutrients (Carrillo-Inungaray et al., 2014; Parvin et al., 2021; Wiser et al., 2016). Therefore, it was ensured that experimental plants have received adequate levels of mineral nutrients with a suitable medium pH in the modified Hoagland nutrient solution (Hoagland and Arnon, 1950). Potassium was the only mineral nutrient which was supplied to the plants at different rates.

Additionally, all plants were exposed to appropriate lighting to avoid impairments in growth due to inadequate or excessive light conditions (Barber & Andersson, 1992; Cakmak, 2005).

Furthermore, sufficient humidity, oxygen, and CO₂ levels are among the factors that must be considered in plant nutrition and growth (Chia & Lim, 2022; Considine & Foyer, 2021; Morison & Lawlor, 1999). In summary, when evaluating the data in Table 4.1, it should be noted that, except for the concentration of the element under deficiency conditions, the other parameters mentioned above were kept as optimal and equal as possible. The findings obtained from this assessment can reflect the genetic differences exhibited by the ecotypes.

In previous studies, three candidate genes (*CESA4*, AT5G44030; *SULTR4;1*, AT5G13550; *MOP9.16*, AT5G24320) consistently showing significant expression differences in GWAS results within previous nitrogen use efficiency studies of *A. thaliana* HapMap population were picked (Erol, 2019). To conduct a group-based rather than individual-based investigation, two groups were formed (Table 4.11): those with early flowering and high nitrogen accumulation (pheno-group 1) and those with late flowering and low nitrogen accumulation (pheno-group 2) (Erol, 2019). One advantage of pooling was the ability to determine whether similar phenotypes exhibit similar behaviors. Although all accessions were more highly expressed in the early-flowering pheno-group 1, the extreme change in expression of the *CESA4* gene was particularly noteworthy (Figure 4.20). Experiments conducted on these two groups demonstrated distinct expression differences between them. The *cellulose synthase A4 (CESA4)* gene, which exhibited the most significant differential expression, was selected for further studies.

Individual plants were subsequently examined based on the data obtained from these groups. Initially, from pheno-group 1, CS28800, CS28833, and CS76199, and from pheno-group 2, CS28140, CS76111, and CS28636 were randomly selected and grown under conditions of 1.6 mM nitrogen deficiency and sufficient nitrogen. Upon examining the expression of the *CESA4* gene, it was found that, except for CS28140, the other ecotypes indeed exhibited behavior consistent with their group classification (Figure 4.21). Since the grouping here was roughly based on some physiological observations, completely homogeneous behavior cannot be expected. For example, in some studies, it is noteworthy that although CIBC2 (CS28140) exhibits high electrolyte leakage under salt stress, the ecotypes Br-0 (CS76101) and WAR (CS28812) show moderate levels of electrolyte leakage. Furthermore, under salt stress, Br-0 demonstrates a significant increase in both dry and fresh weight, whereas CIBC2 shows a considerably lower increase in these measures (Julkowska, 2015). On the other hand, it has been observed that the SNPs in the *CESA4* gene of CIBC2 are identical to those in Wt-3 (CS28833) except for a single nucleotide (Table 4.12). Therefore, it is not surprising that CIBC2 exhibits similar behavior to Wt-3, given that their gene sequences are almost identical.

Many genes are upregulated or downregulated during flowering, and numerous physiological traits show positive or negative correlations with flowering (Atwell et al., 2010). Although the early/late flowering physiological condition considered in this grouping could potentially be linked to a similarity in the level of *CESA4* gene expression, it cannot be directly correlated. Thus, rather than general data obtained from small-scale group studies, the behaviors of individual plants should be considered.

Nitrogen is a natural building block of many organic compounds, including amino acids, and lipids. It is the most crucial nutrient for the maintenance of plant metabolism, growth, and assimilate production, also influencing plant gene expression (Näsholm et al., 2009). The two primary inorganic forms of nitrogen that are directly absorbed by the root system and impact plant enzymatic reactions are nitrate (NO_3^-) and ammonium (NH_4^+) (Singh et al., 2022). Nitrogen deficiency results in chlorosis in leaves, particularly the lower leaves, inhibits bud growth, and overall reduces plant growth (Tang et al., 2023). Its absence during the early vegetative stage of a plant's life negatively impacts crop output, which cannot be rectified by adding nitrogen later (Binder et al., 2000).

It has been demonstrated that organic amendments with a low C/N ratio indirectly increase the production and activity of microbial exo- and endo-cellulases by providing more inorganic nitrogen to plants. This phenomenon has been interpreted as a factor enhancing cellulose degradation (Berg, 2000; Henriksen & Breland, 1999; Recous et al., 1995). In another study, excessive nitrogen application inhibited lignolytic white-rot fungi in the microbiota (Berg, 2000). Therefore, conducting a microbial analysis in rockwool and the plant's rhizosphere might be necessary to determine whether the increased expression of *CESA4* under nitrogen deficiency is due to such secondary effects. Nonetheless, in a study conducted on maize plants, it was observed that glycosyltransferase genes, including *CESA4* (family 2 of glycosyl transferases (GT2) (Beeckman et al., 2002), were down-regulated in the roots of a nitrogen deficiency-tolerant line compared to a nitrogen deficiency-sensitive line (Singh et al., 2022). In *A. thaliana*, one reason for the reduction of *CESA4* gene expression in non-flowering ecotypes under nitrogen deficiency could be their greater sensitivity to nitrogen deficiency compared to flowering ecotypes because plants produce stem tissue during the flowering period, which requires a lot of cellulose (Doblin et al., 2002).

Therefore, developing crop genotypes with higher nitrogen use efficiency (NUE) is crucial for achieving sustainable agriculture, high productivity, minimal chemical input requirements, and

minimal environmental impact. Considering all these factors, the increased gene activity in response to nitrogen deficiency is a promising result. In pursuing sustainable agriculture, it is important to identify genotypes that enhance the production of primary or secondary metabolites under nitrogen deficiency. While genes involved in nitrogen uptake, such as *nitrate transporters (NRTs)*, have been the focus of much research (Singh et al., 2022), it is also crucial to investigate whether plants can still produce metabolites under nitrogen deficiency. Especially, for agricultural crops, the ability to yield efficiently under nitrogen deficiency is just as important as the capacity for adequate nitrogen uptake. In this context, research on genes like *CESA4*, which are not directly associated with nutrient deficiency but are critical for the healthy growth of plants, gains importance.

Moreover, given nitrogen's vital roles outlined above, its deficiency can mask several unpredictable side effects. Therefore, potassium, an essential element that is not a direct building block of organic matter, was included in the experimental setup. Among the mineral nutrients, potassium (K) plays a crucial role in enhancing the survival of crop plants under environmental stress conditions. It is essential for various physiological processes, including photosynthesis, the translocation of photosynthates to sink organs, maintenance of turgor pressure, enzyme activation, and the reduction of excessive uptake of ions in saline and flooded soils (Cakmak, 2005). Therefore, the same experiment was also intended to be investigated under K deficiency conditions. *CESA4* expression was examined in 10 ecotypes of *A. thaliana* grown under conditions with 1.6 mM and 8 mM nitrogen, and 3 mM, 750 μ M, and 187.5 μ M potassium (Figure 4.22). The results indicated that the CS28140 ecotype, which exhibited different behavior from its phenotypic group under nitrogen deficiency, showed similar behavior to other group members under potassium deficiency. This finding suggests that nitrogen may interact more clustered with other genes in various pathways, influencing gene expression changes (Singh et al., 2022; Tang et al., 2023). Members of pheno-group 1, CS28729, CS76199, CS76113, and CS28833, demonstrated high *CESA4* expression under both low nitrogen and low potassium conditions, thereby emerging as stable candidate ecotypes. Conversely, CS76111, CS76208, CS28812, CS76265, and CS28787 did not exhibit significant changes in *CESA4* activity under either condition, supporting the hypothesis of a potential link between the gene's activity and flowering. Based on all the RT-qPCR analyses, CS28812 and CS76111, which consistently showed unchanged *CESA4* expression across all conditions, and CS28833 and CS76199, which consistently exhibited high *CESA4* expression under all conditions, have been tested at different K supply levels. As shown in Figure 4.23, the *CESA4*

gene exhibited consistently low expression in CS28812, while CS28833 demonstrated consistently high expression. The CS28833 accession which shows the most variable results under all conditions and is the most promising nominee in terms of nutrient-use efficiency has been identified as a candidate genotype for further studies.

Some studies have shown that sodium can replace potassium in certain plant species, at least partially. In young olive trees, for instance, the presence of sodium allowed the trees to tolerate extremely low potassium concentrations. Sodium was able to substitute for potassium and bring the photo-assimilation rate to nearly optimal levels (Erel et al., 2014). With sufficient sodium, potassium deficiency did not significantly impair the stomatal control mechanism, regardless of water availability. The beneficial effect of sodium on photosynthesis and carbohydrates under potassium deficiency suggests that sodium plays a positive role in metabolism and photosynthetic reactions, indicating that Na possibly replaces K in some physiological functions (Erel et al., 2014; Rengel et al., 2022). As seen in Table 4.9, sodium accumulation in the tissue of CS28833 accession increased as potassium deficiency intensified. Under conditions where the total potassium content fell below the critical value of 2% (1, 25, 200 μM K) (Reuter & Robinson, 1997), the sodium concentration in the tissues increased by 4-5 times. This suggests that this ecotype may be relatively sodium-use efficient, potentially delaying the onset of deficiency symptoms by effectively utilizing sodium in the K/Na balance. Regarding sodium deficiency, many plants in the *Brassicaceae* family have been found to have an adequate Na concentration ranging from 0.1-1%. In some mustard species, this concentration can drop to as low as 0.02% (Reuter & Robinson, 1997). Although no Na deficiency was observed in CS28833 plants, the change in Na concentration is intriguing. In *Brassicaceae* plants, a K/Na ratio above 1.3% is identified as a critical toxicity threshold (Reuter & Robinson, 1997). Therefore, the increasing Na concentration might indicate a secondary defense mechanism to mitigate this toxicity. Additionally, the determining role of calcium in the regulation and function of Na and K in plant tissues may explain the increased Ca levels under K deficiency conditions compared to the control (Gutiérrez-Boem, 1995). A Ca/Na ratio above 0.3% in *Brassicaceae* tissues is also identified as a critical toxicity threshold (Reuter & Robinson, 1997). Studies have shown that increased Na concentration under sodicity or salinity conditions can lead to a corresponding increase in Ca concentration (Gutiérrez-Boem, 1995). It is also known that K, Ca, and Na are using unspecific transporters/channels during their root uptake. Consequently, there is competition among these cationic nutrients during root uptake (Rengel et al., 2022; Zörb et al., 2014). It is therefore not surprising why under low K supply

more Ca and Na are absorbed and accumulated in plants (Table 4.9). Hence, if a Na change linked to K deficiency occurred in CS28833, this change might indirectly cause an increase in Ca concentration. Indeed, the results in Table 4.9 align with this expectation (see the appendices for Na and Ca content (%) distribution data). Meanwhile, a study has demonstrated that oxidative stress induced by potassium (K^+) deprivation leads to a comprehensive enhancement of antioxidant and NADPH-producing systems in the halophyte *Cakile maritima*, a member of the *Brassicaceae* family, akin to *A. thaliana* (Houmani et al., 2022). Notably, numerous antioxidant enzymes exhibit increased activity in both leaves and roots under conditions of K deficiency. The increase in these antioxidative systems may have also triggered the upregulation of the *CESA4* gene.

By identifying and functionally characterizing the K^+ , NO_3^- , and $H_2PO_4^-$ transporters, crop varieties with high K^+ , NO_3^- , and $H_2PO_4^-$ acquisition efficiency may be genetically engineered, potentially resulting in a significant reduction in the quantity of fertilizer used. Such strategies should focus on the regulatory mechanisms of these transporters, rather than solely on the absorption processes of K^+ , NO_3^- , and $H_2PO_4^-$ (Chen et al., 2008). These three nutrients are far more crucial than the numerous other inorganic minerals that plants require due to their profound influence on plant growth and development. One of the main obstacles to crop production in many low-input agricultural systems worldwide is the poor availability of these three ingredients (Chen et al., 2008). Research should investigate whether the activity of the *CESA4* gene could contribute to developing plant species that are less sensitive to K and N deficiency conditions. However, before this, it is necessary to identify a series of relevant transporters to evaluate the plant's K mechanism. Supporting this, understanding the transcriptional regulatory mechanism is crucial, as the changes in *AtCESA4* activity observed in plants are examined through mRNA. Both plant K^+ channels and transporters undergo significant alterations in K deficiency due to developmental processes and environmental stressors (Chen et al., 2008). Induction of the *HAK/KT* transporter gene by K^+ depletion has been demonstrated (Rubio et al., 2000). Except for the regulatory subunit *AtKCI*, whose expression rises in leaf peripheral tissues under salt stress, the transcription of most *Shaker* K^+ channels in the cell membranes of *Arabidopsis* is unaffected by low K^+ stress (Pilot et al., 2003). Certain data indicate that plant hormones may also significantly impact the transcription of K^+ channels (Chérel et al., 2002; Pilot et al., 2003). Therefore, the striking changes in *CESA4* expression observed with alterations in K levels should be investigated to determine if they are related to K transporters.

The exogenous application of potassium (K) has been shown to increase the biosynthesis of cellulose derivatives in numerous studies (Huang et al., 2023; Yin et al., 2022). In contrast, there are very few studies on the changes in genes responsible for cellulose production in the presence or absence of potassium (Armengaud et al., 2010). This study is one of the few that highlights significant and striking changes in genes not directly associated with potassium in plants under potassium deficiency.

5.2. Association between *CESA4* Expression Level and Compartmentation of Potassium in Different Plant Tissues

Generally, the reduction of chlorosis and necrosis in young leaves and the variation of potassium allocation between tissues of K-deficiency tolerant-like ecotypes raised the question of whether there would be any changes in the *CESA4* gene. As observed in Figures 4.2 and 4.3, the increasing symptoms of potassium deficiency primarily affected older tissues. In early flowering accessions (CS28833, CS76199), stem length varied with different potassium conditions. When evaluating inflorescence lengths, it was observed that plants exhibited the fastest flowering under the most deficient conditions. When investigating whether this change would lead to any alterations in the *CESA4* gene, the CS28812 ecotype at the vegetative stage and the CS28833 ecotype at the early reproductive stage exhibited distinct patterns across different tissues (Figure 4.23). In the CS28812 ecotype, no significant change in *CESA4* expression was observed under 187.5 μM (moderate) and 46.9 μM (marginal) K conditions, while approximately a two-fold increase in expression was noted in older leaves under 750 μM (sub-optimal) K conditions. Conversely, in the CS28833 ecotype, moderate potassium conditions led to the highest *CESA4* expression across all tissues, with the highest expression observed in young leaves among tissues. Both showed down-regulation of the *CESA4* gene in old leaves. Strong carbohydrate accumulation occurs in the source leaves due to the reduction in photosynthetic activity observed in potassium deficiency and the restriction of sucrose transfer from the source to the sink organs. This leads to an excessive decrease in the photosynthetic electron transport chain, which increases the production of reactive oxygen species (ROS) (Cakmak, 2005). This can similarly be shown to cause a decrease in *CESA4* activity in older leaves.

CS28833 accession, which has higher phenotypic plasticity than others, at the early reproductive stage (4 weeks old), the longest shoot was observed at 1 μM K, while the shortest

was in 2000 μM K supply (Figure 4.4). However, as the plants transitioned to the late reproductive stage and began senescence or autophagy, significant changes in the inflorescence parts were noted as expected (Pottier et al., 2019). The 2000 μM K supply plants developed significantly longer and more numerous secondary, tertiary, and quaternary inflorescences (Figure 4.5). In order to assess this, the rosette size and shoot elongation data (Figure 4.1 and Table 4.2) demonstrated statistically significant changes occurring during both the early and late reproductive stages, confirming the purpose of this test. This is actually an indication that plants have evolved to produce the most beneficial response to the perpetuation of their species. As a result of nutrient remobilization, which comes from the tendency of plants to load nutrients into seeds, there are fewer nutrients in senescent organs and more in young organs (Pottier et al., 2014; Shi et al., 2012). In the K-deficient samples, chlorosis and cell death in cauline leaves could be attributed to the inadequate remobilization of K during this stage (Pottier et al., 2019). Potassium (K) tends to be mobilized from source (older) leaves to new growth or developing seeds, as are other nutrients like N, P, S, and metals. The nutrient mobilization linked to senescence enables the recovery of nutrients from aged or injured leaves, offering the evident adaptive benefit of recycling nutrients that can be in short supply in the surroundings or require high energy expenditure (Leopold, 1961). Since little is known about the genes that regulate and maintain the mobilization of products from senescent to young tissues (Himmelblau & Amasino, 2001), examining the role of *CESA4* in this regard could be a valuable contribution to the literature. Understanding this whole mechanism is important to improve seed nutrient contents and to obtain qualified and fortified grains, especially in agricultural crops.

To elucidate these findings, striking variations were observed in the dry matter yield, potassium content distribution, and mineral element analysis results of CS28833 plants at the early-reproductive stage (Tables 4.7, 4.8, 4.9, and 4.10). Tables 4.7 and 4.8 show that the maximum dry matter was observed in the 25 μM and 200 μM K samples, while the dry matter amount decreased in the highest K environment. It was observed that the dry matter weight significantly decreased at the highest K level. In a study conducted on apple dwarf rootstock seedlings, it was shown that the dry matter weight of plants treated with 0 mM and 12 mM K was statistically equal (Xu et al., 2020). Plant dry weight increased from 0 mM K to 6 mM K application but decreased as the supply increased from 6 mM K to 12 mM K. In these plants, the development of photosynthetic parameters, Rubisco, SS, SPS, NR activity, and ^{13}C assimilation consistently showed a similar pattern. This indicates that insufficient or excessive

K supply can inhibit the metabolic or genetic functions of plants and the transport of photosynthetic products from sources to sinks or growth tissues. Therefore, an overdose of potassium might create a "toxic" effect by hindering the plant's access to other elements. In this study, all data has shown that 0 to 12 mM K and 3 to 9 mM K exhibited equivalent responses like conjugates. As already mentioned above, high levels of K may induce a deficiency of other cationic nutrients due to the antagonistic effects of high root uptake of Ca and Mg (Garcia et al., 2022; Rengel et al., 2022; Zörb et al., 2014). Table 4.9 shows that indeed, high levels of K application have a distinct inhibitory effect on root uptake and shoot accumulation of Ca, Mg, and Na. One explanation for why high K applications had a reducing effect on shoot growth of plants could be related to impairments in use of Ca and Mg in cellular functions by excess K (Garcia et al., 2022). These results suggest that determining the "conjugate" values of nutrient elements like potassium in each plant could reduce fertilization requirements. In another study conducted on *A. thaliana* roots, no significant changes were observed in primary lateral root intensity and secondary lateral root length, as K deficiency became more severe (Gruber et al., 2013). This suggests that alternative mechanisms may be in place that prevent the plant from slowing down its growth under potassium deficiency.

As shown in Table 4.9, it is an expected result that there was a significant increase observed in the growth tissue, specifically the stem, of the CS28833 accession grown in environments with potassium concentrations of 1 μ M, 25 μ M, 200 μ M, and 2000 μ M (Leopold, 1961; Pottier et al., 2014, 2019). The notable outcome is that there was only a variation in potassium concentration among the treatments. Therefore, if there were changes in genes related to nutrition, considering that the only variable in the growth conditions was the amount of potassium supplementation, it can be inferred that this change stemmed from potassium-associated mechanisms. In one study, a salt-tolerant tomato accession had a higher Na-substitution capacity when K was present in limited amounts. It was observed that when the Amberly Cross tomato cultivar was grown under low K conditions when Na was present, most of the Na transported to the leaves accumulated in the petioles rather than in the leaf lamina (Figdore et al., 1987). The localization of sodium at different sites of CS28833 can be investigated. Moreover, in a study conducted on Virginia and Burley tobacco varieties, the cellulose content (%) in the stem is approximately twice that of the leaves (Kulić & Radojičić, 2011). In another study, the cellulose content (%) in the stems of transgenic rice plants was found to be 1.5 times higher than that in the leaves (Fan et al., 2018). *CESA4*, one the major actors of cellulose biosynthesis in plants, is a gene that exhibits high activity, particularly in

the secondary cell walls of many plant tissues. Except for flower tissue, significantly high *CESA4* activity can be observed in other tissues (Beekman et al., 2002). However, since potassium (K) plays a significant role in the transportation of many photosynthates, potassium deficiency in plants may lead to a reduction in the transport from leaves to stems, resulting in a decrease in cellulose content in the stem (Marschner et al., 1996). While several researchers (Degl'Innocenti et al., 2009; Gerardeaux et al., 2010; Zhao et al., 2001) claim that K⁺ deficit results in a decrease in leaf area, Jordan-Meille and Pellerin (2004) found that K⁺ deficiency limits the elongation of leaves in maize plants, which in turn influences leaf growth. demonstrated that it had nothing to do with the region's restrictions on the supply of carbohydrates. According to Gerardeaux et al. (2010), sugar starvation of the pharyngeal tissues—possibly via sugar signaling—may be the cause of cotton's declining organ size (leaves, internodes), rather than the absence of photoassimilates and cell turgor. Based on this information, it can be said that more studies are needed to determine whether sugar production is restricted in K deficiency.

The potassium content (%) distribution in leaves and inflorescence stems in Table 4.10 shows that as the K supply increases, the amount of potassium in the leaves also increases. Leaves are source organs where photosynthesis predominantly occurs, making them the areas with the highest demand for potassium under healthy conditions (Kirkby, 2023). On the other hand, as the K supply decreases, more than 65% of the total K content is accumulated in the stem. This indicates that the plant prioritizes nourishing tissues such as seeds and apical meristems by transferring nutrients from aging tissues to these areas, as mentioned above. In the late-reproductive stage of CS28833 plants, higher expression levels were observed in the stem under all potassium deficiency conditions (Figure 4.24). Based on this result, it can be inferred that as the potassium content in the tissue increases, *CESA4* activity may also increase.

To investigate whether this phenomenon is specific to *A. thaliana* and to evaluate its applicability in agricultural crops, the activity of the *CESA4* gene was examined in different tissues of bread wheat (*Triticum aestivum*) plants grown under potassium deficiency. In bread wheat, there are 22 *CESA* genes, including homoeologs across the three genomes. *TaCESA4*, 7, and 8 have been identified as specific to secondary cell wall (SCW) formation, while *TaCESA1*, 2, and 6 are specific to primary cell wall (PCW) formation. *TaCESA3*, 5, and 9 are largely redundant orthologs to PCW *CESAs* based on ortholog analysis. Sequence similarity between *Arabidopsis CESA4* and its orthologs from maize, rice, wheat, and barley has been found to range from 73% to 74% (Kaur et al., 2016). The activity of the *CESA4* gene in wheat

grown under potassium-deficient conditions (0 mg kg^{-1}) is significantly higher compared to wheat grown under adequate potassium conditions (300 mg kg^{-1}), similar to the observations in *A. thaliana* (Figure 4.25). The study by Kaur

and colleagues (2016) indicates that these three SCW genes (*TaCesA4*, 7, 8) and their homoeologs are co-expressed in mature root tissues. It is expected that the genes *TaCesA4A*, *B*, *D*, *TaCesA7B*, *D*, and *TaCesA8B*, *D* will exhibit low expression levels during PCW formation and high expression levels in mature tissues, such as stems immediately after anthesis. Accordingly, as shown in Figure 4.25, it is expected that the relatively more mature tissues, such as the second leaf and second stem, would exhibit higher *CESA4* expression compared to the flag leaf and flag stem. This is because secondary cell wall production is higher in mature tissues, whereas younger tissues predominantly have primary cell walls (Andrews et al., 1999). In a study examining potassium distribution in different wheat genotypes, it was found that under normal conditions, the potassium content in the flag leaf of all the genotypes of interest was significantly lower than that in the third leaf (Rahnama et al., 2011). Asif and colleagues (2018) also reported that in wheat grown with potassium deficiency, the allocation of potassium shifted more toward the grain. Additionally, the stem/leaf potassium ratio increased by 25%. Therefore, under deficiency conditions, the potassium content in the leaves is expected to be lower than that in the stem of bread wheat plants.

5.3. The Potential Correlations of Potassium and the *CESA4* Gene with Flowering Time

Looking back to where the story began, early flowering was one of the most notable physiological changes observed in *CESA4* expression. Accessions that flowered early showed high *CESA4* expression under low potassium conditions in nearly all replicates. However, late-flowering ecotypes reduced their *CESA4* expression as their potassium support decreased (see Section 4.5). This situation strengthens the possibility of a connection between flowering and either the *CESA4* gene or potassium.

The loss of function of *AKT2/3* (a potassium channel) in *Arabidopsis* changes the flowering time characteristic, indicating that the availability of potassium impacts the flowering time (Wang et al., 2021). Other research indicates that *akt2*, *cb14* (calcineurin B-like proteins), and *cipk6* (CBL-interacting protein kinase 6) loss-of-function mutants also display delayed flowering under short-day conditions, hinting at the modulation of ion channels in the

flowering pathway and potassium channel activity through a calcium sensor kinase (Held et al., 2011). Negishi et al. (2018) discovered that mutant plants deficient in the *sodium-potassium root defective1* (*NaKR1*) gene exhibited excessive accumulation of Na⁺ and K⁺ and displayed delayed flowering. NaKR1 is involved in the phloem transport of the flowering locus T (*FT*) protein, which controls flowering time, (Zhu et al., 2016) and enhances the transcription level of *FT* under long-day conditions in a potassium concentration-dependent manner. Therefore, the observation of reduced *FT* expression and late flowering in certain mutants with high potassium content suggests that increased potassium levels may suppress flowering (Negishi et al., 2018). Additionally, this study indicated that plants with high potassium content produced significantly more rosette and cauline leaves compared to wild type (Col-0), indicating that the plants were larger and more developed like the results in Figure 4.1. The fact that increased potassium content in *A. thaliana*, even due to a mutation, results in late flowering suggests that the deficiency of this mineral element could potentially enhance flowering. In *Jatropha curcas*, the overexpression of the *Flowering Locus T* (*FT*) gene, which controls flowering time, has resulted in the upregulation of *cellulose synthase* genes *CESA4*, *CESA7*, and *CESA8* in cell walls (Wu et al., 2022). The counterparts of transcription factors regulating the circadian clock, flowering time, plant defense, and oxidative stress of *A. thaliana* in sugar cane have been observed to increase the expression levels of *CESA4* and *CESA7* (Hosaka et al., 2021). In summary, existing evidence suggests that the expression of the *CESA4* gene, involved in secondary cell wall formation, is associated with flowering time and fiber content in plants like sugarcane and *Jatropha*. The upregulation of *CESA4* appears to coincide with flowering and increased fiber accumulation.

5.4. CRISPR/Cas9-Mediated Engineering of *CESA4* Gene Utilizing PEI-SWNT

To ascertain whether the phenotypic changes resulting from the specified potassium nutrition conditions are attributable to the altered expression levels of the *CESA4* gene, the gene was knocked-out by a CRISPR/Cas9-mediated bioengineering approach. While this knockout remains in its initial stages and it is premature to conduct a functional analysis, the progress achieved thus far appears promising.

Initially, to verify the system, a *phytoene desaturase 3* (*PDS3*) knockout study was conducted using floral dipping transformation (FDT), which achieved higher efficiency (15-20%) than reported in the literature (Song et al., 2018; Verma et al., 2008; Zhang et al., 2006) (Figure

4.17). The *PDS3* gene is a suitable candidate for such determination applications (Yan et al., 2015). When the transformant seeds were placed in a selection medium and germinated, rapid bleaching of the cotyledons was observed, providing results within a week. Additionally, several concentrations of polyethyleneimine functionalized single-walled carbon nanotubes (PEI-SWNT) were determined to be non-toxic, offering a novel, viable and rapid transformation option compared to the literature. While *Agrobacterium tumefaciens*-mediated T-DNA insertion leads to the formation of transgenic plants, there is no clear evidence that PEI-SWNT directly edits the genome of the host (Frank et al., 2019). Therefore, it does not possess the disadvantages associated with the use of transgenic plants, which often raise concerns. Additionally, *A. tumefaciens*-mediated transformation is not a rapid and practical method in terms of applicability (Frank et al., 2019; Zhang et al., 2006). The bacterial growth process, the risk of contamination during application, the necessary cleaning procedures post-application, and the damage inflicted on the plant make this method laborious. In contrast, PEI-SWNT emerges as a cost-effective and time-saving approach. This method eliminates the risks associated with sterility or contamination and can bind to plasmids within half an hour, thereby significantly saving time. Furthermore, it produces minimal waste and does not require disinfectants or similar chemicals used with *A. tumefaciens*, making it a relatively environmentally friendly and sustainable solution.

However, this method has some limitations that need to be addressed: (i) the multiple bands formation in gel electrophoresis of the plasmid construct has not been resolved (Figure 4.12). The consistent presence of the insert band without complete disappearance in any optimization indicates a low quantity of plasmid DNA in the ligation. The bands observed within the expected range of the plasmid weight may be due to flanking or nested ligation of the plasmid, but it is yet to be determined whether this poses a problematic consequence in transformation (Balavoine, 1996). (ii) due to the low yield and content of the constructs, the colony formation time of resistant bacteria after *Escherichia coli* transformation was doubled (Froger & Hall, 2007), causing some delay (Figure 4.13). When the duration of plating is extended, it becomes necessary to continuously maintain the integrity and activity of the antibiotic in the medium and resort to secondary verification methods to ensure that the resulting *E. coli* colonies possess the expected construct. (iii) not working with a gene like *PDS3*, which does not induce quick physiological changes in the cotyledons, makes the selection of transformants challenging. As presented in Figure 4.19, the segregation of transformants results in a lengthy process lasting up to 20 days. The extended duration of this process necessitates weekly changes of the agar

medium where the seedlings are placed. During these changes, avoiding damage to the roots of seedlings is highly challenging and requires gaining expertise and proficiency in handling such situations. Otherwise, there is a risk of causing harm to the roots or shoots of the plant, potentially leading to the loss of transformants. Nonetheless, at the conclusion of this process, it is necessary to confirm homozygosity, possibly through methods like PCR, as there may still be plant species that do not exhibit phenotypic changes and remain non-transformed.

5.5. Conclusion

This study aimed to characterize various potassium-dependent functions of the *CESA4* gene. The tests conducted on the *CESA4* gene, which exhibited increased expression under potassium deficiency, can be said to support the hypotheses of this thesis. In summary, potassium's role in sugar transport renders these outcomes unsurprising. Additionally, the rate of photosynthesis decreases under potassium deficiency. In such conditions, where sugar production and transport are restricted, the plant's cellulose production is likely to decrease. However, in a plant with growth requirements, the production of essential structural components like cellulose is inevitable. Therefore, the plant may attempt to obtain sugar substrates by mobilizing potassium ions to growing organs. On the other hand, the increase in cellulose biosynthesis should not be confused with an increase in the expression of *cellulose synthase* genes. Consequently, increased production of cellulose is not necessarily expected. The key point here is not the increased production of this metabolite, but rather the heightened demand for its production by the plant. With further supporting studies, it can be said that this research will reach its full potential.

This study is one of the few that highlights significant and striking changes in the *CESA4* gene, which is not directly associated with potassium, in plants under potassium deficiency. Additionally, it is one of the rare studies suggesting that potassium or *CESA4* may interact with flowering and that potassium may more strongly support the production of metabolites under deficient conditions rather than adequate ones. This is a highly beneficial outcome for the establishment of sustainable agricultural systems. Lastly, the study has strong implications regarding the dramatic changes in potassium allocation under deficiency conditions. Considering all these factors, it is foreseeable that this research will open new doors in many important areas.

5.6. Future Prospects

Given that this study is a preliminary investigation into gene function characterization, however, there are some questions still unanswered. Nevertheless, the promising results deserve more in-depth study. To validate the hypotheses and establish robust theories, increased trials and further research are required as follows:

To understand the role of the *CESA4* gene in potassium metabolism:

- A comprehensive CRISPR/Cas9-mediated *CESA4* knock-out study should be conducted.
- The relationship between K⁺ pumps and CESA enzyme complexes should be examined.
- It should be investigated whether there is a need for a potassium-dependent compound in CESA enzymatic reactions.

To determine if there is a connection with flowering:

- Periodic analyses of *CESA4* expression throughout the flowering process should be conducted.

To understand if the related functions are tissue-dependent:

- Element analysis and RT-qPCR should be performed on distinct tissues from 4 and 5-week-old plants.
- Elemental analysis and RT-qPCR should be conducted on various tissues of wheat plants.
- Analyses of soluble sugar and cellulose content should be performed in these tissues.

BIBLIOGRAPHY

- Alonso-Blanco, C., El-Assal, S. E. D., Coupland, G., & Koornneef, M. (1998). Analysis of natural allelic variation at flowering time loci in the Landsberg erecta and Cape Verde Islands ecotypes of *Arabidopsis thaliana*. *Genetics*, *149*(2), 749–764. <https://doi.org/10.1093/GENETICS/149.2.749>
- Andrews, M., Sprent, J. I., Raven, J. A., & Eady, P. E. (1999). Relationships between shoot to root ratio, growth and leaf soluble protein concentration of *Pisum sativum*, *Phaseolus vulgaris* and *Triticum aestivum* under different nutrient deficiencies. *Plant, Cell & Environment*, *22*(8), 949–958. <https://doi.org/10.1046/J.1365-3040.1999.00452.X>
- Armengaud, P., Breitling, R., & Amtmann, A. (2010). Coronatine-insensitive 1 (COI1) mediates transcriptional responses of *Arabidopsis thaliana* to external potassium supply. *Molecular Plant*, *3*(2), 390–405. <https://doi.org/10.1093/MP/SSQ012>
- Arnon, D. I. (1950). Criteria of essentiality of inorganic micronutrients for plants, with special reference to molybdenum. *Lotsya*, *3*, 31–38.
- Ashley, M. K., Grant, M., & Grabov, A. (2006). Plant responses to potassium deficiencies: a role for potassium transport proteins. *Journal of Experimental Botany*, *57*(2), 425–436. <https://doi.org/10.1093/JXB/ERJ034>
- Atwell, S., Huang, Y. S., Vilhjálmsson, B. J., Willems, G., Horton, M., Li, Y., Meng, D., Platt, A., Tarone, A. M., Hu, T. T., Jiang, R., Mulyati, N. W., Zhang, X., Amer, M. A., Baxter, I., Brachi, B., Chory, J., Dean, C., Debieu, M., ... Nordborg, M. (2010). Genome-wide association study of 107 phenotypes in *Arabidopsis thaliana* inbred lines. *Nature* *2010* *465*:7298, *465*(7298), 627–631. <https://doi.org/10.1038/nature08800>
- Balavoine, G. (1996). Identification of members of several homeobox genes in a planarian using a ligation-mediated polymerase chain reaction technique. *Nucleic Acids Research*, *24*(8), 1547–1553. <https://doi.org/10.1093/NAR/24.8.1547>
- Barber, J., & Andersson, B. (1992). Too much of a good thing: light can be bad for photosynthesis. *Trends in Biochemical Sciences*, *17*(2), 61–66. [https://doi.org/10.1016/0968-0004\(92\)90503-2](https://doi.org/10.1016/0968-0004(92)90503-2)

- Beeckman, T., Przemeck, G. K. H., Stamatiou, G., Lau, R., Terry, N., De Rycke, R., Inzé, D., & Berleth, T. (2002a). Genetic Complexity of Cellulose Synthase A Gene Function in Arabidopsis Embryogenesis. *Plant Physiology*, *130*(4), 1883. <https://doi.org/10.1104/PP.102.010603>
- Beeckman, T., Przemeck, G. K. H., Stamatiou, G., Lau, R., Terry, N., De Rycke, R., Inzé, D., & Berleth, T. (2002b). Genetic Complexity of Cellulose Synthase A Gene Function in Arabidopsis Embryogenesis. *Plant Physiology*, *130*(4), 1883. <https://doi.org/10.1104/PP.102.010603>
- Berg, B. (2000). Litter decomposition and organic matter turnover in northern forest soils. *Forest Ecology and Management*, *133*(1–2), 13–22. [https://doi.org/10.1016/S0378-1127\(99\)00294-7](https://doi.org/10.1016/S0378-1127(99)00294-7)
- Binder, D. L., Sander, D. H., & Walters, D. T. (2000). Maize Response to Time of Nitrogen Application as Affected by Level of Nitrogen Deficiency. *Agronomy Journal*, *92*(6), 1228–1236. <https://doi.org/10.2134/AGRONJ2000.9261228X>
- Cakmak, I. (2005). The role of potassium in alleviating detrimental effects of abiotic stresses in plants § Summary-Zusammenfassung. *J. Plant Nutr. Soil Sci*, *168*, 521–530. <https://doi.org/10.1002/jpln.200420485>
- Cakmak, I., Hengeler, C., & Marschner, H. (1994). Changes in phloem export of sucrose in leaves in response to phosphorus, potassium and magnesium deficiency in bean plants. *Journal of Experimental Botany*, *45*(9), 1251–1257. <https://doi.org/10.1093/JXB/45.9.1251>
- Carrillo-Inungaray, M. L., Hidalgo-Morales, M., Rodríguez-Jimenes, G. del C., García-Alvarado, M. Á., Ramírez-Lepe, M., Munguía, A. R., Robles-Olvera, V., Carrillo-Inungaray, M. L., Hidalgo-Morales, M., Rodríguez-Jimenes, G. del C., García-Alvarado, M. Á., Ramírez-Lepe, M., Munguía, A. R., & Robles-Olvera, V. (2014). Effect of Temperature, pH and Water Activity on *Penicillium digitatum* Growth. *Journal of Applied Mathematics and Physics*, *2*(10), 930–937. <https://doi.org/10.4236/JAMP.2014.210105>
- Carroll, A., Mansoori, N., Li, S., Lei, L., Vernhettes, S., Visser, R. G. F., Somerville, C., Gu, Y., & Trindade, L. M. (2012). Complexes with Mixed Primary and Secondary Cellulose Synthases Are Functional in Arabidopsis Plants. *Plant Physiology*, *160*(2), 726–737. <https://doi.org/10.1104/PP.112.199208>

- Chen, Y. F., Wang, Y., & Wu, W. H. (2008). Membrane Transporters for Nitrogen, Phosphate and Potassium Uptake in Plants. *Journal of Integrative Plant Biology*, *50*(7), 835–848. <https://doi.org/10.1111/J.1744-7909.2008.00707.X>
- Chérel, I., Michard, E., Platet, N., Mouline, K., Alcon, C., Sentenac, H., & Thibaud, J. B. (2002). Physical and Functional Interaction of the Arabidopsis K⁺ Channel AKT2 and Phosphatase AtPP2CA. *The Plant Cell*, *14*(5), 1133–1146. <https://doi.org/10.1105/TPC.000943>
- Chia, S. Y. Y., & Lim, M. W. W. (2022). A critical review on the influence of humidity for plant growth forecasting You may also like High-Performance QCM Humidity Sensors Using Carbon Nanostructure Material as Sensing Film A critical review on the influence of humidity for plant growth forecasting. *IOP Conf. Ser.: Mater. Sci. Eng*, *1257*, 12001. <https://doi.org/10.1088/1757-899X/1257/1/012001>
- Considine, M. J., & Foyer, C. H. (2021). Oxygen and reactive oxygen species-dependent regulation of plant growth and development. *Plant Physiology*, *186*(1), 79. <https://doi.org/10.1093/PLPHYS/KIAA077>
- Cutler, S., & Somerville, C. (1997). Cellulose synthesis: Cloning in silico. *Current Biology*, *7*, 108–111.
- Degl'Innocenti, E., Hafsi, C., Guidi, L., & Navari-Izzo, F. (2009). The effect of salinity on photosynthetic activity in potassium-deficient barley species. *Journal of Plant Physiology*, *166*(18), 1968–1981. <https://doi.org/10.1016/J.JPLPH.2009.06.013>
- Delmer, D. P. (1999). Cellulose biosynthesis: Exciting times for a difficult field of study. *Annual Review of Plant Biology*, *50*(Volume 50, 1999), 245–276. <https://doi.org/10.1146/ANNUREV.ARPLANT.50.1.245/CITE/REFWORKS>
- Demesa-Arevalo, E., Narasimhan, M., & Simon, R. (2024). Intercellular Communication in Shoot Meristems. *Annual Review of Plant Biology*, *75*(1). <https://doi.org/10.1146/ANNUREV-ARPLANT-070523-035342>
- Demirer, G. S., & Landry, M. P. (2021). *Efficient Transient Gene Knock-down in Tobacco Plants Using Carbon Nanocarriers*. <https://doi.org/10.21769/BioProtoc.3897>

- Ding, L., Wang, K. J., Jiang, G. M., Biswas, D. K., Xu, H., Li, L. F., & Li, Y. H. (2005). Effects of Nitrogen Deficiency on Photosynthetic Traits of Maize Hybrids Released in Different Years. *Annals of Botany*, *96*(5), 925–930. <https://doi.org/10.1093/AOB/MCI244>
- Doblin, M. S., Kurek, I., Jacob-Wilk, D., & Delmer, D. P. (2002). Cellulose Biosynthesis in Plants: from Genes to Rosettes. *Plant and Cell Physiology*, *43*(12), 1407–1420. <https://doi.org/10.1093/PCP/PCF164>
- DREW, M. C. (1975). COMPARISON OF THE EFFECTS OF A LOCALISED SUPPLY OF PHOSPHATE, NITRATE, AMMONIUM AND POTASSIUM ON THE GROWTH OF THE SEMINAL ROOT SYSTEM, AND THE SHOOT, IN BARLEY. *New Phytologist*, *75*(3), 479–490. <https://doi.org/10.1111/J.1469-8137.1975.TB01409.X>
- Eichert, T., & Fernández, V. (2023). Uptake and release of elements by leaves and other aerial plant parts. In *Marschner's Mineral Nutrition of Plants*. Elsevier. <https://doi.org/10.1016/B978-0-12-819773-8.00014-9>
- Erel, R., Ben-Gal, A., Dag, A., Schwartz, A., & Yermiyahu, U. (2014). Sodium replacement of potassium in physiological processes of olive trees (var. Barnea) as affected by drought. *Tree Physiology*, *34*(10), 1102–1117. <https://doi.org/10.1093/TREEPHYS/TPU081>
- Erol, N. O. (2019). *Genetic analysis of nitrogen use efficiency in Arabidopsis thaliana*.
- Eshed Williams, L. (2021). Genetics of Shoot Meristem and Shoot Regeneration. *Annual Review of Genetics*, *55*(Volume 55, 2021), 661–681. <https://doi.org/10.1146/ANNUREV-GENET-071719-020439/CITE/REFWORKS>
- Fan, C., Li, Y., Hu, Z., Hu, H., Wang, G., Li, A., Wang, Y., Tu, Y., Xia, T., Peng, L., & Feng, S. (2018). Ectopic expression of a novel OsExtensin-like gene consistently enhances plant lodging resistance by regulating cell elongation and cell wall thickening in rice. *Plant Biotechnology Journal*, *16*(1), 254–263. <https://doi.org/10.1111/PBI.12766>
- Fathi, A., Farnia, A., & Maleki, A. (2016). Effects of biological nitrogen and phosphorus fertilizers on vegetative characteristics, dry matter and yield of corn. *Applied Field Crops Research*, *29*(1), 1–7. <https://doi.org/10.22092/AJ.2016.109214>
- Fathi, A., & Zeidali, E. (2021). Conservation tillage and nitrogen fertilizer: a review of corn growth, yield and weed management. *Central Asian Journal of Plant Science Innovation*, *1*(3), 121–142. <https://doi.org/10.22034/CAJPSI.2021.03.01>

- Figdore, S. S., Gabelman, W. H., & Gerloff, G. C. (1987). The accumulation and distribution of sodium in tomato strains differing in potassium efficiency when grown under low-K stress. *Plant and Soil*, 99(1), 85–92. <https://doi.org/10.1007/BF02370156/METRICS>
- Fletcher, J. C. (2002). Shoot and floral meristem maintenance in arabidopsis. *Annual Review of Plant Biology*, 53(Volume 53, 2002), 45–66. <https://doi.org/10.1146/ANNUREV.ARPLANT.53.092701.143332/CITE/REFWORKS>
- Frank, U., Kublik, S., Mayer, D., Engel, M., Schloter, M., Durner, J., & Gaupels, F. (2019). A T-DNA mutant screen that combines high-throughput phenotyping with the efficient identification of mutated genes by targeted genome sequencing. *BMC Plant Biology*, 19(1). <https://doi.org/10.1186/S12870-019-2162-7>
- Froger, A., & Hall, J. E. (2007). Transformation of Plasmid DNA into E. coli Using the Heat Shock Method. *Journal of Visualized Experiments : JoVE*, 6(6). <https://doi.org/10.3791/253>
- Garcia, A., Crusciol, C. A. C., Rosolem, C. A., Bossolani, J. W., Nascimento, C. A. C., McCray, J. M., dos Reis, A. R., & Cakmak, I. (2022). Potassium-magnesium imbalance causes detrimental effects on growth, starch allocation and Rubisco activity in sugarcane plants. *Plant and Soil*, 472(1–2), 225–238. <https://doi.org/10.1007/S11104-021-05222-2/FIGURES/4>
- Gazzani, S., Gendall, A. R., Lister, C., & Dean, C. (2003). Analysis of the Molecular Basis of Flowering Time Variation in Arabidopsis Accessions. *Plant Physiology*, 132(2), 1107–1114. <https://doi.org/10.1104/PP.103.021212>
- Gerardeaux, E., Jordan-Meille, L., Constantin, J., Pellerin, S., & Dingkuhn, M. (2010). Changes in plant morphology and dry matter partitioning caused by potassium deficiency in *Gossypium hirsutum* (L.). *Environmental and Experimental Botany*, 67(3), 451–459. <https://doi.org/10.1016/J.ENVEXPBOT.2009.09.008>
- Gierth, M., Mäser, P., & Schroeder, J. I. (2005). The Potassium Transporter AtHAK5 Functions in K⁺ Deprivation-Induced High-Affinity K⁺ Uptake and AKT1 K⁺ Channel Contribution to K⁺ Uptake Kinetics in Arabidopsis Roots. *Plant Physiology*, 137(3), 1105–1114. <https://doi.org/10.1104/PP.104.057216>

- Gonneau, M., Desprez, T., Guillot, A., Vernhettes, S., & Höfte, H. (2014). Catalytic Subunit Stoichiometry within the Cellulose Synthase Complex. *Plant Physiology*, *166*(4), 1709–1712. <https://doi.org/10.1104/PP.114.250159>
- Goodman, H. M., Ecker, J. R., & Dean, C. (1995). The genome of *Arabidopsis thaliana*. *Proceedings of the National Academy of Sciences of the United States of America*, *92*(24), 10831–10835. <https://doi.org/10.1073/PNAS.92.24.10831>
- Gruber, B. D., Giehl, R. F. H., Friedel, S., & von Wirén, N. (2013a). Plasticity of the *Arabidopsis* Root System under Nutrient Deficiencies. *Plant Physiology*, *163*(1), 161–179. <https://doi.org/10.1104/PP.113.218453>
- Gruber, B. D., Giehl, R. F. H., Friedel, S., & von Wirén, N. (2013b). Plasticity of the *Arabidopsis* Root System under Nutrient Deficiencies. *Plant Physiology*, *163*(1), 161–179. <https://doi.org/10.1104/PP.113.218453>
- Gutiérrez-Boem, F. (1995). The K/Na and Ca/Na ratios and rapeseed yield, under soil salinity or sodicity. *Plant and Soil*. https://www.academia.edu/28659223/The_K_Na_and_Ca_Na_ratios_and_rapeseed_yield_under_soil_salinity_or_sodicity
- Hafsi, C., Atia, A., Lakhdar, A., Debez, A., & Abdelly, C. (2011). Differential Responses in Potassium Absorption and Use Efficiencies in the Halophytes *Catapodium rigidum* and *Hordeum maritimum* to Various Potassium Concentrations in the Medium. *Plant Production Science*, *14*(2), 135–140. <https://doi.org/10.1626/PPS.14.135>
- Hafsi, C., Debez, A., & Abdelly, C. (2014). Potassium deficiency in plants: Effects and signaling cascades. *Acta Physiologiae Plantarum*, *36*(5), 1055–1070. <https://doi.org/10.1007/S11738-014-1491-2/FIGURES/4>
- Hamamoto, S., Horie, T., Hauser, F., Deinlein, U., Schroeder, J. I., & Uozumi, N. (2015). HKT transporters mediate salt stress resistance in plants: from structure and function to the field. *Current Opinion in Biotechnology*, *32*, 113–120. <https://doi.org/10.1016/J.COPBIO.2014.11.025>
- Hashimoto, T., E Scherer, G. F., Van Der Straeten, D., Benková, E., Žádníková, P., Smet, D., & Zhu, Q. (2015). *Strategies of seedlings to overcome their sessile nature: auxin in mobility control*. <https://doi.org/10.3389/fpls.2015.00218>

- Hedrich, R. (2012). Ion channels in plants. *Physiological Reviews*, 92(4), 1777–1811. https://doi.org/10.1152/PHYSREV.00038.2011/SUPPL_FILE/VIDEO1.MP4
- Held, K., Pascaud, F., Eckert, C., Gajdanowicz, P., Hashimoto, K., Corratgé-Faillie, C., Offenborn, J. N., Lacombe, B., Dreyer, I., Thibaud, J. B., & Kudla, J. (2011). Calcium-dependent modulation and plasma membrane targeting of the AKT2 potassium channel by the CBL4/CIPK6 calcium sensor/protein kinase complex. *Cell Research* 2011 21:7, 21(7), 1116–1130. <https://doi.org/10.1038/cr.2011.50>
- Henriksen, T. M., & Breland, T. A. (1999). Nitrogen availability effects on carbon mineralization, fungal and bacterial growth, and enzyme activities during decomposition of wheat straw in soil. *Soil Biology and Biochemistry*, 31(8), 1121–1134. [https://doi.org/10.1016/S0038-0717\(99\)00030-9](https://doi.org/10.1016/S0038-0717(99)00030-9)
- Hepler, P. K., Vidali, L., & Cheung, A. Y. (2001). Polarized cell growth in higher plants. *Annual Review of Cell and Developmental Biology*, 17(Volume 17, 2001), 159–187. <https://doi.org/10.1146/ANNUREV.CELLBIO.17.1.159/CITE/REFWORKS>
- Himmelblau, E., & Amasino, R. M. (2001). Nutrients mobilized from leaves of *Arabidopsis thaliana* during leaf senescence. *Journal of Plant Physiology*, 158(10), 1317–1323. <https://doi.org/10.1078/0176-1617-00608>
- Horton, M. W., Hancock, A. M., Huang, Y. S., Toomajian, C., Atwell, S., Auton, A., Mulyati, N. W., Platt, A., Sperone, F. G., Vilhjálmsón, B. J., Nordborg, M., Borevitz, J. O., & Bergelson, J. (2012). Genome-wide patterns of genetic variation in worldwide *Arabidopsis thaliana* accessions from the RegMap panel. *Nature Genetics* 2012 44:2, 44(2), 212–216. <https://doi.org/10.1038/ng.1042>
- Hosaka, G. K., Correr, F. H., Silva, C. C., Sforça, D. A., Barreto, F. Z., Balsalobre, T. W. A., Pasha, A., Souza, A. P. de, Provart, N. J., Carneiro, M. S., & Margarido, G. R. A. (2021). Temporal Gene Expression in Apical Culms Shows Early Changes in Cell Wall Biosynthesis Genes in Sugarcane. *BioRxiv*, 2021.07.01.450585. <https://doi.org/10.1101/2021.07.01.450585>
- Houmani, H., Debez, A., de Freitas-Silva, L., Abdelly, C., Palma, J. M., & Corpas, F. J. (2022). Potassium (K⁺) Starvation-Induced Oxidative Stress Triggers a General Boost of Antioxidant and NADPH-Generating Systems in the Halophyte *Cakile maritima*.

Huang, B., Liao, Q., Fu, H., Ye, Z., Mao, Y., Luo, J., Wang, Y., Yuan, H., & Xin, J. (2023). Effect of potassium intake on cadmium transporters and root cell wall biosynthesis in sweet potato. *Ecotoxicology and Environmental Safety*, 250, 114501. <https://doi.org/10.1016/J.ECOENV.2023.114501>

Julkowska, M. M. (2015). *Tuned to Survive Salt Stress Induced Changes in Arabidopsis*.

Kaiser, W. M. (1982). Correlation between changes in photosynthetic activity and changes in total protoplast volume in leaf tissue from hygro-, meso- and xerophytes under osmotic stress. *Planta*, 154(6), 538–545. <https://doi.org/10.1007/BF00402997/METRICS>

Kaur, S., Dhugga, K. S., Gill, K., & Singh, J. (2016a). Novel Structural and Functional Motifs in cellulose synthase (CesA) Genes of Bread Wheat (*Triticum aestivum*, L.). *PLOS ONE*, 11(1), e0147046. <https://doi.org/10.1371/JOURNAL.PONE.0147046>

Kaur, S., Dhugga, K. S., Gill, K., & Singh, J. (2016b). *Novel Structural and Functional Motifs in cellulose synthase (CesA) Genes of Bread Wheat (Triticum aestivum, L.)*. <https://doi.org/10.1371/journal.pone.0147046>

Kenrick, P., & Crane, P. R. (1997). The origin and early evolution of plants on land. *Nature* 1997 389:6646, 389(6646), 33–39. <https://doi.org/10.1038/37918>

Kirkby, E. A. (2023). Introduction, definition, and classification of nutrients. *Marschner's Mineral Nutrition of Plants*, 3–9. <https://doi.org/10.1016/B978-0-12-819773-8.00016-2>

Knott, D. R. (2011). THE INHERITANCE OF RUST RESISTANCE. VI. THE TRANSFER OF STEM RUST RESISTANCE FROM AGROPYRON ELONGATUM TO COMMON WHEAT. *https://Doi.Org/10.4141/Cjps61-014*, 41(1), 109–123. <https://doi.org/10.4141/CJPS61-014>

Kulić, G. J., & Radojičić, V. B. (2011). ANALYSIS OF CELLULOSE CONTENT IN STALKS AND LEAVES OF LARGE LEAF TOBACCO. *Journal of Agricultural Sciences*, 56(3), 207–215. <https://doi.org/10.2298/JAS1103207K>

Kumar, M., Thammannagowda, S., Bulone, V., Chiang, V., Han, K. H., Joshi, C. P., Mansfield, S. D., Mellerowicz, E., Sundberg, B., Teeri, T., & Ellis, B. E. (2009). An update on the

- nomenclature for the cellulose synthase genes in *Populus*. *Trends in Plant Science*, *14*(5), 248–254. <https://doi.org/10.1016/j.tplants.2009.02.004>
- Kumar, P., Eriksen, R. L., Simko, I., Shi, A., & Mou, B. (2022). Insights into nitrogen metabolism in the wild and cultivated lettuce as revealed by transcriptome and weighted gene co-expression network analysis. *Scientific Reports* *2022 12:1*, *12*(1), 1–17. <https://doi.org/10.1038/s41598-022-13954-z>
- Lebaudy, A., Véry, A. A., & Sentenac, H. (2007). K⁺ channel activity in plants: Genes, regulations and functions. *FEBS Letters*, *581*(12), 2357–2366. <https://doi.org/10.1016/J.FEBSLET.2007.03.058>
- Leopold, A. C. (1961). Senescence in plant development. *Science*, *134*(3492), 1727–1732. <https://doi.org/10.1126/SCIENCE.134.3492.1727/ASSET/7608645D-3B2C-402A-9445-4F3DBC4964F0/ASSETS/SCIENCE.134.3492.1727.FP.PNG>
- Lersten, N. R. (2015). Morphology and Anatomy of the Wheat Plant. *Wheat and Wheat Improvement*, *13*, 33–75. <https://doi.org/10.2134/AGRONMONOGR13.2ED.C2>
- Levy, A. A., & Feldman, M. (2022). Evolution and origin of bread wheat. *The Plant Cell*, *34*(7), 2549. <https://doi.org/10.1093/PLCELL/KOAC130>
- Li, S., Bashline, L., Lei, L., & Gu, Y. (2014). Cellulose Synthesis and Its Regulation. *The Arabidopsis Book / American Society of Plant Biologists*, *12*, e0169. <https://doi.org/10.1199/TAB.0169>
- Li, W., Xu, G., Alli, A., & Yu, L. (2018). Plant HAK/KUP/KT K⁺ transporters: Function and regulation. *Seminars in Cell & Developmental Biology*, *74*, 133–141. <https://doi.org/10.1016/J.SEMCDB.2017.07.009>
- Li, X., Borsics, T., Harrington, H. M., & Christopher, D. A. (2005). Arabidopsis AtCNGC10 rescues potassium channel mutants of *E. coli*, yeast and Arabidopsis and is regulated by calcium / calmodulin and cyclic GMP in *E. coli*. *Functional Plant Biology*, *32*(7), 643–653. <https://doi.org/10.1071/FP04233>
- Li, Y., Huang, Y., Bergelson, J., Nordborg, M., & Borevitz, J. O. (2010). Association mapping of local climate-sensitive quantitative trait loci in *Arabidopsis thaliana*. *Proceedings of the National Academy of Sciences of the United States of America*, *107*(49), 21199–21204. https://doi.org/10.1073/PNAS.1007431107/SUPPL_FILE/PNAS.201007431SI.PDF

- Marschner, H. (1983). General Introduction to the Mineral Nutrition of Plants. *Inorganic Plant Nutrition*, 5–60. https://doi.org/10.1007/978-3-642-68885-0_2
- Marschner, H., Kirkby, E. A., & Cakmak, I. (1996). Effect of mineral nutritional status on shoot-root partitioning of photoassimilates and cycling of mineral nutrients. *Journal of Experimental Botany*, 47 Spec No(SPEC. ISS.), 1255–1263. https://doi.org/10.1093/JXB/47.SPECIAL_ISSUE.1255
- Mitchell-Olds, T. (2001). *Arabidopsis thaliana* and its wild relatives: a model system for ecology and evolution. *Trends in Ecology & Evolution*, 16(12), 693–700. [https://doi.org/10.1016/S0169-5347\(01\)02291-1](https://doi.org/10.1016/S0169-5347(01)02291-1)
- Morgan, J. L. W., Strumillo, J., & Zimmer, J. (2012). Crystallographic snapshot of cellulose synthesis and membrane translocation. *Nature* 2012 493:7431, 493(7431), 181–186. <https://doi.org/10.1038/nature11744>
- Morison, J. I. L., & Lawlor, D. W. (1999). Interactions between increasing CO₂ concentration and temperature on plant growth. *Plant, Cell & Environment*, 22(6), 659–682. <https://doi.org/10.1046/J.1365-3040.1999.00443.X>
- Mu, X., & Chen, Y. (2021). The physiological response of photosynthesis to nitrogen deficiency. *Plant Physiology and Biochemistry*, 158, 76–82. <https://doi.org/10.1016/J.PLAPHY.2020.11.019>
- Mutwil, M., Debolt, S., & Persson, S. (2008). Cellulose synthesis: a complex complex. *Current Opinion in Plant Biology*, 11(3), 252–257. <https://doi.org/10.1016/J.PBI.2008.03.007>
- Näsholm, T., Kielland, K., & Ganeteg, U. (2009). Uptake of organic nitrogen by plants. *New Phytologist*, 182(1), 31–48. <https://doi.org/10.1111/J.1469-8137.2008.02751.X>
- Negishi, K., Endo, M., Abe, M., & Araki, T. (2018). SODIUM POTASSIUM ROOT DEFECTIVE1 regulates FLOWERING LOCUS T expression via the microRNA156–SQUAMOSA PROMOTER BINDING PROTEIN-LIKE3 module in response to potassium conditions. *Plant and Cell Physiology*, 59(2), 404–413. <https://doi.org/10.1093/PCP/PCX199>
- Nieves-Cordones, M., Alemán, F., Martínez, V., & Rubio, F. (2014). K⁺ uptake in plant roots. The systems involved, their regulation and parallels in other organisms. *Journal of Plant Physiology*, 171(9), 688–695. <https://doi.org/10.1016/J.JPLPH.2013.09.021>

- Oosterhuis, D. M., Loka, D. A., Kawakami, E. M., & Pettigrew, W. T. (2014). The Physiology of Potassium in Crop Production. *Advances in Agronomy*, *126*, 203–233. <https://doi.org/10.1016/B978-0-12-800132-5.00003-1>
- Parvin, I., Mondal, C., Sultana, S., Sultana, N., Aminuzzaman, F. M., Parvin, I., Mondal, C., Sultana, S., Sultana, N., & Aminuzzaman, F. M. (2021). Pathological Survey on Early Leaf Blight of Tomato and In Vitro Effect of Culture Media, Temperature and pH on Growth and Sporulation of *Alternaria solani*. *Open Access Library Journal*, *8*(3), 1–17. <https://doi.org/10.4236/OALIB.1107219>
- Pilot, G., Gaymard, F., Mouline, K., Chérel, I., & Sentenac, H. (2003). Regulated expression of Arabidopsis Shaker K⁺ channel genes involved in K⁺ uptake and distribution in the plant. *Plant Molecular Biology*, *51*(5), 773–787. <https://doi.org/10.1023/A:1022597102282/METRICS>
- Plant - Evolution, Paleobotany, Photosynthesis* / *Britannica*. (n.d.). Retrieved May 28, 2024, from <https://www.britannica.com/plant/plant/Evolution-and-paleobotany>
- Pottier, M., Dumont, J., Masclaux-Daubresse, C., & Thomine, S. (2019). Autophagy is essential for optimal translocation of iron to seeds in Arabidopsis. *Journal of Experimental Botany*, *70*(3), 845–858. <https://doi.org/10.1093/JXB/ERY388>
- Pottier, M., Masclaux-Daubresse, C., Yoshimoto, K., & Thomine, S. (2014). Autophagy as a possible mechanism for micronutrient remobilization from leaves to seeds. *Frontiers in Plant Science*, *5*(JAN), 73624. <https://doi.org/10.3389/FPLS.2014.00011/BIBTEX>
- Rahnama, A., Poustini, K., Tavakkol-Afshari, R., Ahmadi, A., & Alizadeh, H. (2011). Growth Properties and Ion Distribution in Different Tissues of Bread Wheat Genotypes (*Triticum aestivum* L.) Differing in Salt Tolerance. *Journal of Agronomy and Crop Science*, *197*(1), 21–30. <https://doi.org/10.1111/J.1439-037X.2010.00437.X>
- Rayon, C., Olek, A. T., & Carpita, N. C. (2014). Towards Redesigning Cellulose Biosynthesis for Improved Bioenergy Feedstocks. *Plants and BioEnergy, Advances in Plant Biology*, *4*, 183–193. https://doi.org/10.1007/978-1-4614-9329-7_11
- Recous, S., Robin, D., Darwis, D., & Mary, B. (1995). Soil inorganic N availability: Effect on maize residue decomposition. *Soil Biology and Biochemistry*, *27*(12), 1529–1538. [https://doi.org/10.1016/0038-0717\(95\)00096-W](https://doi.org/10.1016/0038-0717(95)00096-W)

- Rengel, Z., Cakmak, I., & White, P. (2022). *Marschner's mineral nutrition of plants*. <https://books.google.com/books?hl=tr&lr=&id=YTOGEAAAQBAJ&oi=fnd&pg=PP1&ots=eLbtPgDUum&sig=6XU1CJqSxBV-o-36JKx85oTYnm4>
- Reuter, D. J., & Robinson, J. B. (1997). Plant Analysis: An Interpretation Manual. In *Plant Analysis: An Interpretation Manual*. CSIRO Publishing. <https://doi.org/10.1071/9780643101265>
- Riedelsberger, J., Miller, J. K., Valdebenito-Maturana, B., Piñeros, M. A., González, W., & Dreyer, I. (2021). Plant HKT Channels: An Updated View on Structure, Function and Gene Regulation. *International Journal of Molecular Sciences* 2021, Vol. 22, Page 1892, 22(4), 1892. <https://doi.org/10.3390/IJMS22041892>
- Rubio, F., Guillermo, S. M., & Rodríguez-Navarro, A. (2000). Cloning of Arabidopsis and barley cDNAs encoding HAK potassium transporters in root and shoot cells. *Physiologia Plantarum*, 109(1), 34–43. <https://doi.org/10.1034/J.1399-3054.2000.100106.X>
- Saxena, I. M., & Brown, R. M. (2000). Cellulose synthases and related enzymes. *Current Opinion in Plant Biology*, 3(6), 523–531. [https://doi.org/10.1016/S1369-5266\(00\)00125-4](https://doi.org/10.1016/S1369-5266(00)00125-4)
- Shamekhi, M. A., Mahdavi, H., Mirzadeh, H., Rabiee, A., Mohebbi-Kalhari, D., & Eslaminejad, M. B. (2017). Platelet-Rich Plasma Incorporated Nanostructures for Tissue Engineering Applications. In *Multifunctional Systems for Combined Delivery, Biosensing and Diagnostics*. Elsevier. <https://doi.org/10.1016/B978-0-323-52725-5.00011-3>
- Shi, R., Weber, G., Köster, J., Reza-Hajirezaei, M., Zou, C., Zhang, F., & von Wirén, N. (2012). Senescence-induced iron mobilization in source leaves of barley (*Hordeum vulgare*) plants. *The New Phytologist*, 195(2), 372–383. <https://doi.org/10.1111/J.1469-8137.2012.04165.X>
- Shin, R., & Schachtman, D. P. (2004). Hydrogen peroxide mediates plant root cell response to nutrient deprivation. *Proceedings of the National Academy of Sciences of the United States of America*, 101(23), 8827–8832. https://doi.org/10.1073/PNAS.0401707101/SUPPL_FILE/01707TABLE2.HTML
- Singh, P., Kumar, K., Jha, A. K., Yadava, P., Pal, M., Rakshit, S., & Singh, I. (2022). Global gene expression profiling under nitrogen stress identifies key genes involved in nitrogen

- stress adaptation in maize (*Zea mays* L.). *Scientific Reports*, 12(1), 4211. <https://doi.org/10.1038/S41598-022-07709-Z>
- SIGnAL : Salk Institute Genomic Analysis Laboratory Home Page*. (n.d.). Retrieved May 31, 2024, from <http://signal.salk.edu/>
- Slabaugh, E., Davis, J. K., Haigler, C. H., Yingling, Y. G., & Zimmer, J. (2014). Cellulose synthases: New insights from crystallography and modeling. *Trends in Plant Science*, 19(2), 99–106. <https://doi.org/10.1016/j.tplants.2013.09.009>
- Song, I., Kang, Y. J., Lee, Y. K., Myung, S. C., & Ko, K. (2018). Endoplasmic reticulum retention motif fused to recombinant anti-cancer monoclonal antibody (mAb) CO17-1A affects mAb expression and plant stress response. *PLoS ONE*, 13(9). <https://doi.org/10.1371/JOURNAL.PONE.0198978>
- Sticklen, M. B. (2008). Plant genetic engineering for biofuel production: towards affordable cellulosic ethanol. *Nature Reviews Genetics* 2008 9:6, 9(6), 433–443. <https://doi.org/10.1038/nrg2336>
- Tang, C., Han, M., Yang, X., Shen, T., Gao, Y., Wang, Y., Zhang, S., Chen, D., He, D., & Li, Y. C. (2023). Gene Expression, Enzyme Activity, Nitrogen Use Efficiency, and Yield of Rice Affected by Controlled-Release Nitrogen. *ACS Omega*, 8(26), 23772–23781. https://doi.org/10.1021/ACSOMEGA.3C02113/SUPPL_FILE/AO3C02113_SI_001.PDF
- Taylor, N. G., Howells, R. M., Huttly, A. K., Vickers, K., & Turner, S. R. (2003). Interactions among three distinct CesA proteins essential for cellulose synthesis. *Proceedings of the National Academy of Sciences*, 100(3), 1450–1455. <https://doi.org/10.1073/PNAS.0337628100>
- Tewari, R. K., Kumar, P., Tewari, N., Srivastava, S., & Sharma, P. N. (2004). Macronutrient deficiencies and differential antioxidant responses—influence on the activity and expression of superoxide dismutase in maize. *Plant Science*, 166(3), 687–694. <https://doi.org/10.1016/J.PLANTSCI.2003.11.004>
- The water-culture method for growing plants without soil : Hoagland, D. R. (Dennis Robert), 1884-1949 : Free Download, Borrow, and Streaming : Internet Archive*. (n.d.). Retrieved May 23, 2024, from <https://archive.org/details/watercultureme3450hoag>

- Verma, S. S., Chinnusamy, V., & Bansal, K. C. (2008). A simplified floral dip method for transformation of *Brassica napus* and *B. carinata*. *Journal of Plant Biochemistry and Biotechnology*, *17*(2), 197–200. <https://doi.org/10.1007/BF03263286>
- von Liebig, J. F. (1841). Die organische Chemie in ihrer Anwendung auf Agricultur und Physiologie. *Deutsches Textarchiv (Kernkorpus)*.
- Wang, Y., Chen, Y. F., & Wu, W. H. (2021). Potassium and phosphorus transport and signaling in plants. *Journal of Integrative Plant Biology*, *63*(1), 34–52. <https://doi.org/10.1111/JIPB.13053>
- White, P. J., & Karley, A. J. (2010). Potassium. *Plant Cell Monographs*, *17*, 199–224. https://doi.org/10.1007/978-3-642-10613-2_9
- Wiser, L., Blom, T. J., Wisner, L., & Blom, T. J. (2016). The Effect of Nitrogen and Phosphorus Ratios and Electrical Conductivity on Plant Growth. *American Journal of Plant Sciences*, *7*(12), 1590–1599. <https://doi.org/10.4236/AJPS.2016.712150>
- Wu, J., Wu, Q., Bo, Z., Zhu, X., Zhang, J., Li, Q., & Kong, W. (2022). Comprehensive Effects of Flowering Locus T-Mediated Stem Growth in Tobacco. *Frontiers in Plant Science*, *13*, 922919. <https://doi.org/10.3389/FPLS.2022.922919/FULL>
- Xu, X., Du, X., Wang, F., Sha, J., Chen, Q., Tian, G., Zhu, Z., Ge, S., & Jiang, Y. (2020). Effects of Potassium Levels on Plant Growth, Accumulation and Distribution of Carbon, and Nitrate Metabolism in Apple Dwarf Rootstock Seedlings. *Frontiers in Plant Science*, *11*, 534048. <https://doi.org/10.3389/FPLS.2020.00904/BIBTEX>
- Yan, L., Wei, S., Wu, Y., Hu, R., Li, H., Yang, W., & Xie, Q. (2015). High-Efficiency Genome Editing in Arabidopsis Using YAO Promoter-Driven CRISPR/Cas9 System. *Molecular Plant*, *8*(12), 1820–1823. <https://doi.org/10.1016/J.MOLP.2015.10.004>
- Yin, A., Shen, C., Huang, Y., Fu, H., Liao, Q., Xin, J., & Huang, B. (2022). Transcriptomic analyses of sweet potato in response to Cd exposure and protective effects of K on Cd-induced physiological alterations. *Environmental Science and Pollution Research*, *29*(24), 36824–36838. <https://doi.org/10.1007/S11356-021-18144-4/FIGURES/8>
- Zebanhl, B. J., Sheard, R. W., Zebanhl, B. J., & Sheard, R. W. (2011). Influence of rate and timing of nitrogen fertilization on yield and quality of hard red winter wheat in Ontario. <https://doi.org/10.4141/Cjps92-002>, *72*(1), 13–19. <https://doi.org/10.4141/CJPS92-002>

- Zhang, X., Henriques, R., Lin, S. S., Niu, Q. W., & Chua, N. H. (2006). Agrobacterium-mediated transformation of *Arabidopsis thaliana* using the floral dip method. *Nature Protocols* 2006 1:2, 1(2), 641–646. <https://doi.org/10.1038/nprot.2006.97>
- Zhao, D., Oosterhuis, D. M., & Bednarz, C. W. (2001). Influence of potassium deficiency on photosynthesis, chlorophyll content, and chloroplast ultrastructure of cotton plants. *Photosynthetica*, 39(1), 103–109. <https://doi.org/10.1023/A:1012404204910/METRICS>
- Zhi, H., Zhou, S., Pan, W., Shang, Y., Zeng, Z., & Zhang, H. (2022). The Promising Nanovectors for Gene Delivery in Plant Genome Engineering. *International Journal of Molecular Sciences*, 23(15). <https://doi.org/10.3390/IJMS23158501>
- Zhu, Y., Liu, L., Shen, L., & Yu, H. (2016). NaKR1 regulates long-distance movement of FLOWERING LOCUS T in *Arabidopsis*. *Nature Plants* 2016 2:6, 2(6), 1–10. <https://doi.org/10.1038/nplants.2016.75>
- Zörb, C., Senbayram, M., & Peiter, E. (2014). Potassium in agriculture – Status and perspectives. *Journal of Plant Physiology*, 171(9), 656–669. <https://doi.org/10.1016/J.JPLPH.2013.08.008>

APPENDICES

Primer sequences used in this study are listed below.

>AT5G13550_Left_primer

TCCAGGGGTATAGCATTGCC

>AT5G13550_Right_primer

GAGAGATGGAAGGCGGATGA

>AT5G24320_Left_primer

TTTACGCCTGTACTCTCCGG

>AT5G24320_Right_primer

AGATGACTCCGACGTTCTCC

>AT5G44030_Left_primer

CAATGACCTCTGGCGTAACG

>AT5G44030_Right_primer

CTCCAAACTCATCGGCTTCG

>LBb1.3

ATTTTGCCGATTTTCGGAAC

>SALK_084627_LP

TCTTCCACCAAATCTTGTTGC

>SALK_084627_RP

GCTTCAAAGTCTTTCCCAAC

>SALK_110333_LP

AACCATATGCTTGCGAAATTG

>SALK_110333_RP

AAAACCTTTTCCTTTGTCAACCAC

>Taestivum_CesA4_3D_Fwd

CTCTCCAATGCCGCAACAAT

>Taestivum_CesA4_3D_Rev

CCGCAAAGAGATGAGCAGAC

>Taestivum_CesA4_3A_Fwd

ACGATTTTGGGTGAGTTGGC

>Taestivum_CesA4_3A_Rev

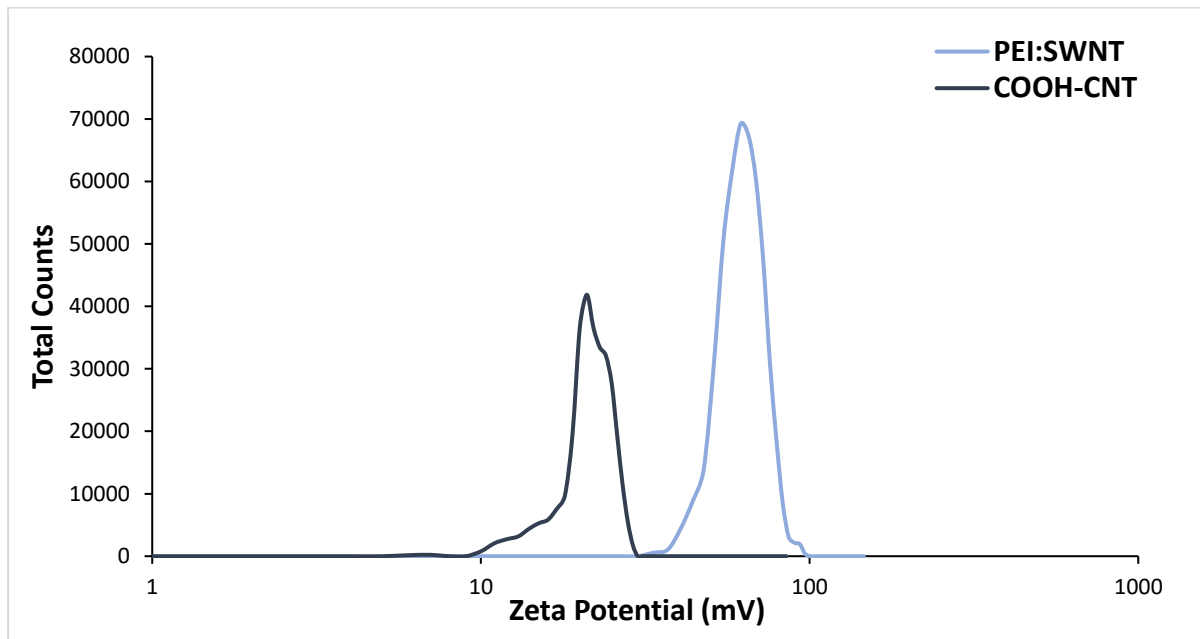
ACGGTAGTGGAAGAAGAGCC

>Taestivum_CesA4_3B_Fwd
AGGGGCTATGAATGCTCTGG
>Taestivum_CesA4_3B_Rev
AGGGTCCATCATGAAGCACA
>Taestivum_TUB_Fwd
CCCTGAGGTTTGATGGTGCT
>Taestivum_TUB_Rev
TGGTGATCTCAGCAACGGAC
>Taestivum_ACT_Fwd
GGAGAAGCTCGCTTACGTG
>Taestivum_ACT_Rev
GGGCACCTGAACCTTTCTGA
>gRNA5_7_Fwd
GTCTTCTCACCGCAAGTTC
>gRNA5_7_Rev
CAGAATTGCTCGTTACGCCA
>gRNA8_Fwd
ACGCCAACAGAAACATCGTC
>gRNA8_Rev
CGACGGCCAACAATCACAT
>AT_EF1ALPHA_F
TTCACCCTTGGTGTCAAGCA
>AT_EF1ALPHA_R
TTTCATCGTACCTGGCCTTGCA

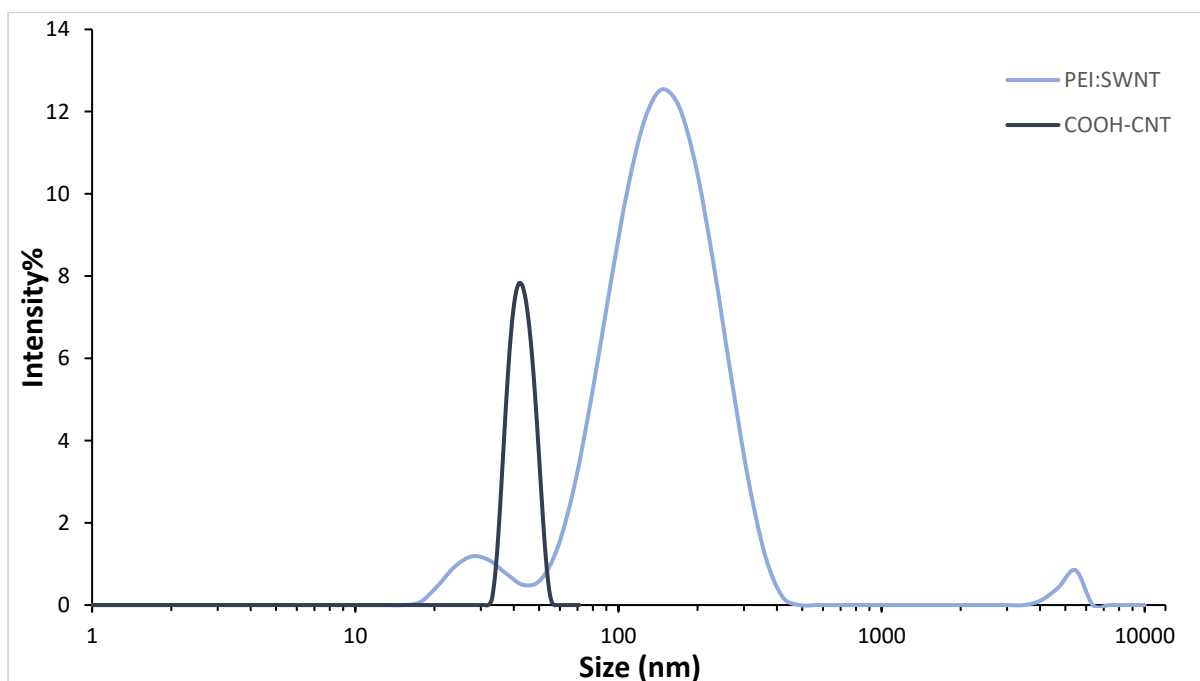
Appendix Table 1. Sodium (Na) and calcium (Ca) distribution in CS28833 tissues under K-deficiency (n=2).

K dose	Tissue	Na Content		Ca Content	
		Distribution	%	Distribution	%
1 μ M	Stem	41,3	\pm 0,03	17,8	\pm 0,02
	Leaf	58,7	\pm 0,03	82,2	\pm 0,02
25 μ M	Stem	21,9	\pm 0,01	12,7	\pm 0,00
	Leaf	78,1	\pm 0,01	87,3	\pm 0,00
200 μ M	Stem	20,1	\pm 0,04	10,7	\pm 0,01
	Leaf	79,9	\pm 0,04	89,3	\pm 0,01

2000 μ M	Stem	22,5	\pm	0,02	11,1	\pm	0,01
	Leaf	77,5	\pm	0,02	88,9	\pm	0,01



Appendix Figure 1. Zeta potential (mV) of PEI:SWNT and COOH-CNT



Appendix Figure 2. Size intensity (nm/%) of PEI:SWNT and COOH-CNT



Appendix Figure 3. Rosette view of 4-week-old CS28833 accession of *A. thaliana* under potassium deficiency